ELSEVIER

Journal of Quantitative Spectroscopy & Radiative Transfer 96 (2005) 139–204

Journal of Quantitative Spectroscopy & Radiative Transfer

www.elsevier.com/locate/jqsrt

The *HITRAN* 2004 molecular spectroscopic database

L.S. Rothman[a,*], D. Jacquemart[a,1], A. Barbe[b], D. Chris Benner[c], M. Birk[d], L.R. Brown[e], M.R. Carleer[f], C. Chackerian Jr.[g], K. Chance[a], L.H. Coudert[h,2], V. Dana[i], V.M. Devi[c], J.-M. Flaud[h,2], R.R. Gamache[j], A. Goldman[k], J.-M. Hartmann[h,2], K.W. Jucks[l], A.G. Maki[m], J.-Y. Mandin[i], S.T. Massie[n], J. Orphal[h,2], A. Perrin[h,2], C.P. Rinsland[o], M.A.H. Smith[o], J. Tennyson[p], R.N. Tolchenov[p], R.A. Toth[e], J. Vander Auwera[f], P. Varanasi[q], G. Wagner[d]

[a]*Harvard-Smithsonian Center for Astrophysics, Atomic and Molecular Physics Division, Cambridge, MA 02138, USA*
[b]*Université de Reims-Champagne-Ardenne, Groupe de Spectrométrie Moléculaire et Atmosphérique, 51062 Reims, France*
[c]*The College of William and Mary, Department of Physics, Williamsburg, VA 23187, USA*
[d]*DLR – Remote Sensing Technology Institute, Wessling, Germany*
[e]*California Institute of Technology, Jet Propulsion Laboratory, Pasadena, CA 91109, USA*
[f]*Université Libre de Bruxelles, Service de Chimie Quantique et Photophysique, C.P. 160/09, B-1050 Brussels, Belgium*
[g]*NASA Ames Research Center, Moffett Field, CA 94035, USA*
[h]*Université Paris-Sud, Laboratoire de Photophysique Moléculaire, 91405 Orsay, France*
[i]*Université Pierre et Marie Curie, Laboratoire de Physique Moléculaire et Applications, 75252 Paris, France*
[j]*Univ. of Mass Lowell, Department of Environmental Earth and Atmospheric Sciences, Lowell, MA 01854, USA*
[k]*University of Denver, Department of Physics, Denver, CO 80208, USA*
[l]*Harvard-Smithsonian Center for Astrophysics, Optical and Infrared Astronomy Division, Cambridge, MA 02138, USA*
[m]*15012 24 Ave, SE, Mill Creek, WA, USA*
[n]*National Center for Atmospheric Research, Boulder, CO 80307, USA*
[o]*NASA Langley Research Center, Atmospheric Sciences, Hampton, VA 23681, USA*
[p]*University College London, Department of Physics and Astronomy, London WC1E 6BT, UK*
[q]*State University of New York at Stony Brook, Stony Brook, NY 11794, USA*

Received 3 August 2004; received in revised form 15 October 2004; accepted 18 October 2004

*Corresponding author. Tel.: +1 617 495 7474; fax: +1 617 496 7519.
E-mail address: lrothman@cfa.harvard.edu (L.S. Rothman).

[1]New address: Université Pierre et Marie Curie, Laboratoire de Dynamique, Interactions et Réactivité, 75252 Paris, France.

[2]Presently at the Universités Paris 7 et 12, Laboratoire Inter-Universitaire des Systèmes Atmosphériques, 94010 Creteil, France.

0022-4073/$ - see front matter
doi:10.1016/j.jqsrt.2004.10.008

Abstract

This paper describes the status of the 2004 edition of the *HITRAN* molecular spectroscopic database. The *HITRAN* compilation consists of several components that serve as input for radiative transfer calculation codes: individual line parameters for the microwave through visible spectra of molecules in the gas phase; absorption cross-sections for molecules having dense spectral features, i.e., spectra in which the individual lines are unresolvable; individual line parameters and absorption cross-sections for bands in the ultra-violet; refractive indices of aerosols; tables and files of general properties associated with the database; and database management software. The line-by-line portion of the database contains spectroscopic parameters for 39 molecules including many of their isotopologues.

The format of the section of the database on individual line parameters of *HITRAN* has undergone the most extensive enhancement in almost two decades. It now lists the Einstein *A*-coefficients, statistical weights of the upper and lower levels of the transitions, a better system for the representation of quantum identifications, and enhanced referencing and uncertainty codes. In addition, there is a provision for making corrections to the broadening of line transitions due to line mixing.

Keywords: HITRAN; Spectroscopic database; Molecular spectroscopy; Molecular absorption; Line parameters; Absorption cross-sections; Aerosols

1. Introduction

This article describes the data and software that have been added, modified, or enhanced in the *HITRAN* (**hi**gh resolution **tran**smission) compilation since the previous update of 2001 [1]. An archival compilation was made available in the summer of 2004 after the 8th biennial *HITRAN* Database conference that took place at the Harvard-Smithsonian Center for Astrophysics, Cambridge MA, 16–18 June 2004. The compilation brings together the *HITRAN* line-transition parameters, infrared cross-sections, UV line-by-line parameters and cross-sections, aerosol refractive indices, and documentation. The new file structure for the compilation is shown in Fig. 1. This compilation, called HAWKS (**H**ITRAN **a**tmospheric **w**or**ks**tation), is available on an anonymous ftp-site. Instructions for accessing the database can be found in the *HITRAN* web-site

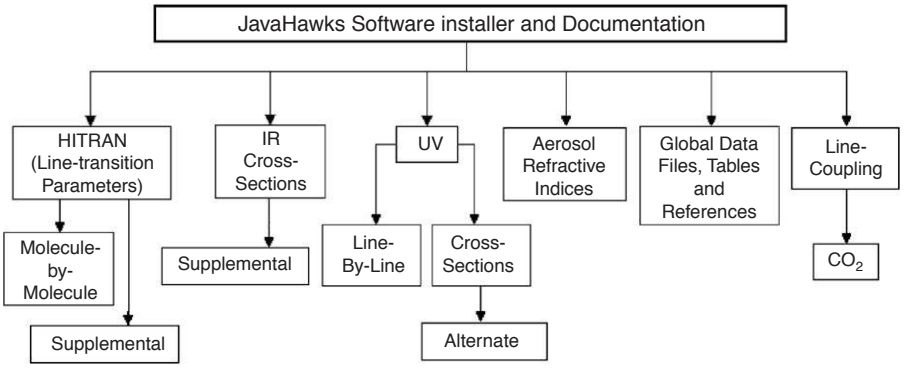

Fig. 1. File structure of the *HITRAN* ftp-site (ftp://cfa-ftp.harvard.edu/pub/hitran04).

(http://cfa-www.harvard.edu/HITRAN). As in previous editions, there is software included called JavaHAWKS which provides a functional and flexible set of functions for managing the database. This software can be installed on a wide set of platforms, running for example Windows, UNIX, Solaris, LINUX, and Mac OS.

The *HITRAN* database is the recognized international standard, used for a vast array of applications including terrestrial atmospheric remote sensing, transmission simulations, fundamental laboratory spectroscopy studies, industrial process monitoring, and pollution regulatory studies. An international *HITRAN* advisory committee, composed of a dozen experts in the field of spectroscopy, has been established under the auspices of NASA. This committee reviews and evaluates new data and makes recommendations for updates and replacements in the compilation.

The most significant of the improvements featured in this newly updated edition of *HITRAN* relates to the line-by-line parameters. In Section 2 of this paper, the new *HITRAN* format for the line-by-line parameters is presented. Section 3 deals with the notable improvements that have been made in the line-by-line portion of the present (2004) compilation. The status of the infrared cross-sections, sets of ultraviolet data, and the aerosol refractive indices of aerosols, is discussed in Sections 4–6.

2. The 2004 HITRAN format

The format of the parameters for each spectral line (equivalent to a record in the database) is given in Table 1. The total length of the record is now 160 characters, an increase from the 100 bytes that had been adopted since the edition of 1986 [2] until the edition of 2000 including updates of 2001 [1]. The parameters presented in Table 1 are described in Table 2. Nine fields have been added in this 160-byte format: three extra uncertainty indices for line-shape parameters and three corresponding reference pointers, a flag for line coupling, which is also known as "line mixing," and the statistical weights of the upper and lower levels of each of the transitions.

The flag used for line coupling is identified in the database by an asterisk (*). Its appearance in the corresponding field of a transition is an alert that information on line coupling is available in the *HITRAN* ftp-site (ftp://cfa-ftp.harvard.edu/pub/hitran04). The current *HITRAN* ftp-site contains several directories (folders) which are illustrated in Fig. 1. One of these directories is called "line-coupling." It contains subdirectories in the cases of those molecules for which line-coupling data are available. These data appear in several files: a "readme" file, programs and input files that introduce line coupling into the usual line-profile model using the Voigt profile. In this edition of *HITRAN*, CO_2 is the only molecule for which line-coupling data have been introduced (see Section 3.2 for details). In the future, line-coupling data will be considered for other molecules, especially CH_4, N_2O, and O_2.

In the format that has been adopted in the present edition, the weighted square of the transition moment has been replaced by the Einstein A-coefficient. There are several reasons for the implementation of this change [3]. The most crucial of these is prompted by the facts that: (a) the Einstein A-coefficients are more desirable for applications in the studies of non-local thermodynamic equilibrium (non-LTE) in the atmosphere, astrophysics, and fundamental physics, and (b) some inconsistencies in the definitions adopted for the transition moment were indeed the sources of inaccuracies in the previous editions of *HITRAN*. A complete and detailed paper [3] dealing with the calculation of the A-coefficients and statistical weights of the energy levels of the upper and lower states in the present edition of the database appears in Ref. [3].

Table 1
Record formats for line-by-line parameters and cross-section data in *HITRAN*

Format for HITRAN Parameters in the line-by-line section, Editions 1986 through 2001 (100-character record)

Parameter	M	I	v	S	$\Re$	γ_{air}	γ_{self}	E''	n_{air}	δ_{air}	V'	V''	Q'	Q''	Ierr	Iref
Field Length	2	1	12	10	10	5	5	10	4	8	3	3	9	9	3	6
FORTRAN Descriptor	I2	I1	F12.6	E10.3	E10.3	F5.4	F5.4	F10.4	F4.2	F8.6	I3	I3	A9	A9	3I1	3I2

Format for HITRAN Parameters in the line-by-line section, 2004 Edition (160-character record)

Parameter	M	I	v	S	A	γ_{air}	γ_{self}	E''	n_{air}	δ_{air}	V'	V''	Q'	Q''	Ierr	Iref	* (flag)	g'	g''
Field Length	2	1	12	10	10	5	5	10	4	8	15	15	15	15	6	12	1	7	7
FORTRAN Descriptor	I2	I1	F12.6	E10.3	E10.3	F5.4	F5.4	F10.4	F4.2	F8.6	A15	A15	A15	A15	6I1	6I2	A1	F7.1	F7.1

Format for cross-section headers

Quantity	Chemical symbol	Wavenumber (cm^{-1}) Minimum	Maximum	Number of points	Temperature (K)	Pressure (torr)	Maximum X-section	Resolution	Common name	Not used	Broadener	Reference number
Field length	20	10	10	7	7	6	10	5	15	4	3	3
FORTRAN Descriptor	A20	F10.3	F10.3	I7	F7.1	F6.1	E10.3	A5	A15	4X	A3	I3

Notes: The quantities of the *HITRAN* line-by-line section in these 100- and 160-character records are defined in Table 2.
The format of the cross-section files did not change from the *HITRAN* 2000 edition to the 2004 edition. The pressure stated in the cross-section header is in torr (760 torr = 1 atm = 1013.25 hPa). The field for resolution is normally given in cm^{-1} since the majority of cross-section measurements were taken with Fourier transform spectrometers. In the case of measurements taken with grating spectrometers, the resolution field is given in milli-Angtroms and is listed as *xxx*mA where "*xxx*" is a number.

Table 2
Description of the quantities present in the 100- and 160-character records of the *HITRAN* line-by-line section

Parameter	Meaning	Field length of the (100/160) character records	Type	Comments or units
M	Molecule number	2/2	Integer	*HITRAN* chronological assignment
I	Isotopologue number	1/1	Integer	Ordering within a molecule by terrestrial abundance
v	Vacuum wavenumber	12/12	Real	cm^{-1}
S	Intensity	10/10	Real	$cm^{-1}/(molecule\,cm^{-2})$ at standard 296 K
$\mathfrak{R}$	Weighted square of the transition moment	10/0	Real	$Debye^2$ (for an electric dipole transition)
A	Einstein A-coefficient	0/10	Real	s^{-1}
γ_{air}	Air-broadened half-width	5/5	Real	HWHM at 296 K (in $cm^{-1}\,atm^{-1}$)
γ_{self}	Self-broadened half-width	5/5	Real	HWHM at 296 K (in $cm^{-1}\,atm^{-1}$)
E''	Lower-state energy	10/10	Real	cm^{-1}
n_{air}	Temperature-dependence exponent for γ_{air}	4/4	Real	unitless, with $\gamma_{air}(T)=\gamma_{air}(T_0)\times(T_0/T)^{n_{air}}$
δ_{air}	Air pressure-induced line shift	8/8	Real	$cm^{-1}\,atm^{-1}$ at 296 K
V'	Upper-state "global" quanta	3/15	Hollerith	see Table 3
V''	Lower-state "global" quanta	3/15	Hollerith	see Table 3
Q'	Upper-state "local" quanta	9/15	Hollerith	see Table 4
Q''	Lower-state "local" quanta	9/15	Hollerith	see Table 4
Ierr	Uncertainty indices	3/6	Integer	Accuracy for 3/6 critical parameters $(v, S, \gamma_{air}/v, S, \gamma_{air}, \gamma_{self}, n_{air}, \delta_{air})$, see Table 5
Iref	Reference indices	6/12	Integer	References for 3/6 critical parameters $(v, S, \gamma_{air}/v, S, \gamma_{air}, \gamma_{self}, n_{air}, \delta_{air})$
*	Flag	0/1	Character	Availability of program and data for the case of line mixing
g'	Statistical weight of the upper state	0/7	Real	See details in Ref. [3]
g''	Statistical weight of the lower state	0/7	Real	See details in Ref. [3]

Notes: For the field-length column, the notation A/B corresponds to the number of characters respectively in the 100- and 160-character records. For example, concerning the weighted square of the transition moment, the number of characters for $\mathfrak{R}$ is 10 in the case of the *HITRAN* 2000 edition [1], and 0 in the case of the *HITRAN* 2004 edition since this parameter has been replaced by the Einstein A-coefficient.

Major effort has gone into making the identifications of quantum numbers of energy levels or states more readily evident in the present edition of the database. Instead of the codes that were adopted for the vibrational levels, and in certain cases for electronic levels, in the previous edition [1], explicit identification of quanta (the so-called global quanta) has been used in the present edition. The field lengths of the global and local quantum identifications have been increased from 9 to 15 characters so that a more consistent and encompassing notation for the assignments could be established. In the current edition, a substantial effort has been made to describe and systematize the format of the database identifying the vibrational and rotational quantum numbers of each molecule in its "line-by-line" section. The global and local identification of the quantum numbers and of their FORTRAN descriptors are summarized, respectively, in Tables 3 and 4. As regards the identification of the quantum numbers used for global identification, the modifications made to the previous notation [1] are as follows. In the case of C_2H_2, the total symmetry + or − of the level has been added in order to specify a precise assignment of the lower vibrational state. In the case of CH_4, in class 10, the notation in Table 3 can now describe each vibrational level of methane [13]. For the identification of the "local quanta," the number of different classes has been decreased to 6 groups in this edition from 11 sub-groups in the previous edition [1], thus creating a more compact format. The format of the rotational quantum numbers J, K, K_a, K_c has been increased from two digits to three digits (allowing for the possibility in the future of values greater than 99 for heavy species). The format of the hyperfine quantum number F has been increased from two digits (I2) or four digits (F4.1) to five digits (denoted as A5 in Table 4 in order to incorporate the two cases of integer (I5) or half-integer (F5.1) numbers). Moreover, an important effort has been made in order to standardize the local quanta identification for each molecule. Such is the case, for example, of NO_2 for which the conventions for the J-coding and the F-coding in *HITRAN* had been different depending on the spectral region (see Table 2 of Ref. [14]). We now have the same convention (see notes of Table 4) for the different spectral regions. This convention has also been adopted for HO_2 (see notes of Table 4).

The definitions of the uncertainty indices used in *HITRAN* have not changed from previous editions and are defined in Table 5. However, uncertainty and reference indices are now also given for the self-broadened half-width, the exponent depicting the temperature-dependence of the air-broadened half-width, and the air pressure-induced line shift in addition to line position, line intensity, and air-broadened half-width. It should be remarked that the code 0 in Table 5 might lend itself to two different meanings in the case of line position or air pressure-induced shift. It means that either the uncertainty in the shift reported is greater than 1 cm^{-1} or was not reported. The word "default" or "constant" (code 1 in Table 5) means a constant value, and the word "average" or "estimate" (code 2 in Table 5) means an average or empirical value.

Table 6 is a summary of the molecules in *HITRAN*, giving the isotopologues or isotopomers[3] (a total of 93 variants), their fractional abundance, spectral coverage, and number of lines.

[3]An isotopologue is a molecular twin, as it were, that differs from the original molecule in the isotopic composition (number of isotopic substitutions) only; for example, $^{13}CH_4$ and $^{12}CH_3D$ are isotopologues of $^{12}CH_4$. An isotopomer (a contraction of 'isotopic isomer'), on the other hand, has the same number of each of the isotopic atoms but differing in their orientation within the molecular structure (giving rise to different spectra), for example $^{16}O^{18}O^{16}O$ is an isotopomer of $^{16}O^{16}O^{18}O$ and so is $^{14}N^{15}NO$ of $^{15}N^{14}NO$.

Table 3
Notation and format for the ten classes of global quanta identification in the *HITRAN* 2004 edition

Class definition for *HITRAN* molecules	Upper- and lower-state "global" quanta
Class 1: Diatomic molecules CO, HF, HCl, HBr, HI, N_2, NO^+	v_1 $\overline{13x}$ I2
Class 2: Diatomic molecules with different electronic levels O_2	X v_1 $\overline{12x}$ A1 I2
Class 3: Diatomic molecules with doublet-Π electronic state NO, OH, ClO	X i v_1 $\overline{7x}$ A1 A3 $\overline{2x}$ I2
Class 4: Linear triatomic N_2O, OCS, HCN	v_1 v_2 l_2 v_3 $\overline{7x}$ I2 I2 I2 I2
Class 5: Linear triatomic with large Fermi resonance CO_2	v_1 v_2 l_2 v_3 r $\overline{6x}$ I2 I2 I2 I2 I1
Class 6: Non-linear triatomic H_2O, O_3, SO_2, NO_2, HOCl, H_2S, HO_2, HOBr	v_1 v_2 v_3 $\overline{9x}$ I2 I2 I2
Class 7: Linear tetratomic C_2H_2	v_1 v_2 v_3 v_4 v_5 l $\pm$ r S I2 I2 I2 I2 I2 I2 A1 I1 A1
Class 8: Pyramidal tetratomic NH_3, PH_3	v_1 v_2 v_3 v_4 S $\overline{5x}$ I2 I2 I2 I2 I2
Class 9: Non-linear tetratomic H_2CO, H_2O_2, COF_2	v_1 v_2 v_3 v_4 v_5 v_6 $\overline{3x}$ I2 I2 I2 I2 I2 I2
Class 10: Pentatomic or greater polyatomic CH_4 CH_3D, CH_3Cl, C_2H_6, HNO_3, SF_6, HCOOH, $ClONO_2$, C_2H_4, CH_3OH	v_1 v_2 v_3 v_4 n C $\overline{3x}$ I2 I2 I2 I2 A2 A2 Individual molecule notation

Notes: Defined in an earlier *HITRAN* edition [2], the global quanta were represented by an index (format I3) which was a code corresponding to the vibrational quantum numbers. In the *HITRAN* 2004 edition, the vibrational quantum numbers are directly incorporated as a 15-character field. v_j is the quantum number associated with the normal mode of vibration j, l_j is the vibrational angular momentum quantum number associated with the degenerate bending mode j, and l is defined as the absolute value of the sum of the vibrational angular momentum quantum number l_j. For classes 2 and 3, X designates the electronic state of the molecule, and for class 3, i corresponds to either $\frac{1}{2}$ or $\frac{3}{2}$, which means $N = J \pm \frac{1}{2}$ depending on the molecules, see Ref. [4, pp. 233–234]. For details of the notation of class 5, see Ref. [5]. For the notation of class 7, see Ref. [6]. Moreover, we added for class 7 the parity u or g of the vibrational level in the S-field for the symmetric isotopologue $^{12}C_2H_2$. For class 8, S is the symmetry of the level (only for NH_3: for PH_3 S is blank). For H_2O_2 in class 9, v_4 has been replaced by the torsional quanta n and τ described in Refs. [7,8]. For CH_4, n is a multiplicity index, and C is the symmetry. Class 10 includes a wide variety of polyatomic molecules; the notation is tailored to each individual molecule.

Table 4
Notation and format for the six groups of local quanta identification in the *HITRAN* 2004 edition

Group classification and *HITRAN* molecules	Upper-state local quanta					Lower-state local quanta				
Group 1: Asymmetric rotors[a]	J'	K'_a	K'_c	F'	Sym′	J''	K''_a	K''_c	F''	Sym″
H_2O, O_3, SO_2, NO_2, HNO_3, H_2CO, HOCl, H_2O_2, COF_2, H_2S, HO_2, HCOOH, $ClONO_2$, HOBr, C_2H_4	I3	I3	I3	A5	A1	I3	I3	I3	A5	A1
Group 2: Diatomic and linear molecules				F'					F''	
CO_2, N_2O, CO, HF, HCl, HBr, HI, OCS, N_2, HCN, C_2H_2, NO^+	10X			A5		5X			A5	
Group 3: Spherical rotors		J'	C'	α'	F'		J''	C''	α''	F''
SF_6, CH_4	2X	I3	A2	I3	A5	2X	I3	A2	I3	A5
Group 4: Symmetric rotors	J'	K'	l'	C'	Sym′	F'	J''	K''	l''	C''	Sym″	F''
CH_3D, CH_3Cl, C_2H_6, NH_3, PH_3, CH_3OH	I3	I3	I2	A2	A1	A4	I3	I3	I2	A2	A1	A4
Group 5: Triplet-Σ ground electronic states				F'					N''	Br	J''	F''	Sym
O_2	10X			A5		1X			I3	A1	I3	A5	A1
Group 6: Doublet-Π ground electronic states[b]				F'					J''	Sym″	F''
NO, OH, ClO	10X			A5		3X			F5.1	A1	A5

Notes: Prime and double primes refer, respectively, to upper and lower states, respectively; *Br* is the *O*-, *P*-, *Q*-, *R*-, or *S*-branch symbol; *J* is the quantum number associated with the total angular momentum excluding nuclear spin; *F* is the quantum number associated with the total angular momentum including nuclear spin. *F* is shown in A5 FORTRAN format in order to accommodate integer (I5) or half-integer values (F5.1). For group 3, the notations *C* and α are described in Ref. [9]. For group 4, the symmetry *C* (which is equal to A+, A− or E) is described in Refs. [10,11]. *N* is the total angular momentum including spin and rotation for O_2. Sym is either the symmetry *e* or *f* for ℓ-type doubling [12], + or − for required symmetry symbols, or *d* or *q* for magnetic-dipole or electric-quadrupole transitions (only for O_2 and N_2).

[a]For NO_2 and HO_2, *N* (the quantum number associated with the rotational angular momentum) is used instead of *J*, and the Sym field +/− (which is not a symmetry) is the *J*-coding defined as follows: + means $J = N + \frac{1}{2}$ and − means $J = N - \frac{1}{2}$.

[b]For OH, the format of branch (Br) in the lower-state quanta field is 2A1 to accommodate the total orbital angular momentum *N* as well as *J*.

Table 5
Uncertainty codes adopted for *HITRAN*

Line position and Air pressure-induced line shift (cm^{-1})		Intensity, half-width (air- and self-) and temperature-dependence	
Code	Uncertainty range	Code	Uncertainty range
0	$\geqslant 1.$ or Unreported	0	Unreported or unavailable
1	$\geqslant 0.1$ and $<1.$	1	Default or constant
2	$\geqslant 0.01$ and <0.1	2	Average or estimate
3	$\geqslant 0.001$ and <0.01	3	$\geqslant 20\%$
4	$\geqslant 0.0001$ and <0.001	4	$\geqslant 10\%$ and $<20\%$
5	$\geqslant 0.00001$ and <0.0001	5	$\geqslant 5\%$ and $<10\%$
6	<0.00001	6	$\geqslant 2\%$ and $<5\%$
		7	$\geqslant 1\%$ and $<2\%$
		8	$<1\%$

Note: Uncertainty indices are provided for six parameters in the *HITRAN* 2004 edition. However, there remain some lines from earlier editions with zero or blank for these indices, since this system was first implemented for three parameters in 1986. Because some contributors do not supply this important information, it is incumbent upon users to consult the references. Sources for these parameters are provided by the reference indices (access to these references can be made in the JavaHAWKS software or the file ref-table.pdf available at the address ftp://cfa-ftp.harvard.edu/pub/hitran04/Global_Data/).

Tables 1–6 should facilitate the user's interpretation of all of the notations used in this (2004) edition of the *HITRAN* database.

3. Line-by-line parameters

This edition of *HITRAN* contains a new entry, namely, the methanol molecule (CH_3OH). The number of transitions included in the database is limited by: (1) a reasonable minimum cutoff in absorption intensity (based on sensitivity of instruments to observe absorption over maximum terrestrial path lengths), (2) lack of sufficient experimental data, or (3) lack of calculated transitions.

The molecules for which data are included in the line-by-line portion of *HITRAN* are mostly composed of small numbers of atoms and have low molecular weights. Large polyatomic molecules have many normal modes of vibration and "heavy" species have fundamentals at very low wavenumbers. For two of the molecules in *HITRAN*, SF_6 and $ClONO_2$, we have put the parameters for this edition in a supplemental folder (see Fig. 1). The rationale for this is that the line-by-line parameters represent only a few bands, and neglect many significant hot bands for the "heavy" species. For most applications, the IR cross-sections of these molecules in the *HITRAN* compilation provide a better simulation.

The following sub-sections cover all molecules whose parameters have been updated since the last edition of *HITRAN* [1]. The descriptions are generally ordered by increasing wavenumber region, and we have attempted to describe the improvements in the line positions and intensities

Table 6
Summary of isotopologues represented in *HITRAN*

No.	Molecule	Isotopologue (AFGL notation)	Fractional abundance	Spectral coverage (cm^{-1})	Number of lines
1	H_2O	161	0.997317	0-25233	36114
		181	0.00199983	0-14519	9548
		171	0.000372	10-11335	6120
		162	0.00031069	0-7514	9628
		182	0.000000623	0-3825	1611
		172	0.000000116	1234-1599	175
2	CO_2	626	0.98420	442-12785	27979
		636	0.01106	497-8105	8836
		628	0.0039471	0-8133	13445
		627	0.000734	0-6962	7739
		638	0.00004434	567-4947	2312
		637	0.00000825	584-3642	1593
		828	0.0000039573	615-3670	721
		728	0.00000147	626-2359	288
3	O_3	666	0.992901	0-4061	183785
		668	0.00398194	0-2114	21718
		686	0.00199097	1-2075	8937
		667	0.000740	0-2122	65106
		676	0.000370	0-2101	31935
4	N_2O	446	0.990333	0-7797	33066
		456	0.0036409	5-5086	4222
		546	0.0036409	4-4704	4592
		448	0.00198582	542-4672	4250
		447	0.000369	550-4430	1705
5	CO	26	0.98654	3-8465	917
		36	0.01108	3-6279	780
		28	0.0019782	3-6267	760
		27	0.000368	3-6339	728
		38	0.00002222	3-6124	712
		37	0.00000413	1807-6197	580
6	CH_4	211	0.98827	0-9200	187128
		311	0.01110	0-6070	28793
		212	0.00061575	7-3307	35519
7	O_2	66	0.995262	0-15928	1431
		68	0.00399141	1-15852	671
		67	0.000742	0-14537	4326
8	NO	46	0.993974	0-9274	100902
		56	0.0036543	1609-2061	699
		48	0.00199312	1601-2039	679
9	SO_2	626	0.94568	0-4093	38566
		646	0.04195	2463-2497	287
10	NO_2	646	0.991616	0-3075	104223
11	NH_3	4111	0.9958715	0-5295	27994
		5111	0.0036613	0-5180	1090
12	HNO_3	146	0.989110	0-1770	271166
13	OH	61	0.997473	0-19268	41166
		81	0.00200014	0-329	295
		62	0.00015537	0-332	912

Table 6 (*continued*)

No.	Molecule	Isotopologue (AFGL notation)	Fractional abundance	Spectral coverage (cm^{-1})	Number of lines
14	HF	19	0.99984425	41-11536	107
15	HCl	15	0.757587	20-13458	324
		17	0.242257	20-10995	289
16	HBr	19	0.50678	16-9759	651
		11	0.49306	16-9758	642
17	HI	17	0.99984425	12-8488	806
18	ClO	56	0.75591	0-1208	3599
		76	0.24172	0-1200	3631
19	OCS	622	0.93739	0-4119	10553
		624	0.04158	0-4116	4186
		632	0.01053	0-4013	2283
		623	0.007399	509-4116	1802
		822	0.001880	0-4042	1096
20	H_2CO	126	0.98624	0-2999	1772
		136	0.01108	0-73	563
		128	0.0019776	0-48	367
21	HOCl	165	0.75579	1-3800	8877
		167	0.24168	1-3800	7399
22	N_2	44	0.9926874	1922-2626	120
		124	0.98511	0-3424	2955
23	HCN	134	0.01107	2-3405	652
		125	0.0036217	2-3420	646
24	CH_3Cl	215	0.74894	0-3173	16411
		217	0.23949	0-3162	14708
25	H_2O_2	1661	0.994952	0-1500	100781
26	C_2H_2	1221	0.97760	604-6686	3232
		1231	0.02197	613-6589	285
27	C_2H_6	1221	0.97699	720-2978	4749
28	PH_3	1111	0.99953283	770-2472	11790
29	COF_2	269	0.98654	725-2002	70601
30	SF_6	29	0.95018	929-964	22901
31	H_2S	121	0.94988	2-4257	12330
		141	0.04214	5-4172	4894
		131	0.007498	5-4099	3564
32	HCOOH	126	0.983898	10-1235	24808
33	HO_2	166	0.995107	0-3676	38804
34	O	6	0.997628	68-159	2
35	$ClONO_2$	5646	0.74957	763-798	21988
		7646	0.23970	765-791	10211
36	NO^+	46	0.993974	1634-2531	1206
37	HOBr	169	0.5056	0-316	2177
		161	0.4919	0-316	2181
38	C_2H_4	221	0.9773	701-3243	12697
		231	0.02196	2947-3181	281
39	CH_3OH	2161	0.98593	0-1408	19899

Note: SF_6 and $ClONO_2$ are relegated to the supplemental directory.

prior to those in the other parameters, when feasible. Future improvements are also mentioned where necessary.

3.1. H_2O (molecule 1)

For water-vapor parameters, a major improvement has been accomplished, especially for the main isotopologue $H_2^{16}O$.

In the pure-rotation region, 952 lines of $HD^{18}O$ have been added to *HITRAN*. Line positions and intensities derive from the JPL catalog [15]. It should be noted that the spectral line parameters of this isotopologue were only listed in the earlier editions of *HITRAN* in the spectral region covering the bands due to the bending mode of vibration of the molecule.

Updates of line positions have been made for 1396 lines of $H_2^{17}O$ and $H_2^{18}O$ from 0 to 500 cm^{-1} based on the work of Toth [16], and of line intensities for 2523 lines of $H_2^{17}O$, $H_2^{18}O$, and $HD^{16}O$ from 0 to 500 cm^{-1} based on the work of Pearson [17].

For the main isotopologue $H_2^{16}O$ between 0 and 800 cm^{-1}, the calculations of Coudert et al. [18–20] have been used to update line positions and line intensities of the 000-000, 010-010, 020-020, 100-100, and 001-001 bands, and to add six new bands into *HITRAN* (100-001, 100-020, 020-100, 020-001, 001-100, 001-020). These updates and improvements are for positions and intensities of 2852 lines involving the first eight vibrational states. At very low wavenumbers, the intensity cutoff S_{cut} used in *HITRAN* is not a constant, but in fact decreases and is related to the effect of the radiation field in the line intensity calculation [21]. For the first seven molecules in *HITRAN*, it is given by

$$S_{cut} = \frac{S_{crit} v}{v_{crit}} \tanh\left(\frac{c_2 v}{2T_0}\right), \tag{1}$$

where, $S_{crit} = 3 \times 10^{-27}$ cm molecule^{-1} at $v_{crit} = 2000\,cm^{-1}$ for water vapor. c_2 is the second radiation constant hc/k (h is Planck's constant, c is the speed of light in vacuum, k is Boltzmann's constant), v is the wavenumber of the transition, and T_0 is a standard temperature. In *HITRAN*, T_0 has traditionally been 296 K.

A complete update for positions and line intensities has been done for all *HITRAN* water-vapor isotopologues between 500 and 8000 cm^{-1} based on the work of Toth [22]. This update does not apply to the lines previously discussed that come from the work of Coudert et al. [18–20].

From 9600 to 11400 cm^{-1}, the line positions and intensities of the isotopologue $H_2^{17}O$, which come from a preliminary study of Camy-Peyret et al. [23], have been updated. The number of lines has been increased to 1063 from 370. Above 11400 cm^{-1}, lines have recently been assigned by Tanaka et al. [24] and will be included in a future update to *HITRAN*.

Nine hundred and eighteen lines of $H_2^{18}O$ have been entered into *HITRAN* in the 12400–14518 cm^{-1} region by drawing upon the work of Tanaka et al. [24,25]. Using the FTS (Fourier Transform Spectroscopy) spectra of water vapor (with significantly enhanced $H_2^{17}O$ and $H_2^{18}O$), which were recorded at the Kitt Peak National Solar Observatory in August 1980, the line positions and the heights of the absorption peaks of the transitions of $H_2^{18}O$ were determined. The conversion of the peak heights of absorption into values of line intensity has been obtained by using the spectra of water vapor in its natural abundance that were recorded in the same spectral region [26]. The quantum assignments of the lines in this spectral region are mostly complete,

while, in some cases, a slight revision of line intensities and line positions, based upon the work of Tanaka et al. [24] is made apparent.

Another significant improvement in the database is in the 9250–9600, 11400–12895, and 13184–25000 cm^{-1} regions, in which the line lists generated from the work of Mérienne et al. [27] and Coheur et al. [28] have been used to replace the previously listed entries for the lines of $H_2^{16}O$. The line positions and line intensities alone have been adopted from Refs. [27,28], while the line assignments are taken from Ref. [29]. The experimental data from Refs. [27,28] are still being analyzed and scrutinized, and improvements are expected in the near future.

There has been a complete overhaul of the line-shape parameters (air-broadened half-widths (γ_{air}), self-broadened half-widths (γ_{self}), and the air-induced line shift (δ_{air})) of $H_2^{16}O$, $H_2^{18}O$ and $H_2^{17}O$. A procedure, described below, was developed that reads the line list for water-vapor, searches in a number of databases for the line-shape data of the particular rotational–vibrational transition, and adds the information based on a scheme of priority. Let us consider firstly the data on air-broadened half-widths. A primary database has been constructed by performing an intercomparison of measured air-broadened half-widths [30] that were determined by averaging two to eight experimental data on each of 3514 transitions and the corresponding and reported experimental uncertainties. A second similar database has been composed of all the single measurements of γ_{air} of 14,355 transitions [30] with the reported uncertainty. Additional databases, as those of *smoothed* γ_{air} values created by Toth [22] (for 7716 transitions) and those calculated using the complex Robert–Bonamy (CRB) method for 6040 rotational–vibrational transitions [31–36], have been set up.

The algorithm given in Ref. [37] to determine an approximate value of γ_{air} allows us to determine an approximate air pressure-induced line shift as well. The method of Ref. [37] is an attempt to fit, for each rotational transition, the experimental and theoretical data by applying Eq. (15) of Ref. [36], which describes the vibrational dependence of γ_{air} and δ_{air}. The coefficients deduced from the fit allow one to obtain any air-broadened half-width or air pressure-induced line shift of transitions having the same rotational quantum numbers but different vibrational quantum numbers. The fits were made using recent experimental [22,27,28,38,39] and theoretical [32–34] data. This approach may be employed as the interim method of determining the approximate values of γ_{air} and δ_{air} for the rotational–vibrational transitions of $H_2^{16}O$, $H_2^{18}O$ and $H_2^{17}O$ until a more robust approach, based upon accurately measured data, surfaces.

The procedure for adding the air-broadened half-width data is based on a preference for the data extracted from the intercomparison database [30], in which the respective uncertainties in the data are identified. If a value does not exist in this database for a given rotational–vibrational transition, the algorithm next searches the database of all air-broadened measurements of the half-width. If a reliable datum exists, with its associated uncertainty and the source from which it was extracted is duly apparent, it is recommended by the algorithm. If such is not the case, then the algorithm recommends the employment of the smoothed data that were created by Toth [22]. If a reliable datum exists, it is used, and the uncertainty code is set to 5. If there is no datum in the latter list, the search is extended to the CRB database [32–36] for the particular rovibrational transition. If the datum is in the CRB database it is used and the uncertainty code set to 5. Finally, if the datum has not been found in the above databases, the approximate air-broadened half-width from the work of Ref. [37] is used with the uncertainty code set to 4.

In the case of the deuterated isotopologues $HD^{16}O$, $HD^{18}O$ and $HD^{17}O$, the measurements and extrapolations performed by Toth [22] have been used in the 500–8000 cm^{-1} region. For all the other transitions of these species, only the data from Ref. [22] that belong to the ν_1, ν_2, and ν_3 bands of $HD^{16}O$ have been used by making the implicit assumption that the dependence upon the vibrational quantum numbers is negligible.

For the self-broadened half-widths, γ_{self}, of $H_2^{16}O$, $H_2^{18}O$, and $H_2^{17}O$, the following procedure has been adopted. For a given rovibrational transition, priority is given to data taken from the database of all values of γ_{self} (10,596 transitions) from Ref. [30]. When the datum existed as a measurement, it was implemented with the corresponding experimental uncertainty along with the suitable reference found in the database. In cases where a measured datum had not been available, we resorted to the adoption of the smoothed data on γ_{self} presented by Toth in Ref. [22] for 7716 transitions. If a measured value was available, it is listed with the uncertainty code assigned to be 5. Finally, if a value had not been found in either the experimental or the extrapolated database, a γ_{self} that has been determined by averaging experimental values as a function of J'' (uncertainty code 2) was adopted.

For the transitions in the pure-rotational bands of $HD^{16}O$ and $HD^{18}O$, we adopted the data from Ref. [22] on corresponding rotational transitions in the ν_1, ν_2, and ν_3 bands of $HD^{16}O$. A study, which is based on the approach of Ref. [37], of the dependence of self-broadened line widths on vibrational quantum numbers, is contemplated as an update of these coefficients in a future *HITRAN* edition.

As the modern atmospheric remote-sensing instruments and experiments are becoming progressively more sophisticated, the need for data on air-induced shifts of the spectral lines of atmospheric gases is emerging. However, it must be recognized that collision-induced line shifts are, more often than not, more difficult to measure than half-widths, and values reported by different laboratories can disagree significantly. It is difficult to archive a set of data that is concordant with the measurements reported by every laboratory. So, the entries in the database in this category have to be regarded as the best estimates that we could provide at the present time. The air pressure-induced line shifts, δ_{air}, for water vapor included in the current edition, have been judiciously chosen from the following five sources: the database compiled by Gamache and Hartmann [30] after a critical intercomparison of all of the published experimental line shift data on 680 transitions, a seemingly comprehensive list cited in Ref. [30] of published experimental line shifts of 8754 transitions, the line shifts reported by Toth [22] on 2978 transitions after he subjected his measured data to a smoothing procedure, the CRB calculated database [32–36] on 6040 transitions, and the complete set of data from Ref. [37], which describes a semi-empirical procedure for generating the list of line parameters in the absence of definitive measurements. The same set of criteria as applied to, and described above for air-broadened widths, has been adopted for the line shifts as well. Top priority has been given to accurate and carefully performed measurements, and the next order of priority is assigned to a CRB calculation, and then falling back to the data of Ref. [37] for a semi-empirical approach as an interim solution. The present attempt is a considerable advance from the lack of these data in the previous edition [1], in which we were only able to assign for most of the transitions a value of zero as an indication that a datum was unavailable for the air-induced line shift.

As it is commonly accepted now, the dependence of a collision-broadened half-width upon temperature is expressed in terms of an exponent, n, under the assumption that the half-width

Table 7
Summary of the temperature-dependence exponents n_{air} of the water-vapor air-broadened half-widths from Ref. [40]

$\|m\|$	n_{air}
0	0.78
1	0.78
2	0.78
3	0.77
4	0.73
5	0.69
6	0.64
7	0.59
8	0.53
9	0.49
10	0.45
11	0.41
12	0.39
13	0.37
14	0.36
15	0.36
16	0.38
$\geqslant 17$	0.41

varies as the negative power n of the temperature. The exponents of the air-broadened half-widths, n_{air}, in the current database are the estimated values given in Ref. [40], which addresses the 6-μm region. It should be noted that these values are only $|m|$-dependent ($m = -J''$ for $\Delta J = -1$, $m = J''$ for $\Delta J = 0$, and $m = J'' + 1$ for $\Delta J = +1$, where J'' is the rotational quantum number in the lower state of a radiative transition resulting from absorption). These exponents have now been used for all the assigned transitions of all of the isotopologues of water vapor throughout this database. Table 7 summarizes these entries. A default exponent of 0.68 has been adopted for n_{air} for unassigned lines.

3.2. CO_2 (molecule 2)

Among the recent studies on carbon dioxide, we highlight the global calculation by Tashkun et al. [41] on the positions and intensities of the lines of $^{12}C^{16}O_2$, $^{13}C^{16}O_2$, $^{12}C^{16}O^{18}O$ and $^{12}C^{16}O^{17}O$. This enterprise of calculation resulted in the establishment of the so-called "Carbon Dioxide Spectroscopic Database at 296 K" with the acronym *CDSD*-296. This work has been compared with earlier calculations that used the Direct Numerical Diagonalization (DND) technique [42], and has been found to be an improvement. Following the procedure that has been employed previously [43], high-quality experimental data have been preferred. For this reason, the data of *CDSD*-296 have been adopted in order to update *HITRAN* only in situations in which high-quality observational data were unavailable.

We have added two line lists in the pure-rotational spectral region in this edition for the isotopologues $^{16}O^{12}C^{18}O$ and $^{16}O^{12}C^{17}O$. Although their permanent dipole moments are quite small, their effects are apparently identifiable in spectroscopic observations. Thus we felt that the

data on these transitions deserved to be included in the database. The positions, line intensities, and the energies of the lower states of the transitions are derived from the JPL catalog [15]. It should be noted that the hyperfine structure of the $^{16}O^{12}C^{17}O$ isotopologue is resolved.

It can be stated that a significant update has indeed been accomplished on the line positions. For the principal isotopologue of CO_2, namely, $^{12}C^{16}O_2$, the recent work of Miller and Brown [44] has been used to update the line positions of 83 bands in a considerably large infrared spectral region. Fig. 2 shows the dramatic improvement in the residuals due to the new line positions that are identified in the 2-μm region. This improvement is typical of what has been achieved in the latest update in the database on this molecule. Furthermore, the calculation by Tashkun et al. [41] has been used to improve the database on line positions that had previously been presented in HITRAN92 [45] as calculations using spectroscopic constants [43] coming from a DND calculation [42], from Venus observations [46], and from the calculation by Rothman and Benedict [47] for the other isotopologues. The work of Tashkun et al. [41] has led to this update of line positions of 51 bands of $^{12}C^{16}O_2$, 8 bands of $^{13}C^{16}O_2$, 4 bands of $^{12}C^{16}O^{18}O$, and 12 bands of $^{12}C^{16}O^{17}O$. This update covers the entire infrared region.

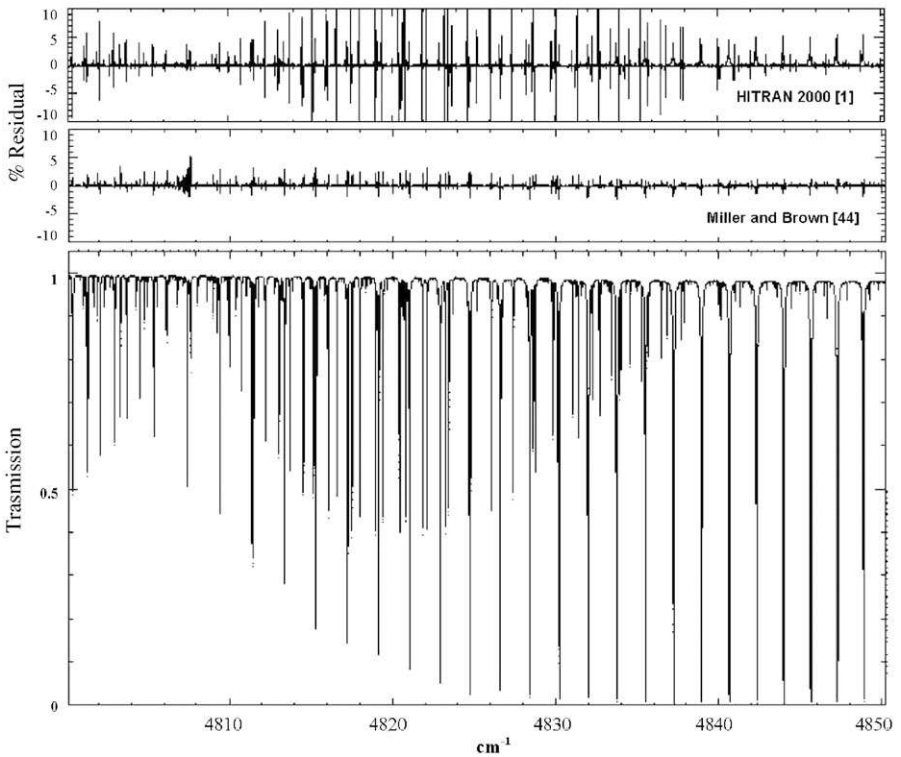

Fig. 2. Comparison between experimental (solid line) and simulated (dashed line) CO_2 laboratory spectra in the 2-μm region. The experimental conditions of the bottom panel are 30 torr CO_2 and 25 m path. Top panel: residuals from simulating the experimental spectrum using the previous *HITRAN* database [1]. RMS error = 2.75%. Middle panel: simulation residuals using the line positions reported in Miller and Brown [44] with unpublished intensity data. RMS error = 0.11%.

As recommended by Goldman et al. [48], the work of Ding et al. [49] has been used to update the line positions in the $2\nu_1 + 3\nu_3$ band triad around 9550 cm^{-1} of $^{12}C^{16}O_2$. The spectroscopic constants of Ref. [49] have also been used to update the line positions of the two hot bands 20031-10001 and 20032-10002 around 8230 cm^{-1} involving the levels of the $2\nu_1 + 3\nu_3$ triad (the vibrational quantum number notation used for this molecule is shown in Table 3). For the interacting 21113-11102, 21113-11101, 12212-02201, 40002-11102, and 23301-02201 bands of $^{12}C^{16}O_2$ in the 3-μm region, the line positions have been taken from Benner [50]. The positions of the two laser bands of $^{12}C^{16}O^{17}O$ have also been updated from Ref. [51]. A summary of the improvements pertaining to the line positions is given in Table 8.

Numerous experimental studies have been reported in the open literature on line intensities of this molecule since the last update of *HITRAN* [1] was announced in this journal. Several research efforts have been recognized in the preparation of the current edition: Mandin et al. [52] on the 10012-10001 band of $^{12}C^{16}O_2$ centered at 2225 cm^{-1}; Claveau et al. [51] on three hot bands of $^{16}O^{12}C^{17}O$ between 550 and 765 cm^{-1}; Ref. [53] on the $\nu_2 + \nu_3 - \nu_2$ band of $^{16}O^{12}C^{17}O$ and the laser bands of $^{16}O^{12}C^{17}O$ and $^{16}O^{12}C^{18}O$; Teffo et al. [54,55] on the 10031-00001 and 10032-00001 bands of the main isotopologue centered at 8294 cm^{-1} and at 8192 cm^{-1} [54] and on the ν_3-fundamental of $^{16}O^{13}C^{17}O$ [55]; Henningsen and Simonsen [56] on the $2\nu_1 + 2\nu_2 + \nu_3$ band of $^{12}C^{16}O_2$ at 6348 cm^{-1}; Kshirasagar et al. [57] for the data on the $2\nu_3$ band of $^{16}O^{12}C^{18}O$ at 4639 cm^{-1}; Ref. [58] for the data on the 00031-10001 and 00031-10002 bands of $^{12}C^{16}O_2$ at 5584 cm^{-1}; Giver et al. [59] for the data on the five bands of $^{12}C^{16}O_2$ between 5218 cm^{-1} and 5349 cm^{-1}; Devi et al. [60] for data on the 33 bands of $^{12}C^{16}O_2$ between 3090 and 3850 cm^{-1}; and Benner [50] for the data on the five interacting bands around 3400 cm^{-1}. We also used the calculation, *CDSD*-296 [41], in order to replace the line intensities that arose from an early calculation by Rothman and Benedict [47]. In essence, the line intensities for four bands of $^{12}C^{16}O_2$ and 15 bands of $^{12}C^{16}O^{17}O$ have thus been updated. A summary of the bands for which the line intensities have been updated is presented in Table 9. It should be noted that the 23301-02201 band centered at 3554.964 cm^{-1}, which was not present in the 2000 *HITRAN* edition [1], has been added from the work of Benner [50].

The previous edition of *HITRAN* [1] had no CO_2 line parameters at wavenumbers above 9650 cm^{-1}. However, in the present edition we have added parameters for the 10041-00001, 10051-00001, 10052-00001 and 00051-00001 bands of the $^{12}C^{16}O_2$ isotopologue. The spectral line positions stem from Campargue et al. [61], and the line positions in the 10051-00001 band have been confirmed independently by Lucchesini [62]. Line intensities are drawn from Ref. [63], but, since the data are deemed to be not highly accurate, a code 3 (i.e., uncertainty in the measurement in excess of 20%) has been adopted. These four bands are of particular interest in the studies of the atmosphere of Venus.

Concerning the air- and self-broadened half-widths, and the temperature dependence of the air-broadened widths, the values recommended in Ref. [45] for the *HITRAN* 92 edition have been used for all CO_2 transitions in subsequent editions of the database, including the present one. Air pressure-induced line shifts have been added for the two laser bands of $^{12}C^{16}O_2$ at 9.4 and 10.4 μm, based on the work of Devi et al. [64]. These shifts have also been adopted for the laser bands of the other isotopologues, by assuming that the dependence upon the type of isotopologue is negligible. Values of shifts have been retained from the previous *HITRAN* edition for the bands at 4.3 μm, but otherwise there has been no attempt to give non-zero values of δ_{air} for the majority of carbon dioxide bands at this time.

Table 8
Bands of CO_2 for which the line positions have been updated

Band center (cm^{-1})	Upper vib $v_1v_2l_2v_3r$	Lower vib $v_1v_2l_2v_3r$	v_{min} (cm^{-1})	v_{max} (cm^{-1})	Number of lines	J_{min}	J_{max}	Ref.
$^{12}C^{16}O_2$ isotopologue								
608.8	1 0 0 1 2	0 1 1 1 1	576	644	67	1	47	[44]
618.0	1 0 0 0 2	0 1 1 0 1	546	687	136	1	91	[44]
645.1	2 3 3 0 3	2 2 2 0 3	645	646	15	10	24	[41]
654.9	0 1 1 1 1	0 0 0 1 1	607	708	98	1	67	[44]
655.3	0 2 2 1 1	0 1 1 1 1	621	696	144	1	52	[44]
667.4	0 1 1 0 1	0 0 0 0 1	593	752	153	0	102	[44]
667.8	0 2 2 0 1	0 1 1 0 1	600	750	275	1	94	[44]
688.7	1 1 1 0 1	1 0 0 0 1	625	756	126	0	84	[44]
710.8	1 0 0 1 1	0 1 1 1 1	677	745	67	1	47	[44]
720.8	1 0 0 0 1	0 1 1 0 1	649	791	137	1	92	[44]
741.7	1 1 1 0 1	0 2 2 0 1	675	802	233	2	81	[44]
791.4	1 1 1 0 1	1 0 0 0 2	737	849	109	0	74	[44]
927.2	01 1 1 1	1 1 1 0 1	868	964	138	1	60	[44]
961.0	0 0 0 1 1	1 0 0 0 1	886	1002	75	0	74	[44]
1063.7	0 0 0 1 1	1 0 0 0 2	986	1105	77	0	76	[44]
2076.9	1 1 1 0 1	0 0 0 0 1	2010	2145	127	0	88	[44]
2224.7	1 0 0 1 2	1 0 0 0 1	2158	2264	68	0	68	[44]
2274.4	0 6 6 1 1	0 6 6 0 1	2244	2299	62	6	34	[41]
2275.8	1 4 4 1 1	1 4 4 0 1	2251	2297	42	4	28	[41]
2277.2	2 2 2 1 1	2 2 2 0 1	2259	2294	23	10	22	[41]
2278.4	1 4 4 1 2	1 4 4 0 2	2243	2306	77	4	39	[41]
2280.6	2 2 2 1 2	2 2 2 0 2	2250	2305	61	4	34	[41]
2281.7	2 2 2 1 3	2 2 2 0 3	2243	2310	85	2	42	[41]
2286.8	0 5 5 1 1	0 5 5 0 1	2234	2322	133	5	56	[41]
2311.7	0 1 1 2 1	0 1 1 1 1	2246	2350	162	1	67	[44]
2324.1	0 2 2 1 1	0 2 2 0 1	2227	2371	250	2	92	[44]
2324.2	0 0 0 2 1	0 0 0 1 1	2244	2366	80	1	79	[44]
2326.6	1 0 0 1 1	1 0 0 0 1	2231	2372	91	0	90	[44]
2327.4	1 0 0 1 2	1 0 0 0 2	2231	2374	93	0	92	[44]
2336.6	0 1 1 1 1	0 1 1 0 1	2227	2384	278	1	101	[44]
2349.1	0 0 0 1 1	0 0 0 0 1	2230	2397	109	0	108	[44]
2429.4	1 0 0 1 1	1 0 0 0 2	2364	2467	66	0	66	[44]
3365.3	3 1 1 0 2	1 0 0 0 1	3331	3403	33	8	48	[41]
3398.2	2 1 1 1 3	1 1 1 0 1	3374	3420	46	6	28	[50]
3465.4	2 0 0 1 3	1 0 0 0 1	3410	3505	61	0	60	[44]
3496.1	2 3 3 1 3	1 3 3 0 2	3464	3522	68	3	36	[41]
3505.0	1 4 4 1 2	0 4 4 0 1	3461	3537	108	4	48	[41]
3506.7	3 1 1 1 4	2 1 1 0 3	3473	3534	73	2	38	[41]
3518.7	2 2 21 3	1 2 2 0 2	3468	3554	124	2	54	[41]
3527.8	2 2 2 1 2	1 2 2 0 1	3484	3559	100	2	47	[41]
3542.6	2 1 1 1 3	1 1 1 0 2	3476	3586	171	1	70	[50]
3543.1	4 0 0 0 2	1 1 1 0 2	3502	3592	82	1	63	[50]
3552.9	1 2 2 1 2	0 2 2 0 1	3476	3598	203	2	78	[50]
3555.0	2 3 3 0 1	0 2 2 0 1	3504	3611	188	2	68	[50]
3555.9	2 1 1 1 2	1 1 1 0 1	3492	3593	152	1	64	[44]

Table 8 (*continued*)

Band center (cm^{-1})	Upper vib $v_1v_2l_2v_3r$	Lower vib $v_1v_2l_2v_3r$	ν_{min} (cm^{-1})	ν_{max} (cm^{-1})	Number of lines	J_{min}	J_{max}	Ref.
3568.2	2 0 0 1 3	1 0 0 0 2	3490	3615	81	0	80	[44]
3589.7	2 0 0 1 2	1 0 0 0 1	3506	3628	79	0	78	[44]
3612.8	1 0 0 1 2	0 0 0 0 1	3509	3661	99	0	98	[44]
3659.3	0 2 2 1 1	0 0 0 0 1	3582	3715	82	4	86	[44]
3692.4	2 0 0 1 2	1 0 0 0 2	3606	3731	81	0	80	[44]
3703.2	3 1 1 1 1	2 1 1 0 1	3680	3723	43	6	27	[41]
3703.5	2 2 2 1 2	1 2 2 0 2	3651	3736	124	2	54	[41]
3704.1	2 3 3 1 2	1 3 3 0 2	3675	3727	56	3	32	[41]
3711.5	2 0 0 1 1	1 0 0 0 1	3635	3757	79	0	78	[44]
3712.4	2 3 3 1 1	1 3 3 0 1	3689	3733	42	7	28	[41]
3713.7	2 1 1 1 1	1 1 1 0 1	3648	3755	166	1	68	[44]
3713.8	2 2 2 1 1	1 2 2 0 1	3665	3747	118	2	52	[41]
3714.8	1 0 0 1 1	0 0 0 0 1	3610	3763	99	0	98	[44]
3724.1	1 5 5 1 1	0 5 5 0 1	3702	3743	33	5	25	[41]
3726.4	1 4 4 1 1	0 4 4 0 1	3678	3759	119	4	51	[41]
3814.3	2 0 0 1 1	1 0 0 0 2	3753	3854	65	0	64	[44]
3980.6	0 1 1 2 1	0 2 2 0 1	3975	4003	59	8	47	[44]
4005.9	0 0 0 2 1	0 1 1 0 1	3934	4029	78	2	63	[44]
4416.1	3 1 1 0 4	0 0 0 0 1	4426	4452	16	12	42	[41]
4687.8	3 00 1 4	1 0 0 0 1	4652	4719	42	2	42	[44]
4722.6	3 2 2 1 4	1 2 2 0 2	4705	4740	23	10	22	[41]
4733.5	2 3 3 1 3	0 3 3 0 1	4696	4763	87	3	42	[41]
4735.6	4 0 0 1 5	2 0 0 0 3	4712	4757	24	6	28	[41]
4753.5	3 1 1 0 2	0 0 0 0 1	4706	4800	72	2	60	[41]
4755.7	3 1 1 1 4	1 1 1 0 2	4712	4792	102	1	50	[41]
4768.6	2 2 2 1 3	0 2 2 0 1	4711	4807	144	2	60	[44]
4784.7	2 0 0 2 3	0 0 0 1 1	4762	4805	21	7	27	[41]
4786.7	3 1 1 1 3	1 1 1 0 1	4750	4814	78	2	41	[44]
4790.6	3 0 0 1 4	1 0 0 0 2	4733	4834	65	0	64	[44]
4807.7	2 1 1 1 3	0 1 1 0 1	4741	4854	91	1	72	[44]
4808.2	4 0 0 0 2	0 1 1 0 1	4758	4857	80	1	55	[41]
4839.7	3 0 0 1 3	1 0 0 0 1	4780	4874	61	0	60	[44]
4853.6	2 0 0 1 3	0 0 0 0 1	4772	4903	85	0	84	[44]
4910.6	2 0 0 2 2	0 0 0 1 1	4872	4937	41	1	41	[41]
4912.2	4 0 0 1 4	2 0 0 0 3	4879	4936	35	2	36	[41]
4920.2	3 2 2 1 3	1 2 2 0 2	4893	4942	49	6	30	[41]
4922.6	4 0 0 1 3	2 0 0 0 2	4889	4946	35	2	36	[41]
4937.3	4 0 0 1 2	2 0 0 0 1	4922	4953	8	12	20	[41]
4941.5	2 3 3 1 2	0 3 3 0 1	4897	4972	103	3	47	[41]
4942.5	3 0 0 1 3	1 0 0 0 2	4872	4978	69	0	68	[44]
4946.8	3 1 1 1 2	1 1 1 0 1	4900	4979	102	1	50	[44]
4953.4	2 2 2 1 2	0 2 2 0 1	4890	4991	158	2	64	[44]
4959.7	3 0 0 1 2	1 0 0 0 1	4892	4996	67	0	66	[44]
4965.4	2 1 1 1 2	0 1 1 0 1	4884	5007	198	1	77	[44]
4977.8	2 0 0 1 2	0 0 0 0 1	4881	5018	89	0	88	[44]
5028.5	2 0 0 21	0 0 0 1 1	5000	5052	31	3	33	[41]
5062.4	3 0 0 1 2	1 0 0 0 2	5002	5096	61	0	60	[44]

Table 8 (*continued*)

Band center (cm^{-1})	Upper vib $v_1v_2l_2v_3r$	Lower vib $v_1v_2l_2v_3r$	v_{min} (cm^{-1})	v_{max} (cm^{-1})	Number of lines	J_{min}	J_{max}	Ref.
5099.7	2 0 0 1 1	0 0 0 0 1	5017	5148	85	0	84	[44]
5114.9	3 0 0 1 1	1 0 0 0 1	5060	5155	61	0	60	[44]
5123.2	2 1 1 1 1	0 1 1 0 1	5050	5167	185	1	73	[44]
5127.0	3 1 1 1 1	1 1 1 0 1	5086	5158	91	1	45	[44]
5139.4	2 2 2 1 1	0 2 2 0 1	5081	5176	145	2	60	[44]
5151.4	2 3 3 1 1	0 3 3 0 1	5112	5181	90	3	43	[41]
5217.7	3 0 0 1 1	1 0 0 0 2	5176	5251	48	0	46	[44]
5315.7	0 1 1 2 1	0 0 0 0 1	5251	5342	93	0	64	[44]
5584.4	0 0 0 3 1	1 0 0 0 1	5541	5601	39	2	40	[44]
5687.2	0 0 0 3 1	1 0 0 0 2	5638	5703	42	2	42	[44]
5972.5	3 2 2 1 4	0 2 2 0 1	5949	5995	46	6	29	[41]
5998.6	4 0 0 1 5	1 0 0 0 2	5967	6028	37	2	38	[41]
6020.8	3 1 1 1 4	0 1 1 0 1	5975	6059	108	1	52	[44]
6076.0	3 0 0 1 4	0 0 0 0 1	6019	6121	66	0	66	[44]
6149.4	4 1 1 1 4	1 1 1 0 2	6160	6164	5	14	18	[41]
6170.1	3 2 2 1 3	0 2 2 0 1	6132	6198	82	2	41	[44]
6175.1	4 0 0 1 4	1 0 0 0 2	6130	6207	50	0	50	[44]
6196.2	3 1 1 1 3	0 1 1 0 1	6137	6233	136	1	60	[44]
6205.5	4 0 0 1 3	1 0 0 0 1	6160	6232	47	0	46	[44]
6227.9	3 0 0 1 3	0 0 0 0 1	6150	6266	75	0	74	[44]
6308.3	4 0 0 1 3	1 0 0 0 2	6260	6335	49	0	48	[44]
6346.3	4 0 0 1 2	1 0 0 0 1	6303	6376	47	0	46	[44]
6347.9	3 0 0 1 2	0 0 0 0 1	6271	6385	73	0	74	[44]
6356.3	3 1 1 1 2	0 1 1 0 1	6297	6392	134	1	59	[44]
6359.3	3 2 2 1 2	0 22 0 1	6322	6386	80	2	40	[41]
6387.9	4 1 1 0 1	0 0 0 0 1	6348	6430	45	8	52	[41]
6503.1	3 0 0 1 1	0 0 0 0 1	6447	6545	63	0	62	[44]
6532.7	4 0 0 1 1	1 0 0 0 1	6506	6557	29	4	32	[41]
6536.4	3 1 1 1 1	0 1 1 0 1	6489	6572	107	1	51	[44]
6562.4	3 2 2 1 1	0 2 2 0 1	6547	6577	15	11	19	[41]
6870.8	1 1 1 3 2	1 1 1 0 2	6848	6885	30	9	24	[41]
6905.8	1 0 0 3 1	1 0 0 0 1	6850	6922	47	0	46	[44]
6907.1	1 0 0 3 2	1 0 0 0 2	6846	6924	51	0	50	[44]
6935.1	0 1 1 3 1	0 1 1 0 1	6846	6952	156	1	65	[44]
6972.6	0 0 0 3 1	0 0 0 0 1	6856	6989	79	0	78	[44]
7284.0	4 0 0 1 5	0 0 0 0 1	7253	7314	37	2	38	[41]
7414.5	4 1 1 1 4	0 1 1 0 1	7386	7438	57	4	32	[41]
7460.5	4 0 0 1 4	0 0 0 0 1	7411	7494	54	0	54	[44]
7583.3	4 1 1 1 3	0 1 1 0 1	7550	7608	70	2	37	[41]
7593.7	4 0 0 1 3	0 0 0 0 1	7535	7623	57	0	56	[44]
7734.4	4 0 0 1 2	0 0 0 0 1	7687	7766	51	0	50	[44]
7757.6	4 1 1 1 2	0 1 1 0 1	7741	7773	18	11	21	[44]
7920.8	4 0 0 1 1	0 0 0 0 1	7897	7944	25	6	30	[41]
8103.6	2 0 0 3 3	1 0 0 0 2	8080	8119	18	8	26	[41]
8135.9	1 1 1 3 2	0 1 1 0 1	8079	8154	98	1	48	[41]
8192.6	1 0 0 3 2	0 0 0 0 1	8099	8210	70	0	70	[44]
8231.6	2 0 0 3 2	1 0 0 0 2	8207	8246	18	8	26	[49]

Table 8 (*continued*)

Band center (cm^{-1})	Upper vib $v_1v_2l_2v_3r$	Lower vib $v_1v_2l_2v_3r$	ν_{min} (cm^{-1})	ν_{max} (cm^{-1})	Number of lines	J_{min}	J_{max}	Ref.
8243.2	2 0 0 3 1	1 0 0 0 1	8224	8256	11	10	20	[49]
8276.8	1 1 1 3 1	0 1 1 0 1	8216	8293	101	1	49	[41]
8294.0	1 0 0 3 1	0 0 0 0 1	8206	8310	65	0	64	[44]
9517.0	2 0 0 3 2	0 0 0 01	9454	9533	51	0	50	[49]
9631.4	2 0 0 3 1	0 0 0 0 1	9583	9649	42	2	42	[49]
$^{13}C^{16}O_2$ isotopologue								
573.7	1 3 3 0 2	0 4 4 0 1	573	574	25	7	31	[41]
595.7	2 1 1 0 3	1 2 2 0 2	579	597	40	5	31	[41]
619.8	2 1 1 0 3	2 0 0 0 3	591	650	57	2	42	[41]
637.8	1 3 3 0 2	1 2 2 0 2	613	669	100	2	41	[41]
649.7	0 5 5 0 1	0 4 4 0 1	625	682	92	4	41	[41]
2225.0	0 5 5 1 1	0 5 5 0 1	2206	2243	24	5	23	[41]
2227.8	1 3 3 1 2	1 3 3 0 2	2202	2249	44	7	29	[41]
2229.7	2 1 1 1 3	2 1 1 0 3	2202	2253	56	4	32	[41]
$^{16}O^{12}C^{18}O$ isotopologue								
561.1	1 2 2 0 2	0 3 3 0 1	547	562	68	7	29	[41]
647.7	1 2 2 0 2	1 1 1 0 2	617	685	266	1	49	[41]
2287.1	1 2 2 1 2	1 2 2 0 2	2251	2315	170	2	43	[41]
2295.0	0 3 3 1 1	0 3 3 0 1	2241	2330	284	3	59	[41]
$^{16}O^{12}C^{17}O$ isotopologue								
586.9	1 1 1 0 2	0 2 2 0 1	548	626	294	2	53	[41]
650.0	1 2 2 0 2	1 1 1 0 2	620	685	244	1	46	[41]
665.1	0 2 2 0 1	0 1 1 0 1	614	726	427	1	74	[41]
665.5	0 3 3 0 1	0 2 2 0 1	623	715	348	2	62	[41]
681.4	1 2 2 0 1	1 1 1 0 1	656	712	208	1	41	[41]
732.3	1 1 1 0 1	0 2 2 0 1	691	771	302	2	54	[41]
748.1	1 2 2 0 1	0 3 3 0 1	733	749	72	7	29	[41]
964.0	0 0 0 1 1	1 0 0 0 1	925	991	85	1	43	[51]
1067.7	00 0 1 1	1 0 0 0 2	1024	1098	97	0	48	[51]
2306.7	1 1 1 1 2	1 1 1 0 2	2253	2342	258	1	58	[41]
2315.1	0 2 2 1 1	0 2 2 0 1	2246	2355	362	2	71	[41]
2317.3	1 0 0 1 1	1 0 0 0 1	2249	2356	141	0	70	[41]
2319.0	1 0 0 1 2	1 0 0 0 2	2249	2359	145	0	72	[41]
2327.6	0 1 1 1 1	0 1 1 0 1	2248	2370	416	1	80	[41]

Note: Upper vib and Lower vib use the AFGL vibrational notation for carbon dioxide [5]. The sixth column indicates the number of lines that have been replaced in *HITRAN*.

It is to be noted that a recent work on line positions of the $^{16}O^{13}C^{16}O$ and $^{16}O^{13}C^{18}O$ isotopologues in the near-infrared from Miller et al. [65] will be taken into account in the next *HITRAN* edition.

Carbon dioxide is the first molecule for which line-coupling data are introduced into the *HITRAN* database. These data have been researched by Hartmann and are based on Refs. [66,67]. They can be found on the *HITRAN* ftp-site (see Fig. 1). A detailed "readme" file gives recommendations on how to implement the line coupling in the line-by-line codes of users. The package of subroutines and input file allows one to take into account line coupling for 306 Q branches of CO_2 isotopologues between 469 and 6935 cm^{-1}. Table 10 summarizes the Q branches of CO_2 for which line-coupling data have been supplied with the *HITRAN* compilation.

3.3. O_3 (molecule 3)

We have implemented a major improvement on the entire list of lines of ozone.

In the pure-rotation region, the positions, the intensities, and the lower energy levels of all of the transitions of the two isotopologues $^{16}O^{16}O^{17}O$ and $^{16}O^{17}O^{16}O$ have been updated by drawing upon the JPL catalog [15]. The significant difference between this and the previous *HITRAN* edition is in resolution of the hyperfine structure of these two isotopologues. It should be noted that the JPL catalog contains measured as well as calculated line positions. As a rule, when several lines of different hyperfine components are reported with the same wavenumber, thereby implying that they could not be resolved, such an unresolved observed feature is designated as a blend of those components in the database.

Using the *MIPAS* (*M*ichelson *I*nterferometer for *P*assive *A*tmospheric *S*ounding) database [20], the line positions and intensities of forty-nine infrared bands of $^{16}O_3$ and the ν_1 and ν_3 bands of the $^{16}O^{16}O^{18}O$ and $^{16}O^{18}O^{16}O$ isotopologues have been updated. Furthermore, seventeen bands of $^{16}O_3$, a band each of $^{16}O^{16}O^{18}O$ and $^{16}O^{18}O^{16}O$, and three bands of $^{16}O^{16}O^{17}O$ and $^{16}O^{17}O^{16}O$ have been introduced. In Table 11 is presented a summary of all the ozone bands that have been added or updated.

Wagner et al. [68] have enabled us to improve the data on the line positions and intensities in the ν_2 fundamental and the "hot bands,"[4] $2\nu_2-\nu_2$, $\nu_1+\nu_2-\nu_2$, and $\nu_2+\nu_3-\nu_2$ bands of the main isotopologue in the 14-μm region. Additionally, six other bands in the 1613–1903 cm^{-1} spectral region (previously unlisted in *HITRAN*), three "hot" bands in the 1872–2288 cm^{-1} region, and three cold bands in the 2590–3006 cm^{-1} region for $^{16}O_3$ have been incorporated into *HITRAN*. These latter 12 bands come from the work of Ref. [69].

Except for the intensities of the bands discussed above, the intensities of all of the other bands (including those of the species with their isotopic variants) have been divided by 1.04 in order to account for the change in the absolute intensities of the two fundamental bands, ν_1 and ν_3, upon which the other data were based [70].

We used the polynomial expressions given in Ref. [68] for the air-broadened half-widths in order to update the previously "scaled calculation" [45]. In apparent contrast to the previous calculation, the data of Ref. [68], as well as the air-broadened width measurements of [71,72], show neither a strong K_a dependence nor a large difference between the $J-K_a-K_c$ sub-bands.

[4] A "hot" band, by its conventional definition, is a vibrational–rotational transition that occurs with the same change in the vibrational quanta as that representing a transition from the ground vibrational level of the molecule, but it implies a transition that takes places from an excited ("hot") vibrational level of energy.

Table 9
Bands of CO_2 for which the line intensities have been updated

Band center (cm^{-1})	Upper vib $v_1v_2l_2v_3r$	Lower vib $v_1v_2l_2v_3r$	v_{min} (cm^{-1})	v_{max} (cm^{-1})	Number of lines	Sum of line intensities	Ref.
$^{12}C^{16}O_2$ isotopologue							
2224.7	1 0 0 1 2	1 0 0 0 1	2158	2264	68	1.12E-22	[52]
3181.5	2 1 1 0 3	0 0 0 0 1	3131	3239	78	1.19E-23	[60]
3275.2	3 0 0 0 3	0 1 1 0 1	3232	3317	65	1.91E-24	[60]
3305.7	3 1 1 0 3	1 0 0 0 2	3270	3344	36	4.42E-25	[60]
3339.4	2 1 1 0 2	0 0 0 0 1	3279	3398	105	1.02E-22	[60]
3340.5	2 2 2 0 2	0 1 1 0 1	3294	3394	145	8.19E-24	[60]
3341.7	2 3 3 0 2	0 2 2 0 1	3311	3379	55	4.04E-25	[60]
3365.3	3 1 1 0 2	1 0 0 0 1	3331	3403	33	3.27E-25	[60]
3396.9	3 0 0 0 2	0 1 1 0 1	3349	3441	52	1.92E-24	[60]
3398.2	2 1 1 1 3	1 1 1 0 1	3374	3420	46	2.52E-25	[50]
3465.4	2 0 0 1 3	1 0 0 0 1	3410	3505	61	1.49E-23	[60]
3496.1	2 3 3 1 3	1 3 3 0 2	3464	3522	68	6.37E-25	[60]
3500.7	2 1 1 0 1	0 0 0 0 1	3445	3561	100	6.18E-23	[60]
3505.0	14 4 1 2	0 4 4 0 1	3461	3537	108	3.67E-24	[60]
3518.7	2 2 2 1 3	1 2 2 0 2	3468	3554	124	1.14E-23	[60]
3527.6	3 0 0 1 4	2 0 0 0 3	3476	3565	57	8.61E-24	[60]
3528.1	1 3 3 1 2	0 3 3 0 1	3467	3568	162	1.01E-22	[60]
3530.0	2 2 2 0 1	0 1 1 0 1	3488	3580	131	4.15E-24	[60]
3542.6	2 1 1 1 3	1 1 1 0 2	3476	3586	171	2.81E-22	[50]
3543.1	4 0 0 0 2	1 1 1 0 2	3502	3592	82	1.09E-23	[50]
3552.9	1 2 2 1 2	0 2 2 0 1	3476	3598	203	2.80E-21	[50]
3555.0	2 3 3 0 1	0 2 2 0 1	3504	3611	188	2.78E-23	[50]
3555.9	2 1 1 1 2	1 1 1 0 1	3492	3593	152	9.39E-23	[60]
3556.8	3 0 0 1 3	2 0 0 0 2	3506	3591	55	5.69E-24	[60]
3566.1	1 0 0 2 2	0 0 0 1 1	3509	3604	62	2.05E-23	[60]
3568.2	2 0 0 1 3	1 0 0 0 2	3490	3615	81	3.09E-21	[60]
3589.7	2 0 0 1 2	1 0 0 0 1	3506	3628	79	1.60E-21	[60]
3659.3	0 2 2 1 1	0 0 0 0 1	3582	3715	82	1.93E-22	[50]
3667.5	1 0 0 2 1	0 0 0 1 1	3606	3704	64	3.47E-23	[60]
3676.7	3 0 0 1 2	2 0 0 0 2	3626	3711	55	7.09E-24	[60]
3679.6	3 0 0 1 3	2 0 0 0 3	3622	3710	57	8.07E-24	[60]
3692.4	2 0 0 1 2	1 0 0 0 2	3606	3731	81	3.64E-21	[60]
3700.3	2 1 1 1 2	1 1 1 0 2	3629	3738	170	2.87E-22	[60]
3711.5	2 0 0 1 1	1 0 0 0 1	3635	3757	79	2.93E-21	[60]
3713.7	2 1 1 1 1	1 1 1 0 1	3648	3755	166	2.22E-22	[60]
3726.6	1 2 2 1 1	0 2 2 0 1	3646	3770	208	4.68E-21	[60]
3727.4	1 3 3 1 1	0 3 3 0 1	3662	3766	168	1.76E-22	[60]
3799.5	3 0 0 1 2	2 0 0 0 3	3774	3819	24	1.35E-25	[60]
3814.3	2 0 0 1 1	1 0 0 0 2	3753	3854	65	5.90E-23	[60]
3858.1	2 1 1 1 1	1 1 1 0 2	3818	3888	87	1.84E-24	[60]
4808.2	4 0 0 0 2	0 1 1 0 1	4758	4857	80	2.44E-23	[41]
5061.8	1 2 2 1 1	0 0 0 0 1	4992	5112	69	4.47E-24	[41]
5217.7	3 0 0 1 1	1 0 0 0 2	5176	5251	48	2.13E-24	[59]
5247.8	1 0 0 2 2	0 1 1 0 1	5217	5271	61	1.37E-24	[59]
5291.1	0 2 2 2 1	0 1 1 0 1	5248	5316	130	3.52E-24	[59]

Table 9 (*continued*)

Band center (cm^{-1})	Upper vib $v_1v_2l_2v_3r$	Lower vib $v_1v_2l_2v_3r$	v_{min} (cm^{-1})	v_{max} (cm^{-1})	Number of lines	Sum of line intensities	Ref.
5315.7	0 1 1 2 1	0 0 0 0 1	5251	5342	93	4.72E-23	[59]
5349.3	1 0 0 2 1	0 1 1 0 1	5301	5357	43	5.77E-25	[59]
5584.4	0 0 0 3 1	1 0 0 0 1	5541	5601	39	5.58E-25	[58]
5687.2	0 0 0 3 1	1 0 0 0 2	5641	5703	40	6.31E-25	[58]
6347.9	3 0 0 1 2	0 0 0 0 1	6271	6385	73	4.42E-22	[56]
6387.9	4 1 1 0 1	0 0 0 0 1	6348	6430	45	2.45E-25	[41]
8192.6	1 0 0 3 2	0 0 0 0 1	8099	8210	70	4.15E-23	[54]
8294.0	1 0 0 3 1	0 0 0 0 1	8194	8310	71	6.18E-23	[54]
$^{16}O^{12}C^{18}O$ isotopologue							
966.3	0 0 0 1 1	1 0 0 0 1	918	997	108	2.01E-24	[51]
1072.7	0 0 0 1 1	1 0 0 0 2	1020	1107	118	5.19E-24	[51]
4639.5	0 0 0 2 1	0 0 0 0 1	4579	4663	115	1.44E-23	[57]
$^{16}O^{12}C^{17}O$ isotopologue							
586.9	1 1 1 0 2	0 2 2 0 1	548	626	294	4.23E-24	[41]
607.6	2 0 0 0 3	1 1 1 0 2	578	640	123	5.41E-25	[41]
607.6	1 0 0 0 2	0 1 1 0 1	554	659	208	1.05E-22	[53]
644.4	1 1 1 0 2	1 0 0 0 2	601	693	183	1.74E-23	[41]
650.0	1 2 2 0 2	1 1 1 0 2	620	685	244	1.27E-24	[41]
665.1	02 2 0 1	0 1 1 0 1	614	726	427	9.55E-22	[41]
681.4	1 2 2 0 1	1 1 1 0 1	656	712	208	6.17E-25	[41]
686.1	1 1 1 0 1	1 0 0 0 1	643	732	178	1.12E-23	[41]
711.3	1 0 0 0 1	0 1 1 0 1	659	765	210	1.30E-22	[53]
713.5	2 0 0 0 1	1 1 1 0 1	688	742	105	3.07E-25	[41]
724.5	2 0 0 0 2	1 1 1 0 2	700	749	89	1.90E-25	[41]
732.3	1 1 1 0 1	0 2 2 0 1	691	771	302	4.94E-24	[41]
748.1	1 2 2 0 1	0 3 3 0 1	733	749	72	9.72E-26	[41]
789.8	1 1 1 0 1	1 0 0 0 2	762	821	114	4.08E-25	[41]
964.0	0 0 0 1 1	1 0 0 0 1	925	991	85	4.00E-25	[51]
1067.7	0 0 0 1 1	1 0 0 0 2	1024	1098	97	8.34E-25	[51]
2306.7	1 1 1 1 2	1 1 1 0 2	2253	2342	258	1.17E-23	[41]
2315.1	0 2 2 1 1	0 2 2 0 1	2246	2355	362	2.03E-22	[41]
2317.3	1 0 0 1 1	1 0 0 0 1	2249	2356	141	8.20E-23	[41]
2319.0	1 0 0 1 2	1 0 0 0 2	2249	2359	145	1.36E-22	[41]
2327.6	0 1 1 1 1	0 1 1 0 1	2244	2370	434	5.20E-21	[41]
$^{16}O^{13}C^{17}O$ isotopologue							
2274.1	0 0 0 1 1	0 0 0 0 1	2198	2316	157	7.33E-22	[60]

Note: Upper vib and Lower vib use the AFGL vibrational notation for carbon dioxide [5]. The sixth column indicates the number of lines that have been replaced in *HITRAN*. Units of the seventh column are $cm^{-1}/(molecule \times cm^{-2})$.

Table 10
Summary of CO_2 bands for which line-coupling data for the Q branches are available in the 2004 *HITRAN* edition

Upper vib $v_1v_2l_2v_3r$	Lower vib $v_1v_2l_2v_3r$	ν_{min} (cm^{-1})	ν_{max} (cm^{-1})	Number of lines
$^{12}C^{16}O_2$ isotopologue				
2 0 0 0 3	1 1 1 0 1	469.0	471.5	70
1 3 3 0 2	1 2 2 0 1	479.9	485.3	70
1 2 2 0 2	1 1 1 0 1	508.2	514.9	70
2 1 1 0 3	2 0 0 0 2	510.3	523.1	70
2 1 1 0 2	2 0 0 0 1	542.2	544.0	70
1 1 1 0 2	1 0 0 0 1	544.3	551.3	74
1 4 4 0 2	0 5 5 0 1	555.5	557.8	70
1 3 3 0 2	0 4 4 0 1	566.6	568.9	70
2 1 1 0 2	1 2 2 0 1	571.1	578.6	70
1 2 2 0 2	0 3 3 0 1	579.4	581.8	70
2 2 2 0 3	1 3 3 0 2	579.5	581.4	70
2 2 2 0 3	1 3 3 0 2	579.5	581.4	70
2 0 0 0 2	1 1 1 0 1	585.2	594.3	70
1 1 1 0 2	0 2 2 0 1	591.1	597.3	79
2 1 1 0 3	1 2 2 0 2	591.8	597.7	70
3 0 0 0 3	2 1 1 0 2	594.6	603.2	70
1 0 0 1 2	2 0 0 0 1	605.0	608.8	70
3 0 0 0 4	2 1 1 0 3	607.5	611.2	70
1 0 0 0 2	0 1 1 0 1	610.4	618.0	90
2 0 0 0 3	1 1 1 0 2	612.0	615.9	74
2 1 1 0 3	2 0 0 0 3	633.1	639.4	70
1 1 1 1 2	1 0 0 1 2	634.9	640.7	70
2 2 2 0 3	2 1 1 0 3	640.5	646.8	70
2 3 3 0 3	2 2 2 0 3	645.1	648.6	70
1 1 1 0 2	1 0 0 0 2	647.1	655.7	84
1 2 2 0 2	1 1 1 0 2	652.6	659.3	75
0 1 1 1 1	0 0 0 1 1	654.9	659.9	70
0 2 2 1 1	0 1 1 1 1	655.3	660.4	70
1 3 3 0 2	1 2 2 0 2	655.6	659.1	70
0 3 3 1 1	0 2 2 1 1	655.7	659.3	70
1 4 4 0 2	1 3 3 0 2	657.7	661.1	70
1 5 5 0 2	1 4 4 0 2	659.3	662.7	70
0 1 1 0 1	0 0 0 0 1	667.4	678.0	102
0 2 2 0 1	0 1 1 0 1	667.8	676.5	94
0 3 3 0 1	0 2 2 0 1	668.1	673.4	86
2 1 1 0 2	2 0 0 0 2	668.2	676.1	70
0 4 4 0 1	0 3 3 0 1	668.5	672.5	76
2 2 2 0 2	2 1 1 0 2	668.6	675.2	70
0 5 5 0 1	0 4 4 0 1	668.8	672.2	70
0 6 6 0 1	0 5 5 0 1	669.2	672.5	70
1 1 1 1 1	1 0 0 1 1	675.8	681.4	70
1 4 4 0 1	1 3 3 0 1	680.1	683.3	70
1 3 3 0 1	1 2 2 0 1	681.5	685.0	70
1 2 2 0 1	1 1 1 0 1	683.9	689.9	73
1 1 1 0 1	1 0 0 0 1	688.7	696.5	84
2 2 2 0 1	2 1 1 0 1	694.7	702.5	70
2 1 1 0 1	2 0 0 0 1	703.5	708.7	70

Table 10 (*continued*)

Upper vib $v_1v_2l_2v_3r$	Lower vib $v_1v_2l_2v_3r$	ν_{min} (cm^{-1})	ν_{max} (cm^{-1})	Number of lines
1 0 0 1 1	0 1 1 1 1	705.8	710.8	70
1 0 0 0 1	0 1 1 0 1	713.3	720.8	92
2 0 0 0 1	1 1 1 0 1	717.2	720.3	72
3 0 0 0 2	2 1 1 0 2	718.0	724.9	70
3 0 0 0 1	2 1 1 0 1	721.8	724.4	70
2 0 0 0 2	1 1 1 0 2	728.1	738.7	72
1 1 1 0 1	0 2 2 0 1	733.9	741.7	81
2 1 1 0 1	1 2 2 0 1	734.6	741.7	70
2 1 1 0 2	1 2 2 0 2	745.5	754.3	70
3 0 0 0 3	2 1 1 0 3	747.5	761.1	70
2 2 2 0 1	1 3 3 0 1	751.4	755.1	70
1 2 2 0 1	0 3 3 0 1	753.2	757.5	70
2 2 2 0 2	1 3 3 0 2	761.3	767.3	70
1 3 3 0 1	0 4 4 0 1	766.3	770.5	70
1 4 4 0 1	0 5 5 0 1	777.4	781.7	70
2 1 1 0 2	2 0 0 0 3	791.0	792.3	70
1 1 1 0 1	1 0 0 0 2	791.5	797.3	74
1 2 2 0 1	1 1 1 0 2	827.8	832.6	70
2 1 1 0 1	2 0 0 0 2	829.5	840.8	70
1 3 3 0 1	1 2 2 0 2	857.2	858.9	70
2 0 0 0 1	1 1 1 0 2	860.8	864.7	70
0 1 1 1 1	1 1 1 0 1	908.2	927.2	70
2 1 1 0 1	1 2 2 0 2	909.0	915.6	70
0 1 1 1 1	1 1 1 0 2	1051.7	1071.5	70
2 0 0 0 3	0 1 1 0 1	1879.2	1881.0	70
2 1 1 0 3	1 0 0 0 2	1896.1	1904.9	70
1 3 3 0 2	0 2 2 0 1	1905.5	1910.1	70
1 2 2 0 2	0 1 1 0 1	1917.6	1923.5	70
1 1 1 0 2	0 0 0 0 1	1932.5	1939.9	74
2 1 1 0 2	1 0 0 0 1	1951.2	1955.5	70
2 0 0 0 2	0 1 1 0 1	1995.4	2003.8	70
2 1 1 0 2	1 0 0 0 2	2054.0	2057.8	70
2 2 2 0 2	1 1 1 0 2	2074.4	2079.0	70
1 1 1 0 1	0 0 0 0 1	2076.9	2084.6	80
1 2 2 0 1	0 1 1 0 1	2093.3	2097.9	70
1 3 3 0 1	0 2 2 0 1	2107.1	2109.9	70
2 1 1 0 1	1 0 0 0 1	2112.5	2120.2	70
1 4 4 0 1	0 3 3 0 1	2119.0	2121.5	70
2 2 2 0 1	1 1 1 0 1	2120.5	2126.4	70
3 0 0 0 2	1 1 1 0 2	2122.8	2131.8	70
2 0 0 0 1	0 1 1 0 1	2127.5	2129.8	70
3 0 0 0 1	1 1 1 0 1	2147.6	2148.2	70
2 1 1 0 1	0 2 2 0 1	2159.9	2166.5	70
2 2 2 0 1	0 3 3 0 1	2189.6	2194.1	70
2 1 1 0 1	1 0 0 0 2	2215.3	2222.6	70
0 5 5 1 1	0 5 5 0 1	2272.3	2286.7	70
2 1 1 1 3	2 1 1 0 3	2273.1	2293.6	70
2 1 1 1 2	2 1 1 0 2	2273.2	2293.4	70

Table 10 (*continued*)

Upper vib $v_1v_2l_2v_3r$	Lower vib $v_1v_2l_2v_3r$	ν_{min} (cm^{-1})	ν_{max} (cm^{-1})	Number of lines
1 3 3 1 1	1 3 3 0 1	2273.7	2288.4	70
1 3 3 1 2	1 3 3 0 2	2276.1	2290.6	70
0 2 2 2 1	0 2 2 1 1	2284.3	2299.2	70
0 4 4 1 1	0 4 4 0 1	2284.5	2299.2	70
1 2 2 1 1	1 2 2 0 1	2286.2	2301.0	70
1 2 2 1 2	1 2 2 0 2	2288.1	2302.9	70
1 1 1 1 1	1 1 1 0 1	2294.0	2313.8	70
0 1 1 2 1	0 1 1 1 1	2294.1	2311.7	70
1 1 1 1 2	1 1 1 0 2	2296.0	2315.2	70
0 3 3 1 1	0 3 3 0 1	2296.8	2311.6	70
0 2 2 1 1	0 2 2 0 1	2309.1	2324.1	70
0 1 1 1 1	0 1 1 0 1	2315.2	2336.6	77
2 1 1 0 3	0 0 0 0 1	3181.5	3191.0	70
3 0 0 0 3	0 1 1 0 1	3266.1	3275.2	70
2 1 1 0 2	0 0 0 0 1	3339.4	3344.0	70
2 2 2 0 2	0 1 1 0 1	3340.5	3344.3	70
3 0 0 0 2	0 1 1 0 1	3389.5	3396.9	70
1 4 4 1 2	0 4 4 0 1	3491.7	3504.9	70
2 1 1 0 1	0 0 0 0 1	3500.7	3508.7	70
2 2 2 1 3	1 2 2 0 2	3503.4	3518.6	70
1 3 3 1 2	0 3 3 0 1	3514.6	3528.0	70
2 2 2 0 1	0 1 1 0 1	3530.0	3535.0	70
2 1 1 1 2	1 1 1 0 1	3534.1	3555.9	70
1 2 2 1 2	0 2 2 0 1	3539.2	3552.8	70
3 0 0 0 1	0 1 1 0 1	3557.4	3558.0	70
1 1 1 1 2	0 1 1 0 1	3562.8	3580.3	70
2 1 1 1 2	1 1 1 0 2	3677.6	3700.3	70
2 2 2 1 2	1 2 2 0 2	3686.3	3703.5	70
2 1 1 1 1	1 1 1 0 1	3694.4	3713.7	70
2 2 2 1 1	1 2 2 0 1	3699.2	3713.8	70
1 1 1 1 1	0 1 1 0 1	3704.2	3723.2	70
1 4 4 1 1	0 4 4 0 1	3710.7	3726.3	70
1 2 2 1 1	0 2 2 0 1	3711.4	3726.6	70
1 3 3 1 1	0 3 3 0 1	3712.0	3727.3	70
0 1 1 2 1	0 2 2 0 1	3946.3	3980.5	70
0 0 0 2 1	0 1 1 0 1	3970.3	4005.9	70
3 1 1 0 3	0 0 0 0 1	4591.1	4601.3	70
3 1 1 0 2	0 0 0 0 1	4753.5	4757.8	70
2 2 2 1 3	0 2 2 0 1	4754.3	4768.5	70
2 3 3 1 2	0 3 3 0 1	4926.1	4941.5	70
2 2 2 1 2	0 2 2 0 1	4937.5	4953.4	70
2 1 1 1 2	0 1 1 0 1	4944.4	4965.4	70
2 1 1 1 1	0 1 1 0 1	5104.7	5123.2	70
2 2 2 1 1	0 2 2 0 1	5124.1	5139.4	70
1 0 0 2 2	0 1 1 0 1	5213.9	5247.8	70
0 2 2 2 1	0 1 1 0 1	5263.1	5291.1	70
0 1 1 2 1	0 0 0 0 1	5290.4	5315.7	70
3 1 1 1 3	0 1 1 0 1	6174.5	6196.2	70

Table 10 (*continued*)

Upper vib $v_1v_2l_2v_3r$	Lower vib $v_1v_2l_2v_3r$	ν_{min} (cm^{-1})	ν_{max} (cm^{-1})	Number of lines
3 1 1 1 2	0 1 1 0 1	6334.3	6356.3	70
1 1 1 2 2	0 0 0 0 1	6515.1	6537.9	70
1 1 1 2 1	0 0 0 0 1	6654.8	6679.7	70
0 2 2 3 1	0 2 2 0 1	6852.7	6897.7	70
0 1 1 3 1	0 1 1 0 1	6886.7	6935.1	70
$^{13}C^{16}O_2$ isotopologue				
1 1 1 0 2	1 0 0 0 1	526.5	537.0	70
1 3 3 0 2	0 4 4 0 1	572.6	573.7	70
12 2 0 2	0 3 3 0 1	584.2	585.3	70
2 1 1 0 3	1 2 2 0 2	591.8	598.3	70
1 1 1 0 2	0 2 2 0 1	595.9	600.7	70
2 0 0 0 2	1 1 1 0 1	601.3	608.0	70
2 0 0 0 3	1 1 1 0 2	608.6	611.0	70
1 0 0 0 2	0 1 1 0 1	614.5	617.3	78
2 1 1 0 3	2 0 0 0 3	619.8	626.1	70
1 1 1 0 2	1 0 0 0 2	630.7	636.2	70
1 2 2 0 2	1 1 1 0 2	635.1	640.6	70
0 1 1 1 1	0 0 0 1 1	636.8	641.6	70
1 3 3 0 2	1 2 2 0 2	637.7	641.0	70
2 1 1 0 2	2 0 0 0 2	644.6	652.1	70
0 1 1 0 1	0 0 0 0 1	648.5	656.5	90
0 2 2 0 1	0 1 1 0 1	648.8	655.3	81
0 3 3 0 1	0 2 2 0 1	649.1	652.3	70
0 4 4 0 1	0 3 3 0 1	649.4	652.6	70
0 5 5 0 1	0 4 4 0 1	649.7	652.9	70
1 3 3 0 1	1 2 2 0 1	661.1	664.5	70
1 2 2 0 1	1 1 1 0 1	663.2	668.6	70
1 1 1 0 1	1 0 0 0 1	667.0	672.9	70
2 1 1 0 1	2 0 0 0 1	683.2	688.9	70
2 0 0 0 1	1 1 1 0 1	708.2	713.5	70
1 0 0 0 1	0 1 1 0 1	713.2	721.6	76
2 1 1 0 1	1 2 2 0 1	726.8	733.5	70
1 1 1 0 1	0 2 2 0 1	732.5	739.8	70
2 0 0 0 2	1 1 1 0 2	737.2	748.5	70
1 3 3 0 1	0 4 4 0 1	760.3	765.7	70
1 1 1 0 1	1 0 0 0 2	771.3	772.1	70
1 2 2 0 1	1 1 1 0 2	800.1	805.3	70
1 1 1 0 2	0 0 0 0 1	1896.5	1904.8	70
2 0 0 0 2	0 1 1 0 1	1988.6	1996.6	70
1 1 1 0 1	0 0 0 0 1	2037.1	2040.7	70
1 2 2 0 1	0 1 1 0 1	2051.5	2054.7	70
2 1 1 0 1	1 0 0 0 1	2063.7	2070.0	70
1 3 3 0 1	0 2 2 0 1	2064.1	2065.4	70
2 0 0 0 1	0 1 1 0 1	2095.5	2102.1	70
2 1 1 0 1	0 2 2 0 1	2127.9	2136.5	70
0 4 4 1 1	0 4 4 0 1	2222.6	2236.6	70
1 2 2 1 2	1 2 2 0 2	2224.5	2239.3	70

Table 10 (*continued*)

Upper vib $v_1v_2l_2v_3r$	Lower vib $v_1v_2l_2v_3r$	ν_{min} (cm^{-1})	ν_{max} (cm^{-1})	Number of lines
1 1 1 1 2	1 1 1 0 2	2231.4	2250.7	70
1 1 1 1 1	1 1 1 0 1	2231.7	2250.6	70
0 3 3 1 1	0 3 3 0 1	2234.0	2248.3	70
0 2 2 1 1	0 2 2 0 1	2245.4	2260.0	70
0 1 1 1 1	0 1 1 0 1	2254.1	2271.8	70
1 2 2 1 2	0 2 2 0 1	3461.5	3473.7	70
1 1 1 1 1	0 1 1 0 1	3619.0	3639.2	70
1 2 2 1 1	0 2 2 0 1	3625.2	3641.5	70
1 3 3 1 1	0 3 3 0 1	3625.6	3641.6	70
2 1 1 1 2	0 1 1 0 1	4850.9	4871.4	70
2 1 1 1 1	0 1 1 0 1	4992.4	5013.8	70
0 1 1 2 1	0 0 0 0 1	5144.2	5168.6	70
$^{16}O^{12}C^{18}O$ isotopologue				
1 1 1 0 2	1 0 0 0 1	535.9	539.0	70
2 0 0 0 2	1 1 1 0 1	556.1	564.9	70
1 2 2 0 2	0 3 3 0 1	558.0	561.1	70
1 1 1 0 2	0 2 2 0 1	571.2	576.6	70
1 0 0 0 2	0 1 1 0 1	591.2	597.0	72
2 0 0 0 3	1 1 1 0 2	594.5	599.0	70
1 1 1 0 2	1 0 0 0 2	642.3	648.2	70
1 2 2 0 2	1 1 1 0 2	647.7	653.3	70
0 1 1 0 1	0 0 0 0 1	662.4	669.8	88
0 2 2 0 1	0 1 1 0 1	662.8	668.3	77
0 3 3 0 1	0 2 2 0 1	663.2	666.5	70
0 4 4 0 1	0 3 3 0 1	663.6	666.9	70
1 2 2 0 1	1 1 1 0 1	678.9	684.0	70
1 1 1 0 1	1 0 0 0 1	683.5	688.3	70
1 0 0 0 1	0 1 1 0 1	700.4	703.5	75
2 0 0 0 2	1 1 1 0 2	705.4	712.5	70
2 0 0 0 1	1 1 1 0 1	706.0	707.8	70
1 1 1 0 1	0 2 2 0 1	719.8	724.4	70
1 2 2 0 1	0 3 3 0 1	736.9	739.9	70
1 1 1 0 1	1 0 0 0 2	789.9	797.5	70
1 1 1 0 2	0 0 0 0 1	1901.7	1906.9	70
1 1 1 0 1	0 0 0 0 1	2049.3	2056.2	70
1 2 2 0 1	0 1 1 0 1	2065.9	2071.2	70
2 0 0 0 1	0 1 1 0 1	2094.7	2095.0	70
1 1 1 1 1	1 1 1 0 1	2277.4	2296.8	70
0 3 3 1 1	0 3 3 0 1	2281.0	2295.0	70
1 1 1 1 2	1 1 1 0 2	2281.7	2299.4	70
0 2 2 1 1	0 2 2 0 1	2293.1	2307.4	70
0 1 1 1 1	0 1 1 0 1	2302.7	2319.7	70
$^{16}O^{12}C^{17}O$ isotopologue				
2 0 0 0 2	1 1 1 0 1	570.0	579.1	70
1 1 1 0 2	0 2 2 0 1	581.6	586.8	70
1 0 0 0 2	0 1 1 0 1	602.5	607.6	70

Table 10 (*continued*)

Upper vib $v_1v_2l_2v_3r$	Lower vib $v_1v_2l_2v_3r$	ν_{min} (cm^{-1})	ν_{max} (cm^{-1})	Number of lines
2 0 0 0 3	1 1 1 0 2	603.2	607.6	70
1 1 1 0 2	1 0 0 0 2	644.4	650.8	70
1 2 2 0 2	1 1 1 0 2	650.0	655.6	70
0 1 1 0 1	0 0 0 0 1	664.7	671.3	81
0 2 2 0 1	0 1 1 0 1	665.1	670.0	70
0 3 3 0 1	0 2 2 0 1	665.5	668.9	70
1 2 2 0 1	1 1 1 0 1	681.4	686.5	70
1 1 1 0 1	1 0 0 0 1	686.1	691.2	70
1 0 0 0 1	0 1 1 0 1	707.6	711.3	70
2 0 0 0 1	1 1 1 0 1	710.2	713.5	70
2 0 0 0 2	1 1 1 0 2	715.6	724.5	70
1 1 1 0 1	0 2 2 0 1	727.1	732.3	70
1 2 2 0 1	0 3 3 0 1	744.5	748.1	70
1 1 1 0 1	1 0 0 0 2	789.8	796.3	70
1 1 1 0 2	0 0 0 0 1	1916.7	1923.0	70
1 1 1 0 1	0 0 0 0 1	2062.1	2068.5	70
0 2 2 1 1	0 2 2 0 1	2300.5	2315.1	70
0 1 1 1 1	0 1 1 0 1	2310.7	2327.6	70
1 1 1 1 2	0 1 1 0 1	3541.8	3558.7	70
1 1 1 1 1	0 1 1 0 1	3684.7	3702.1	70
$^{16}O^{13}C^{18}O$ isotopologue				
1 0 0 0 2	0 1 1 0 1	598.2	601.6	70
0 1 1 0 1	0 0 0 0 1	643.3	648.1	71
0 2 2 0 1	0 1 1 0 1	643.7	648.2	70
1 0 0 0 1	0 1 1 0 1	694.0	699.0	70
0 2 2 1 1	0 2 2 0 1	2229.2	2242.8	70
0 1 1 1 1	0 1 1 0 1	2238.3	2254.4	70
$^{16}O^{13}C^{17}O$ isotopologue				
1 0 0 0 2	0 1 1 0 1	606.7	609.6	70
0 1 1 0 1	0 0 0 0 1	645.7	650.7	70
0 2 2 0 1	0 1 1 0 1	646.1	650.9	70
1 0 0 0 1	0 1 1 0 1	703.1	709.4	70
0 1 1 1 1	0 1 1 0 1	2245.2	2262.4	70
$^{18}O^{12}C^{18}O$ isotopologue				
0 1 1 0 1	0 0 0 0 1	657.3	661.8	70
0 2 2 0 1	0 1 1 0 1	657.8	662.0	70
0 1 1 1 1	0 1 1 0 1	2285.9	2301.8	70
$^{17}O^{12}C^{18}O$ isotopologue				
0 1 1 0 1	0 0 0 0 1	659.7	664.2	70

Note: For the non-symmetric isotopologues of CO_2, the Q branch possesses both e- and f-type transitions for each J'' (none of the data are $\Sigma \leftarrow \Sigma$). In this case, line-coupling data are supplied for each transition type.

Table 11
Summary of the ozone bands which have been updated in *HITRAN* or added from the *MIPAS* database [20]

Upper vib $v_1v_2v_3$	Lower vib $v_1v_2v_3$	ν_{min} (cm^{-1})	ν_{max} (cm^{-1})	Number of lines	Sum of line intensities
$^{16}O^{16}O^{16}O$					
0 2 1	0 1 1	612	770	923	1.8824E-22
1 2 0	1 1 0	629	766	668	1.1351E-22
0 0 2	1 0 0	918	1048	981	3.1436E-21
1 0 1	1 0 0	918	1181	2684	6.0065E-20
1 0 2	1 0 1	921	1003	1148	7.9910E-22
1 1 1	1 1 0	924	1018	1425	2.0344E-21
0 0 1	0 0 0	928	1244	7416	1.3664E-17
0 1 1	0 1 0	929	1218	3956	4.4570E-19
0 0 3	1 0 1	931	1016	201	4.0176E-23
2 0 1	2 0 0	931	1009	808	2.8433E-22
0 1 2	1 1 0	931	1017	211	3.7350E-23
0 0 2	0 0 1	932	1194	3268	1.6156E-19
0 2 1	0 2 0	933	1062	2125	1.4700E-20
0 0 3	0 0 2	934	1021	1388	1.6040E-21
1 0 1	0 0 1	934	1202	2600	5.0402E-21
0 1 2	0 1 1	935	1032	1797	5.8154E-21
1 2 1	1 2 0	937	990	286*	4.0473E-23
1 1 2	1 1 1	939	969	26*	2.4853E-24
0 3 1	0 3 0	940	1019	961*	4.6499E-22
1 0 2	0 0 2	940	1015	214	4.6153E-23
0 2 2	0 2 1	942	1009	670*	1.8133E-22
1 0 0	0 0 0	943	1273	6749	5.1954E-19
0 1 3	0 1 2	944	993	264*	3.5856E-23
1 1 1	0 1 1	947	1091	267	6.2728E-23
1 1 0	0 1 0	947	1233	3931	1.2249E-20
2 0 0	1 0 0	955	1216	3022	3.1850E-21
1 2 0	0 2 0	959	1179	1031	2.4030E-22
2 0 0	0 0 1	976	1232	2100	8.0229E-21
2 1 0	1 1 0	1084	1158	201	3.4255E-23
2 0 1	0 0 2	1099	1160	427	7.9395E-23
2 1 0	0 1 1	1130	1201	614	1.6078E-22
3 0 0	1 0 1	1158	1210	212	2.7170E-23
0 0 2	0 1 0	1319	1431	107	1.9842E-23
0 2 0	0 0 0	1332	1495	1127	4.3259E-22
1 0 1	0 1 0	1358	1435	1043	9.5455E-22
0 1 1	0 0 0	1634	1927	3415	5.1506E-20
0 2 1	0 1 0	1644	1749	1365	3.2891E-21
1 1 0	0 0 0	1666	1963	3695	2.2823E-20
1 2 0	0 1 0	1712	1877	1621	1.3196E-21
0 0 3	1 0 0	1860	2094	1301	1.1896E-21
0 0 4	1 0 1	1868	1905	91*	9.6770E-24
0 0 2	0 0 0	1882	2278	5339	1.0771E-19
1 0 2	1 0 0	1885	2066	1182	3.7277E-22
0 0 3	0 0 1	1894	2089	1923	1.4636E-21
0 1 2	0 1 0	1902	2112	2577	3.0415E-21

Table 11 (*continued*)

Upper vib $v_1v_2v_3$	Lower vib $v_1v_2v_3$	ν_{min} (cm^{-1})	ν_{max} (cm^{-1})	Number of lines	Sum of line intensities
1 0 1	0 0 0	1913	2322	5865	1.1884E-18
1 0 3	0 0 2	1924	1986	536*	1.1492E-22
1 1 1	0 1 0	1929	2221	2614	3.9287E-20
2 0 0	0 0 0	1935	2322	5024	3.2412E-20
0 0 4	0 0 2	1943	1982	20*	2.4744E-24
1 1 2	0 1 1	1962	2036	984*	4.9302E-22
1 0 2	0 0 1	1965	2067	2187	1.4125E-20
0 1 3	0 1 1	1976	2032	67*	8.5047E-24
2 0 2	1 0 1	1992	2050	435*	7.9399E-23
0 2 2	0 2 0	1993	2067	209*	3.2910E-23
1 2 1	0 2 0	1995	2080	1307*	1.2856E-21
2 1 1	1 1 0	1999	2074	873*	3.5388E-22
2 0 1	1 0 0	1999	2133	1986	1.0015E-20
1 3 1	0 3 0	2001	2043	134*	1.4683E-23
3 0 1	2 0 0	2012	2066	309*	4.5660E-23
2 0 1	0 0 1	2014	2206	1006	2.5377E-22
3 0 0	1 0 0	2023	2280	904	2.1541E-22
2 1 0	0 1 0	2065	2258	1722	7.4254E-22
2 2 0	0 2 0	2136	2154	20*	2.3853E-24
3 0 0	0 0 1	2160	2303	1100	8.1572E-22
0 2 1	0 0 0	2347	2430	886	3.9777E-22
$^{16}O^{16}O^{18}O$					
0 0 1	0 0 0	954	1124	4343	5.0599E-20
1 0 0	0 0 0	968	1178	6045	4.2543E-21
1 0 1	0 0 0	2031	2114	2571*	4.6343E-21
$^{16}O^{18}O^{16}O$					
0 0 1	0 0 0	934	1071	2184	2.5550E-20
1 0 0	0 0 0	969	1146	1018	4.7827E-22
1 0 1	0 0 0	1988	2075	1424*	2.3525E-21
$^{16}O^{16}O^{17}O$					
0 0 1	0 0 0	968	1067	3314*	9.5805E-21
1 0 0	0 0 0	988	1158	1764*	3.1376E-22
1 0 1	0 0 0	2049	2122	1774*	8.3593E-22
$^{16}O^{17}O^{16}O$					
0 0 1	0 0 0	958	1057	1644*	4.7081E-21
1 0 0	0 0 0	986	1154	492*	8.5858E-23
1 0 1	0 0 0	2031	2101	861*	4.0123E-22

Note: An asterisk sign (*) in the column of the number of lines signifies that the corresponding band was absent in the *HITRAN* 2000 database. Units of the last column are $cm^{-1}/(molecule \times cm^{-2})$.

For the self-broadened widths, we used the empirical polynomial expressions of Smith [73] based on experimental results for the $\nu_1, \nu_2, \nu_2+\nu_3, \nu_1+\nu_3$, and $2\nu_3$ bands [71,72,74]. For most transitions, where J'' is not equal to K_a'', we used the following expression:

$$\gamma_{\text{self}} = 0.1064 - 7.46\times10^{-6}J(J+1) - 1.40\times10^{-4}K^2, \tag{2}$$

for which $J = J''$ for $\Delta J \leqslant 0$, and $J = J'$ for $\Delta J > 0$, and where $K = K_a''$ for $\Delta K_a \leqslant 0$, and $K = K_a'$ for $\Delta K_a > 0$. Eq. (2) is applicable for J'' up to at least 50, but with $K_a'' \leqslant 13$. Beyond these values, a constant value has been adopted from the last reliable combination of J'' and K_a''.

For lines with $J'' = K_a''$, we adopted the following empirical formula:

$$\gamma_{\text{self}} = 0.1190 - 4.20\times10^{-4}J(J+1) + 1.21\times10^{-6}(J(J+1))^2. \tag{3}$$

Furthermore, Eq. (3) applies to $J'' \leqslant 12$ only. There do not seem to be any measurements reported on $J'' = K_a''$ transitions for $J'' > 12$. Consequently, the value of γ_{self} for $J'' = K_a'' = 12$ transitions has been assumed for $J'' = K_a''$ lines at higher rotational quantum numbers.

We used the polynomial expressions presented in Ref. [68] for the dependence of the air-widths upon temperature. The authors of Refs. [71,72] have also reported the dependence of the air-broadened widths upon temperature in the ν_1 and ν_2 bands. Drouin et al. [75] present a series of pressure-broadened widths, and of their dependence upon temperature, in the submillimeter region. These data will be assessed for the next *HITRAN* edition.

The mean values of the air-induced line shifts, −0.0007, −0.0008, −0.0007, −0.003, and −0.008 $\text{cm}^{-1}\,\text{atm}^{-1}$, apply to the ν_1, ν_2, ν_3, $\nu_1+\nu_3$, and $3\nu_3$ bands, respectively. These average values have been based upon Refs. [71,72,76,77], as no rotational quantum-number dependence of the pressure-induced line shifts has been ascertained with statistical significance from the presently available measurements.

3.4. N_2O (molecule 4)

For nitrous oxide, the line list has been almost completely revised. For positions and intensities we have used the line list of Toth [78] that covers the five isotopologues present in *HITRAN* between 500 and 7500 cm^{-1} with a minimum line strength of 2.02×10^{-25} cm^{-1}/(molecule cm^{-2}). Note that in this line list [78], the values of the bands centered below 900 cm^{-1} come from Johns et al. [79] for the ν_2 band of $^{14}N_2^{16}O$, and have been estimated [78] for the other bands, since research from the earlier work did not cover these bands. Furthermore, we replaced the line positions and intensities listed in Ref. [78] for the laser band (00^01-10^00) in the 10-μm region with the measurements by Daumont et al. [80], since both calculations [80,81] and new measurements [80], while in mutual agreement, show large differences with the data of Toth [78,82]. The line positions and intensities listed in the previous edition of *HITRAN* [1] have been retained for the lines in the 0–50 cm^{-1} region. Note that a recent work from Daumont et al. [83] has been performed between 3800 and 5300 cm^{-1}. More than 3000 line intensities have been measured in 66 bands, and 47 parameters of an effective dipole moment were fitted to experimental line intensities [83,84]. This work will be taken into account in a future *HITRAN* edition.

For the air-broadened widths, a polynomial fit to the experimental results from Toth [85], Lacome et al. [86], and Nemtchinov et al. [87] has been used for all lines of all isotopologues. The

expressions used for the air-broadened half-widths (in $cm^{-1}\,atm^{-1}$ at 296 K) are

$$\gamma_{air} = 0.0964, \quad 0 \leqslant |m| \leqslant 1, \tag{4}$$

$$\gamma_{air} = 0.0964 - 1.72 \times 10^{-3}|m| + 3.81 \times 10^{-5}|m|^2 - 2.96 \times 10^{-7}|m|^3, \quad 2 \leqslant |m| \leqslant 67, \tag{5}$$

$$\gamma_{air} = 0.0632, \quad |m| > 67, \tag{6}$$

where the running index m is $-J''$ in the P-branch, J'' in the Q-branch, and $J''+1$ in the R-branch. It should be emphasized that the formulae given as functions of $|m|$, which we have employed for the broadening parameters described here and throughout this article, are purely empirical and lack any physical interpretation.

A polynomial fit to the measurements by Toth [82] has been used for the self-broadened half-widths of all the lines of all of the isotopologues. The expressions used for the self-broadened half-widths (in $cm^{-1}\,atm^{-1}$ at 296 K) are

$$\gamma_{self} = 0.127, \quad 0 \leqslant |m| \leqslant 1, \tag{7}$$

$$\gamma_{self} = 0.1238 - 1.803 \times 10^{-3}|m| + 2.54 \times 10^{-5}|m|^2 - 1.4 \times 10^{-7}|m|^3, \quad 2 \leqslant |m| \leqslant 86, \tag{8}$$

$$\gamma_{self} = 0.0676, \quad |m| > 86. \tag{9}$$

An average value of 0.75 was assumed for the exponent n in the expression for the temperature dependence of the air-broadened half-width of every line, as is apparent from Refs. [86,87].

An expression given in Ref. [78] for the air pressure-induced line shift parameters as a function of wavenumber and $|m|$ has been used for all the lines excepting those located between 0 and 45 cm^{-1}. Zero has been adopted as the default value for the latter (a reasonable assumption consistent with the usual vibrational dependence expected for pressure-induced line shifts).

3.5. CO (molecule 5)

Several updates are apparent in the current edition for carbon monoxide. For the first overtone of $^{12}C^{16}O$ located near 2.4 μm, line intensities have been updated using the measurements of Brault et al. [88]. It is expected that a question may arise, quite rightfully so, as to our choice of Ref. [88] as the source for the intensities of this band, while several, just as recent and excellent, measurements by other authors [89,90] have appeared in the literature. Ref. [88] contains an appealing and authoritative discourse on the use of (a) a seemingly correct line shape, which, since it exhibits the dependence of the collision-broadening mechanism upon the relative speed of collision (“speed dependent” line shape), is deemed preferable and (b) the effect of line mixing. The other two sources employed the conventional Voigt line shape, and the readers are left to judge the accuracy of the employment of the different line shapes by different authors. These new results show that the line intensities of the previous *HITRAN* edition [1] were systematically larger by 4.2% than those of Ref. [88], as had already been pointed out by the authors of Refs. [89,90], where the measured intensities were reported to be 1 to 6% smaller than those reported in Ref. [1].

In the case of the second overtone (3-0) of $^{12}C^{16}O$ located around 1.6 μm, different groups [91–94] have shown that the intensity values that they measured were smaller than the entries in

previous edition of *HITRAN* by 5–7%. This observation was discussed at *HITRAN* conferences and other workshops. While the data in Refs. [93,94] are in concordance, we chose the calculated values of Sung and Varanasi [94], which were fitted to their experimental data, to update *HITRAN*.

Recent laboratory measurements [89,94,95] of air-broadened widths agree in the fundamental, the first overtone, and the second overtone bands, with the discrepancies being within ±2% for transitions with $3<|m|<19$. Outside this range of values of m, the air-broadened half-widths listed in Ref. [1] were 3–10% smaller than the measured values. For this reason, we chose to update the air-broadened half-widths using a fourth-order polynomial [96] derived from fitting the measurements of Refs. [89,94,95,97]. The root mean square (RMS) error of this fit is about 1.3%. For $1\leqslant|m|\leqslant26$, we used the following expression:

$$\gamma_{\text{air}} = 0.08555 - 6.385\times10^{-3}|m| + 5.627\times10^{-4}|m|^2 - 2.341\times10^{-5}|m|^3 + 3.457\times10^{-7}|m|^4. \tag{10}$$

Since the above expression results in air-broadened widths 5% larger than the previous *HITRAN* values [1] for $|m|$ near 26, to extrapolate beyond $|m| = 26$ we multiplied the previous *HITRAN* values by 1.05.

The entries in Ref. [1] of self-broadened line widths and recently reported measured data [88–94,98–104] all agree within ±5% for $J<25$. However, in order to achieve better accuracy, especially for higher J values, a fourth-order polynomial fit [96] of the measurements of Refs. [89,90,92–94,98–107] has been used to update the self-broadened half-widths. The RMS of this fit is 2.5%. For $1\leqslant|m|\leqslant35$, we used the following expression:

$$\gamma_{\text{self}} = 0.09130 - 5.295\times10^{-3}|m| + 3.764\times10^{-4}|m|^2 - 1.338\times10^{-5}|m|^3 + 1.649\times10^{-7}|m|^4. \tag{11}$$

For $|m|>35$ we adopted a constant half-width equal to the value at $|m| = 35$, $0.0413\,\text{cm}^{-1}\,\text{atm}^{-1}$. Average differences from the previous *HITRAN* edition [1] are +3% for $|m|\sim6$, −2% for $|m|\sim11$–16, and −5% to −10% for $|m|>25$.

The exponent n_{air} for the dependence of air-broadened half-widths has been updated for all CO transitions by means of a polynomial fit [96] of the measurements by Zou and Varanasi [89] in the 1-0 and 2-0 bands and by Connor and Radford [97] for the 0-0 band. The RMS error between the polynomial approximation and experimental data is about 2.7%. Then, for $1\leqslant|m|\leqslant20$, we used the fourth degree polynomial,

$$n_{\text{air}} = 0.7900 - 0.0316|m| + 6.34\times10^{-3}|m|^2 - 4.61\times10^{-4}|m|^3 + 1.04\times10^{-5}|m|^4. \tag{12}$$

For $|m|>20$, where the measured values are sparse and more uncertain, we adopted a constant value of 0.67. The average difference from the entries in the previous *HITRAN* edition [1] is +13%.

Air pressure-induced line shifts of lines in the 1-0, 2-0 and 3-0 bands of $^{12}C^{16}O$ have made their debut in the current edition of the database. The measurements by Zou and Varanasi [89] have been adopted for the lines in the *P*-branch for $1\leqslant|m|\leqslant23$ and in the *R*-branch for $1\leqslant|m|\leqslant25$ for the fundamental band. Beyond this range of $|m|$, we used constant values extrapolated from the measurements, $-0.0035\,\text{cm}^{-1}\,\text{atm}^{-1}$ in the *P*-branch and $-0.0030\,\text{cm}^{-1}\,\text{atm}^{-1}$ in the *R*-branch. For the lines in the first overtone band, we adopted the measurements by Zou and Varanasi [89] for

$1 \leqslant |m| \leqslant 19$ in the *P*-branch and for $1 \leqslant |m| \leqslant 22$ in the *R*-branch. Beyond this range of $|m|$, we used constant values extrapolated from the measurements, $-0.0050\,cm^{-1}\,atm^{-1}$ in the *P*-branch and $-0.0052\,cm^{-1}\,atm^{-1}$ in the *R*-branch. For the second overtone, the experimental values of Sung and Varanasi [94], who reported air pressure-induced line shifts ranging between -0.003 and $-0.009\,cm^{-1}\,atm^{-1}$, have been used in the range $1 \leqslant |m| \leqslant 18$ in the *P*-branch and $1 \leqslant |m| \leqslant 21$ in the *R*-branch. Outside this range, we used the constant values extrapolated from the measurements, $-0.0076\,cm^{-1}\,atm^{-1}$ in the *P*-branch and $-0.0080\,cm^{-1}\,atm^{-1}$ in the *R*-branch. For the other bands, a zero value has been kept to indicate the lack of measurements.

3.6. CH_4 (molecule 6)

Some 48,000 methane parameters that appeared in *HITRAN* 2000 were completely replaced by updated linelists of over 240,000 lines. Most of the revisions made in the region from 0 to $6185\,cm^{-1}$ were described by Brown et al. [9] as the 2001 update (which was available on the *HITRAN* website). Calculated positions and intensities of $^{12}CH_4$ and $^{13}CH_4$ were all based on successful modeling of the dyad (v_2, v_4) and pentad ($2v_4$, v_2+v_4, v_1, v_3, $2v_2$). For the deuterated species $^{12}CH_3D$, bands in the fundamental regions of the triad (v_3, v_6, v_5) and nonad (v_2, v_1, v_4 plus six combination/overtone bands) were also calculated. To accommodate astronomy requirements, weak lines with intensities of $10^{-27}\,cm^{-1}/(molecule \times cm^{-2})$ were included, along with hot bands in the dyad and pentad regions, resulting in a substantial increase in the number of transitions. Since at wavenumbers above $3400\,cm^{-1}$ data were available for $^{12}CH_4$ only, these data were based largely on empirical values, as were all the pressure-broadened half-widths. Additional details are given by Brown et al. [9].

Following the update performed in 2001, two additional changes were made in the spectral region below $1600\,cm^{-1}$. In the pure-rotation region, the quantum number *K* of $^{12}CH_3D$ had been omitted in the previous *HITRAN* editions and, so, a new line list was taken from the JPL catalog [15]. In the dyad region, a few of the air pressure-induced line shifts of $^{12}CH_4$ were revised after the revelation of systematic errors by a comparison with the analysis of the atmospheric spectra obtained in the *MIPAS* experiment [20].

A major improvement was also accomplished for the near-infrared parameters of the lines of CH_4 between 4800 and $9200\,cm^{-1}$. Firstly, 4937 line positions and intensities measured by Brown [108] in the 4800–5500 cm^{-1} region were used to replace the entries in Ref. [1] that were only for 273 lines located between 4800 and $4938\,cm^{-1}$. Additionally, 35,320 measured positions and intensities of lines between 6180 and $9200\,cm^{-1}$ have made their debut here. These parameters were obtained using high-resolution laboratory spectra recorded with the McMath–Pierce Fourier transform spectrometer. The sum of the intensities for all these new lines is $7.09 \times 10^{-20}\,cm^{-1}/(molecule \times cm^{-2})$ near 296 K (which is slightly less than the intensity of the R(0) line of the v_3-fundamental band). Nearly 99% of the new entries are unassigned, with most of the identified transitions belonging to the $4v_4$ band near 2 μm, the v_2+2v_3 band near 1.3 μm, and the $3v_3$ band near 1.1 μm. Without proper quantum assignments, a database cannot lead to an accurate prediction of methane's spectra at temperatures that are significantly different from 296 K. However, it is hoped that the availability of this list will aid in the development of new remote-sensing applications in the near-infrared and encourage efforts to interpret this portion of the methane spectrum. The prospects for future improvements are discussed by Brown et al. [9].

3.7. O_2 (molecule 7)

The A bands of the isotopologues $^{18}O^{16}O$ and $^{17}O^{16}O$ are centered at 0.76 μm, and the line parameters in these bands have been updated. This band of $^{17}O^{16}O$ was absent in the previous *HITRAN* edition [1]. The positions, the intensities, and the air- and self-broadened half-widths in that band have been added using the work of Camy-Peyret et al. [109]. For $^{18}O^{16}O$, only the positions have been updated, using Ref. [109].

3.8. NO (molecule 8)

In atmospheric applications in which non-local thermodynamic equilibrium (NLTE) needs to be considered, data on weak lines of nitric oxide with high lower-state energies are required. The calculation by Goldman et al. [110] for $^{14}N^{16}O$ has been adopted for the high-v (vibrational) and high-J transitions; according to this calculation, the weakest line intensity of this file is equal to $1.5\times10^{-95}\,\mathrm{cm^{-1}/(molecule\times cm^{-2})}$ at the standard reference temperature of 296 K in the database. The line positions and intensities from this calculation have been used to replace the previous parameters calculated by Gillis and Goldman [111]. Furthermore, this calculation has also resulted in the enhancement of the previous version of *HITRAN* [1] in terms of the addition of transitions with high-J values of existing bands, and also transitions of 243 new high-vibrational bands including forbidden bands. The maximum values for the vibrational and rotational quantum numbers are now $v=14$ and $J=126$ for the bands updated from Ref. [110]. The $^2\Pi_{1/2}$ electronic state (denoted X1/2 in the "global" quanta field, see Table 3, Class 3), has $J=N-\frac{1}{2}$, whereas the $^2\Pi_{3/2}$ electronic state (denoted X3/2), has $J=N+\frac{1}{2}$.

In addition, the air-broadened half-widths have been updated for all bands with $\Delta v\geqslant0$ (except for the bands with $\Delta v=2$) by using algorithms deduced from Refs. [112,113] that were previously [1] used only for the fundamental and the hot band (2-1). For the $\frac{3}{2}$ components and for $m<26.5$

$$\gamma_{\mathrm{air}}=0.06850-1.89\times10^{-3}|m|+1.03\times10^{-4}|m|^2-2.57\times10^{-6}|m|^3, \tag{13}$$

with the default value $0.045\,\mathrm{cm^{-1}\,atm^{-1}}$ for $m\geqslant26.5$.

For the $\frac{1}{2}$ components and for $m<26.5$

$$\gamma_{\mathrm{air}}=0.06818-2.61\times10^{-3}|m|+1.58\times10^{-4}|m|^2-3.71\times10^{-6}|m|^3, \tag{14}$$

with the default value $0.045\,\mathrm{cm^{-1}\,atm^{-1}}$ for $m\geqslant26.5$. For $\Delta v=2$ bands, we retained the *HITRAN* [1] algorithms based on Refs. [114–116].

For the self-broadened widths of all lines of all of the isotopologues, polynomial expressions were deduced from the measurements by Pine et al. [116] for the 2-0 band. The dependence of the widths upon vibrational quantum numbers was neglected in the application of the data to other vibrational bands. But a difference was introduced between the $\frac{1}{2}-\frac{1}{2}$ and $\frac{3}{2}-\frac{3}{2}$ sub-bands, as observed by Pine et al. [116]. The widths of the $\frac{1}{2}-\frac{1}{2}$ sub-band were extrapolated to the $\frac{3}{2}-\frac{1}{2}$ forbidden sub-band, and those of the $\frac{3}{2}-\frac{3}{2}$ sub-band were extrapolated to the $\frac{1}{2}-\frac{3}{2}$ forbidden sub-band. The self-broadened half-widths were calculated using the following least squares fits, which were performed on Pine's experimental data (in $\mathrm{cm^{-1}\,atm^{-1}}$) at 296 K:

For the $\frac{1}{2}-\frac{1}{2}$ and $\frac{3}{2}-\frac{1}{2}$ sub-bands:

$$\gamma_{\mathrm{self}}=0.075-3.05\times10^{-3}|m|+1.94\times10^{-4}|m|^2-4.09\times10^{-6}|m|^3,\quad |m|\leqslant17.5, \tag{15}$$

$$\gamma_{\text{self}} = 0.0596, \quad |m| \geqslant 18.5. \tag{16}$$

For the $\frac{3}{2} - \frac{3}{2}$ and $\frac{1}{2} - \frac{3}{2}$ sub-bands:

$$\gamma_{\text{self}} = 0.0748 - 1.48 \times 10^{-3}|m| + 4.73 \times 10^{-5}|m|^2, \quad |m| \leqslant 15.5, \tag{17}$$

$$\gamma_{\text{self}} = 0.0629, \quad |m| \geqslant 16.5. \tag{18}$$

The dependence of γ_{air} upon temperature is given in terms of an analysis of the values of the exponent n_{air}, which was based on the measurements [117] of the N_2-broadened half-widths. The values from this analysis have been adopted for all of the lines of all of the isotopologues. They are $|m|$-dependent until $J'' = 16.5$ (with a constant value for $J'' > 16.5$) and are summarized for the $^2\Pi_{1/2}$ and $^2\Pi_{3/2}$ components in Table 12.

The previous *HITRAN* edition [1] had contained air pressure-induced line shifts reported in Ref. [113] for $\Delta v = 1$ transitions and in Ref. [118] for $\Delta v = 2$ transitions, but included some interchanges of data between the two bands. These mistakes have been corrected in the current edition.

3.9. SO_2 (molecule 9)

There are no modifications made in the line parameters since the previous edition of *HITRAN* [1]. However, a calculated line list in the 8-μm region by Chu et al. [119] shows considerable differences from *HITRAN* [1]. In the v_1 band, the line intensities in *HITRAN* have been found to be larger by about 15%, on the average, while in the v_3 band, they are too large by 10–20%

Table 12
Summary of temperature-dependence exponents n_{air} for air-broadened half-widths of NO used in *HITRAN* 2004 for lower levels corresponding to the $^2\Pi_{1/2}$ and $^2\Pi_{3/2}$ components

$\lvert m\rvert$	n_{air}	
	$^2\Pi_{1/2}$	$^2\Pi_{3/2}$
0.5	0.79	0.74
1.5	0.79	0.74
2.5	0.78	0.74
3.5	0.69	0.68
4.5	0.71	0.63
5.5	0.70	0.67
6.5	0.64	0.65
7.5	0.69	0.67
8.5	0.73	0.73
9.5	0.70	0.64
10.5	0.68	0.70
11.5	0.70	0.71
12.5	0.67	0.68
13.5	0.72	0.66
14.5	0.63	0.83
15.5	0.63	0.74
16.5	0.51	0.67
$\geqslant$ 17.5	0.60	0.70

depending upon the rotational quantum numbers. This calculated line list should be available upon request from the authors. It should be noted that the results of Ref. [119] were corroborated by recent measurements of Sumpf [120]. Henningsen [121] has recently reported line intensities and self-broadened widths in the v_3 band, and that the modeling for both the line intensities and the self-broadened widths appeared to be in good agreement with the data of Refs. [119,120].

3.10. NO_2 (molecule 10)

As was pointed out in the work of Perrin et al. [14], the coding of the rotational quantum numbers N, K_a, K_c, J and F has been defined differently for nitrogen dioxide depending on spectral regions. In the present edition, the coding for these quantum numbers has been standardized according to Ref. [14]. For all nitrogen dioxide bands in *HITRAN* 2004, we use N instead of J, i.e., in the field of J (see Table 4) we put the N quantum number. In the sym field, we use the following convention for all lines: + or − signifying respectively that $J = N + \frac{1}{2}$ or $N - \frac{1}{2}$. Finally, in the field of F, we put F instead of $F - J$ as had been done previously [1].

No new analyses of positions and intensities were included, but the air-broadened half-widths, the air pressure-induced shifts, and the exponent for the temperature dependence of the air-broadened half-widths were revised throughout the database for nitrogen dioxide using empirical expressions and measurements by Benner et al. [122]. In this study, multispectrum retrievals of over 1000 transitions of v_3 were performed by placing constraints on spin-doubled transition pairs in order to improve the precision of the measurements. The experimental accuracies were thought to be 3% or better due to the agreement with other studies, as shown in Ref. [122]. The widths, and, to some extent, the pressure-induced shifts, were found to vary smoothly as a function of the quantum numbers and so quadratic functions were used at each K_a to reproduce the measured widths and shifts. For pressure-induced shifts, the value computed from the constants was scaled by the ratio of the band center of the transition to that of v_3. No pattern was discerned for the air-broadening temperature dependence exponents, and a simple linear equation in m (in this case $m = N''$ for P and Q branch transitions and $N'' + 1$ for R-branch transitions) was fit to these measurements. For selected widths, the RMS deviation was 2.5%. Based on these results, we updated the air-broadened half-widths and pressure shifts for all NO_2 transitions. For v_3 transitions, individual measurements of the half-widths, pressure-induced shifts and the temperature dependence of the widths were inserted on a line-by-line basis. For all other transitions, the empirical expressions were used.

3.11. NH_3 (molecule 11)

There are no changes in the line parameters of ammonia since the previous edition of *HITRAN* [1]. The current status of this molecule and prospects for improvements were discussed by Kleiner et al. [123].

3.12. HNO_3 (molecule 12)

Several updates have been introduced in the case of nitric acid in the current edition. Recently, Zu et al. [124] showed in the 683 GHz region a comparison between an observed spectrum and the

calculations using both the JPL catalog [15] and the previous *HITRAN* database [1], and concluded that the calculation based upon the JPL catalogue was more accurate than that using *HITRAN*. Therefore, the older line list for the pure-rotation band in *HITRAN* [1], which covered the 0–43 cm^{-1} region, has been replaced by the line list of the JPL catalog [15] which, furthermore, extends the spectral coverage to 0–84 cm^{-1}.

In the far infrared, two hot bands, $2\nu_9$–ν_9 and ν_5–ν_9, have been added. Line positions are from a simulation based on analyses of rotational spectra [125], in which intensities were scaled relative to those in the ν_9 fundamental using both laboratory and atmospheric spectra [125].

The intensities of the ν_5 and $2\nu_9$ bands have been normalized based on an accurate analysis of the 11-μm region using new laboratory high-resolution Fourier transform spectra [126]. The individual line intensities of the ν_5 and $2\nu_9$ bands given in *HITRAN* have been multiplied by the factor 0.879.

The two hot bands, $\nu_5+\nu_9-\nu_9$ and $3\nu_9-\nu_9$, located at 885.424 and 830.6 cm^{-1}, respectively, have been updated. These two bands had been removed from *HITRAN* 96 [127] and replaced by the hot band $\nu_5+\nu_9-\nu_9$ from Goldman et al. [128] in *HITRAN* 2000 [1]. In the current edition, the $3\nu_9-\nu_9$ band has been added using the line positions and intensities from Refs. [20,129]. In the $\nu_5+\nu_9-\nu_9$ band, which is the most commonly used for the retrieval of HNO_3 in the atmosphere, the positions and the intensities have been updated from Ref. [130].

Chackerian et al. [131] compared their measurements of the integrated absorption cross-sections with the entries in the 2000 edition of *HITRAN* that were based on Ref. [132], and showed in Table 4 of their article important differences in the two data sets. Using updates described above for the ν_5, $2\nu_9$, $\nu_5+\nu_9-\nu_9$ and $3\nu_9-\nu_9$ bands, the sum of line intensities between 820 and 950 cm^{-1}, multiplied by 1.29955 (see Ref. [131]), is 2.446×10^{-17} $cm^{-1}/(molecule\times cm^{-2})$, which is in good agreement with 2.424×10^{-17} $cm^{-1}/(molecule\times cm^{-2})$ given in Ref. [131], thereby confirming that the updates described above are indeed an improvement over the previous edition [1]. However, we find in the 1160–1240 and 1240–1400 cm^{-1} regions a large difference between the sum of *HITRAN* values of the intensities and the cross-sections reported by Chackerian et al. (see Table 4 of Ref. [131]). A scaling factor of 1.066 was determined by comparing the sum of the integrated cross-sections of Ref. [131] with the previous *HITRAN* intensities in the 1240–1400 cm^{-1} region. For the 1160–1240 cm^{-1} spectral region, because *HITRAN* does not contain the $\nu_6+\nu_7$ band, the cross-sections of Ref. [131] cannot be used to rescale *HITRAN* intensities. Therefore, the same scaling factor derived from the 1240–1400 cm^{-1} region was applied to the *HITRAN* 2000 line intensities in the ν_3 and ν_4 bands to obtain the current *HITRAN* intensities.

In a recent study, Boone and Bernath [133] have performed the retrievals of the volumetric mixing ratios of nitric acid from the spectra observed in the Atmospheric Chemistry Experiment (ACE). The retrievals were of tropical occultation, Arctic occultation, and a northern mid-latitude occultation taken in 2004. Comparisons are presented in Fig. 3 using both the *HITRAN* 2000 edition [1] and the current edition. For the three prominent bands of HNO_3 studied, it can be seen that the application of the new edition of *HITRAN* has reduced discrepancies significantly.

Prior to this edition, the self-broadened half-widths were set equal to zero for most of the lines of nitric acid. We have now assigned a constant value of 0.8 cm^{-1} atm^{-1} of this parameter for all of the lines. This value was chosen following Refs. [124,134].

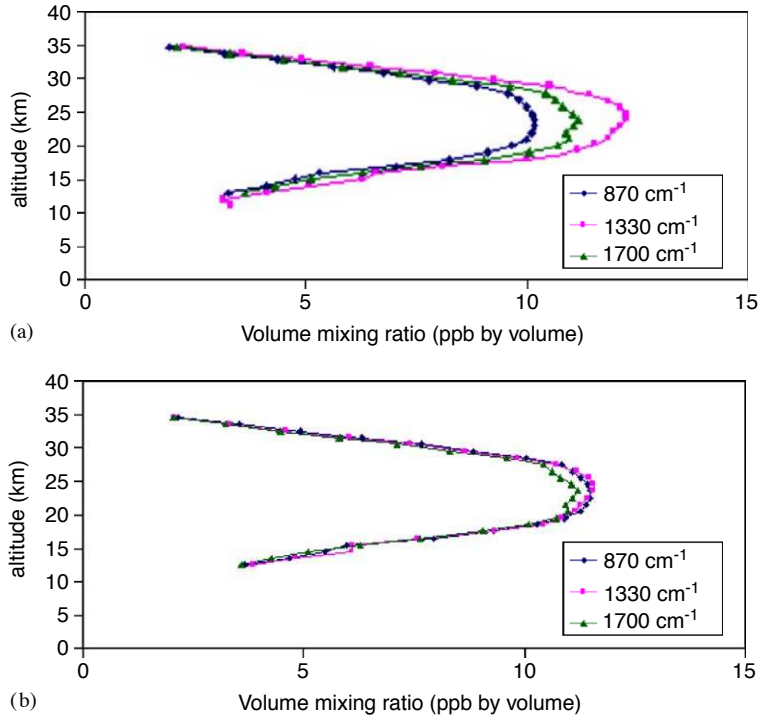

Fig. 3. Atmospheric HNO_3 profiles from an Arctic occultation in February 2004 by the Atmospheric Chemistry Experiment [133], retrieved using three different bands of HNO_3. (a) Retrieval using the *HITRAN* 2000 database [1]. (b) Retrieval using *HITRAN* 2004 line parameters.

3.13. OH (molecule 13)

Line intensities and positions have been updated in the pure rotation bands, $X^2\Pi_{1/2}(v'=0)$—$X^2\Pi_{1/2}(v''=0)$, $X^2\Pi_{3/2}(v'=0)$—$X^2\Pi_{3/2}(v''=0)$ and $X^2\Pi_{1/2}(v'=0)$—$X^2\Pi_{3/2}(v''=0)$, of the two isotopologues ^{18}OH and OD based on Ref. [15]. It should be noted that the hyperfine structure of the lines had been reported in *HITRAN* [1] for both of these isotopologues. Furthermore, hyperfine structure has been added for many lines of the $X^2\Pi_{1/2}(v'=0)$—$X^2\Pi_{1/2}(v''=0)$, $X^2\Pi_{1/2}(v'=1)$—$X^2\Pi_{1/2}(v''=1)$, $X^2\Pi_{1/2}(v'=2)$—$X^2\Pi_{1/2}(v''=2)$, $X^2\Pi_{1/2}(v'=0)$—$X^2\Pi_{3/2}(v''=0)$, $X^2\Pi_{3/2}(v'=0)$—$X^2\Pi_{3/2}(v''=0)$, $X^2\Pi_{1/2}(v'=1)$—$X^2\Pi_{3/2}(v''=1)$, $X^2\Pi_{3/2}(v'=1)$—$X^2\Pi_{3/2}(v''=1)$, $X^2\Pi_{1/2}(v'=2)$—$X^2\Pi_{3/2}(v''=2)$, and $X^2\Pi_{3/2}(v'=2)$—$X^2\Pi_{3/2}(v''=2)$ bands of ^{16}OH by drawing upon the work of Goldman et al. [135]. The predicted line positions used in the current edition of *HITRAN* for high J and high v ($v>3$) transitions could be improved using the recent work of Colin et al. [136]. For the air-broadened half-widths and their temperature dependence, we used the data reported in Ref. [127] for ^{16}OH.

3.14. HF (molecule 14)

The line parameters of hydrogen fluoride have not undergone a revision and remain the same as in the previous edition of *HITRAN* [1].

3.15. HCl (molecule 15)

Theoretically, the hyperfine structure is defined for hydrogen chloride as the coupling between the total angular momentum (excluding the nuclear spins) and the nuclear spins I(Cl) and I(H). Normally, the hyperfine quantum number F is equal to the vectorial summation of J, I(Cl) and I(H). In the previous *HITRAN* edition [1], in the-pure-rotation region, the coupling with I(H) was unresolved, and hence the lines were listed with the F'' quantum number, an integer which is the vectorial sum of J and I(Cl) only. In the pure-rotation region, the line list in the current edition is a combination of the JPL catalog [15] and the previous edition of *HITRAN* [1]. The hyperfine lines R(0)–R(15) in the 0-0-band of $H^{35}Cl$ are from the JPL catalog, and we retained the R(16)–R(21) lines from the previous *HITRAN* edition [1] and the hyperfine structure was unresolved in these lines. The same procedure has been done for the 0-0 band of $H^{37}Cl$. For the 1-1 bands of the two isotopologues, we kept the data that were in the previous *HITRAN* edition, which are very similar to those in the JPL catalog [15].

3.16. HBr (molecule 16)

The line parameters of hydrogen bromide line parameters remain the same as those in the previous edition of *HITRAN* [1].

3.17. HI (molecule 17)

The line parameters of hydrogen iodide are the same as in the previous edition of *HITRAN* [1]. The recent work of Bulanin et al. [137], which was mentioned in Ref. [138] that describes the status of the spectroscopic parameters of HBr and HI in the year 2000, is now available. It presents new intensities and line widths in the fundamental band of HI.

3.18. ClO (molecule 18)

The line parameters of chlorine monoxide remain the same as those listed in the previous edition of *HITRAN* [1].

3.19. OCS (molecule 19)

Recently performed high-resolution line intensity measurements in the 3- to 5-μm region of the spectrum of the main isotopologue of carbonyl sulfide by Régalia-Jarlot et al. [139] showed discrepancies with entries in the previous edition of *HITRAN* [1]. In particular, the line intensities measured by Régalia-Jarlot et al. for the v_3 band of $^{16}O^{12}C^{32}S$ are, on the average, 12.4% higher than those that were compiled in *HITRAN* [1]. This discrepancy has also been confirmed by Vander Auwera et al. [140] recently. The value of the square of the vibrational transition dipole moment measured by the authors of Ref. [139] is 0.1313 (Debye^2), while the value measured by authors of Ref. [140] is 0.1380 (Debye^2). It should be noted that the intensities measured by Régalia-Jarlot et al. exhibited a dependence on the rotational quantum number, whereas Vander Auwera et al. had not found it in their measurements. The value of 0.1313 (Debye^2) given in

Ref. [139] corresponds to $J = 0$. Because of the significant difference with *HITRAN* and despite the disagreement on the rotational dependence of the vibrational transition dipole moment, we decided to update the line intensities in the current edition using the average of the values taken from Refs. [139,140], i.e., 0.1346 (Debye^2). In this update we neglected the dependence on J of the vibrational transition dipole moment, in agreement with the predictions of the global model of Rbaihi et al. [141]. In addition, we updated the line intensities of the $\nu_1 + \nu_3$ band located around 2900 cm^{-1} according to the work of Régalia-Jarlot et al. [139], as entries in the previous edition of *HITRAN* [1] were found to be high by about 12%. Such a change is in agreement with recent measurements by Vander Auwera et al. [140]. In the cases of the $3\nu_1$ and $2\nu_1 + 2\nu_2$ bands around 3.8 μm, the intensities reported by Régalia-Jarlot et al. [139] are lower than *HITRAN* [1] by 7.6% and 7.4%, respectively. However, since the data of Strugariu et al. [142] are in good agreement with the intensities listed in *HITRAN* [1], we have not revised the data on these bands in the current edition. Line intensities in the $2\nu_3$ band of $^{16}O^{12}C^{32}S$ were also updated by adopting the data of Bermejo et al. [143]. The revised intensities are 7% higher than those in the previous edition of *HITRAN* [1].

3.20. H_2CO (molecule 20)

The line parameters of formaldehyde remain the same as in the previous edition of *HITRAN* [1]. However, a new analysis of the ν_2, ν_3, ν_4 and ν_6 bands yielding line positions and intensities in the 5–10 μm region has been reported by Perrin et al. [144]. This work will be considered for inclusion in a future edition of *HITRAN*.

3.21. HOCl (molecule 21)

The positions and intensities of the pure rotation lines of hypochlorous acid corresponding to transitions in its ground state were updated, and transitions within the (001) level were added by adopting the data from Ref. [145].

The parameters were updated in the ν_2 bands of $HO^{35}Cl$ and $HO^{37}Cl$ that are located in the 1178–1321 cm^{-1} region by adopting the results reported in Ref. [146]. Furthermore, the air-broadened half-width of all of the lines in the ν_2 band was set to the average of the measured values reported for two lines by Shorter et al. [147], i.e., 0.1 cm^{-1} atm^{-1}. The previously used default value 0.5 for the exponent n_{air} in the relation for the dependence of the air-broadened half-widths upon temperature was replaced by 0.7.

3.22. N_2 (molecule 22)

The line parameters of nitrogen have not been revised. It has been remarked in Ref. [148] that the intensities may be erroneous by about 2%, and additional measurements need to be performed on these quadrupole lines at 4.3 μm.

3.23. HCN (molecule 23)

A major update has been accomplished for the hydrogen cyanide line list. Line positions and intensities throughout the infrared have been revisited by Maki et al. [149]. The improvements

apply to the three isotopologues present in *HITRAN* in the pure-rotation region and in the infrared from 500 to 3425 cm^{-1}. This work has greatly increased the amount of HCN data in *HITRAN* from 772 transitions in the 2000 edition [1] to 4253 transitions in the present edition. However, transitions appearing at wavenumbers larger than 3425 cm^{-1} have not been considered.

Air-broadened half-widths, self-broadened half-widths, the exponent in the formula for the temperature dependence of the air-broadened half-width, and air pressure-induced line shifts have been updated using polynomials that were fit to the data reported by Devi et al. [150,151] and Rinsland et al. [152].

The polynomial used for air-broadened half-widths of lines with $|m| \leqslant 29$ is

$$\gamma_{\text{air}} = 0.1583 - 0.01102|m| + 7.78 \times 10^{-4}|m|^2 - 2.43 \times 10^{-5}|m|^3 + 2.65 \times 10^{-7}|m|^4. \quad (19)$$

For $|m| > 29$, a constant air-broadened half-width of 0.088 $cm^{-1}\,atm^{-1}$ has been used. Eq. (19) has been obtained by fitting 114 measurements, obtained for the ν_1 band [152] and the $2\nu_2$ band [151], which do not show any apparent vibrational dependence. Eq. (19) has thus been applied for all bands of the three isotopologues.

The following polynomial has been adopted for the self-broadened half-widths of lines with $|m|$ between 1 and 32:

$$\gamma_{\text{self}} = 0.404 + 0.177|m| - 7.49 \times 10^{-3}|m|^2 - 5.5 \times 10^{-4}|m|^3 + 3.42 \times 10^{-5}|m|^4 - 4.79 \times 10^{-7}|m|^5. \quad (20)$$

For $|m| > 32$, a constant self-broadened half-width of 0.15 $cm^{-1}\,atm^{-1}$ has been used. Eq. (20) has been obtained by fitting 67 measurements obtained for the ν_1 band [150]. In the absence of any experimental evidence that there is a dependence of the self-broadened line widths on vibrational quantum numbers [150,151], Eq. (20) has been applied for all of the lines in all of the bands listed in the database for the three isotopologues.

The temperature-dependence of air-broadened half-widths has been updated using the following polynomial for the exponent n_{air} by fitting 52 measurements in the ν_1 band [152]:

$$n_{\text{air}} = 0.8185 - 0.0415|m| + 7.79 \times 10^{-3}|m|^2 - 4.54 \times 10^{-4}|m|^3 + 8.31 \times 10^{-6}|m|^4. \quad (21)$$

The latter polynomial has been used for all bands of the three isotopologues of HCN for transitions between $|m| = 1$ and $|m| = 22$. Above $|m| = 22$, a constant value of 0.79 has been adopted.

Different polynomials have been used for the air pressure-induced line shifts in the *P*- and *R*-branches of the ν_1 and $2\nu_2$ bands of $H^{12}C^{14}N$. For the ν_1 band, we used the following expressions:

$$\delta^P_{\text{air}} = -2.897 \times 10^{-3} - 3.18 \times 10^{-4}|m| + 2.29 \times 10^{-5}|m|^2 - 4.67 \times 10^{-7}|m|^3, \quad (22)$$

$$\delta^R_{\text{air}} = 1.57 \times 10^{-4} - 5.15 \times 10^{-4}|m| + 2.17 \times 10^{-5}|m|^2 - 4.24 \times 10^{-7}|m|^3. \quad (23)$$

Eq. (22) is the result of obtaining the best fit of the measurements [152] on the lines with $|m| \leqslant 29$. For $|m| > 29$, the constant value of $-0.0044\,cm^{-1}\,atm^{-1}$ has been adopted. Eq. (23) has been obtained by fitting measurements [152] on lines with $|m| \leqslant 27$. For $|m| > 27$, the constant value of $-0.0065\,cm^{-1}\,atm^{-1}$ has been adopted. For the $2\nu_2$ band, we used the following expressions:

$$\delta^P_{\text{air}} = -2.114 \times 10^{-3} + 6.63 \times 10^{-4}|m| - 4.62 \times 10^{-5}|m|^2 + 1.19 \times 10^{-6}|m|^3, \quad (24)$$

$$\delta^{R}_{\text{air}} = 1.407 \times 10^{-3} + 2.68 \times 10^{-4}|m| - 2.40 \times 10^{-5}|m|^2 + 4.74 \times 10^{-7}|m|^3. \quad (25)$$

These polynomials, which have been obtained by fitting the measurements [151] on 28 lines in the *P*-branch and 28 lines in the *R*-branch, apply only to lines with $|m| \leqslant 28$. For $|m| > 28$, a constant value of $-0.0072\,\text{cm}^{-1}\,\text{atm}^{-1}$ has been adopted in the *P*-branch, while a constant value of $0.0005\,\text{cm}^{-1}\,\text{atm}^{-1}$ has been adopted in the *R*-branch. For the other bands, new measurements are needed, and extrapolation cannot be pursued using the results obtained for lines in the v_1 and $2v_2$ bands. Therefore, the air pressure-induced line shift has been set at zero for the other bands, thereby meaning that data are lacking. Recent measurements for the v_2 region by Devi and co-workers [153] have been proposed for consideration in a future update of the database.

It should be noted that, since some self-broadened half-widths of HCN are larger than $1.0\,\text{cm}^{-1}\,\text{atm}^{-1}$, this parameter can be read in the FORTRAN format F5.4, but cannot be written in that format. As special care has to be exercised, we recommend writing it in F5.3.

3.24. CH_3Cl (molecule 24)

A line list for the v_2, v_5, and $2v_3$ triad of vibrational bands of methyl chloride appearing in the 6- to 8-μm region has been added in this edition. The positions, intensities, and self-broadened widths are based upon the data of Chackerian et al. [154]. A polynomial expression for the self-broadened half-widths that considers *J*-dependence but not *K*-dependence, provided by this source of data, has been used to update the self-broadened half-widths of lines in all of the other bands of the two isotopologues considered in the database. An update of the air-broadened half-widths has been performed for all CH_3Cl lines in *HITRAN* using three sets of data calculated by Bouanich et al. [155] in the pure-rotation, parallel, and perpendicular bands. Considering that the uncertainty of the air-broadened half-widths is 5% for most lines in the calculation, we used the same calculations for the two isotopologues. Moreover, the constant value of 0.7 for n_{air} based on Ref. [155] has been preferred to the previous 0.5 default value for all lines of the two isotopologues. The pure-rotation bands for the two isotopologues have also been added to the database, using the positions, the intensities and the lower state energy of the JPL catalog [15]. It should be noted that the hyperfine structure is resolved in these two bands.

3.25. H_2O_2 (molecule 25)

A line list of hydrogen peroxide covering the pure-rotation region from 0 to $1427\,\text{cm}^{-1}$, prepared by Perrin et al. [7], has been included in the new *HITRAN* edition. This line list contains the torsional quantum numbers *n* and τ (see the global quanta field in Table 3). It should be noted that the previous versions of *HITRAN* did not contain lines between 99.8 and $1000\,\text{cm}^{-1}$, and did not include the torsional quantum number. Furthermore, the strong *Q* branch near $93.5\,\text{cm}^{-1}$, which is useful for atmospheric applications, was lacking. All these data can be found in the new line list.

Improvements for the v_6 band can be found in the work of Klee et al. [8]. A calculated line list of this band could replace the entries currently in *HITRAN* in the future.

3.26. C_2H_2 (molecule 26)

Recently, El Hachtouki and Vander Auwera [156] measured line intensities for five bands observed in the 1.5-μm region. This region, extending from 6448 to 6686 cm^{-1}, contains the $\nu_1 + \nu_3$ bands of $^{12}C_2H_2$ and $^{12}C^{13}CH_2$ and three hot bands of $^{12}C_2H_2$ associated with this combination band. Because this spectral region corresponds to the emission range of "telecom" diode lasers, the availability of such data can prove to be useful. Therefore, those data have been introduced into the current edition. The line positions were calculated using the constants reported by Kou et al. [157]. It should be noted that accurate line positions with uncertainty not exceeding 5×10^{-6} cm^{-1} are available for lines in the $\nu_1 + \nu_3$ band of $^{12}C_2H_2$ and $^{13}C_2H_2$ [158]. The air- and self-broadened half-widths, their temperature dependence, and the air pressure-induced line shifts were calculated using the polynomial expansion and the constants reported by Jacquemart et al. [6]. Furthermore, we added the parity symbols *u* or *g* for the vibrational symmetry for the isotopologue $^{12}C_2H_2$. It is indeed necessary to have this symmetry in order to determine the intensity alternation and, thus, to be able to calculate the statistical weights of the upper and lower levels [3].

3.27. C_2H_6 (molecule 27)

A line list prepared by Pine and Rinsland [159] for lines in the $^pQ_3$ sub-branch in the ν_7 band of ethane has completely replaced the old data in *HITRAN* [1]. It contains line positions, intensities, lower-state energies, air-broadened half-widths, and air pressure-induced line shift parameters. These new data represent a significant improvement over those used in earlier atmospheric applications.

3.28. PH_3 (molecule 28)

The line list of phosphine has been completely revised and expanded in the current edition. The line positions and line intensities in the 10-μm region are from Ref. [160], while those in the 5-μm region are from Ref. [161]. The air- and self-broadened half-widths from Ref. [160] replace the old default constant values that previously were listed in the earlier editions of *HITRAN* for this molecule.

The symmetry components A+, A−, and E of the C_{3v} group [10,11] have been added in the rotational field (*C* field: see Table 4).

3.29. COF_2 (molecule 29)

An unfortunate typographical error was detected in the previous editions of the database on the line list for carbonyl fluoride in the 5.1-μm region. The assignment of the rotational quantum numbers of the lower-state energy level was mistakenly interchanged with the assignment of those of the upper energy level. This error has been corrected in the current edition, and a new calculation has been generated [162]. The number of lines has more than doubled (28884 versus 13149 in the previous edition) because the degenerate pair of each doublet of lines of the symmetric top has been kept as separate lines.

3.30. SF_6 (molecule 30)

For sulfur hexafluoride, rotational quantum numbers J, R, C, N in the previous edition [1] have been replaced by J, C, α as has been done previously for methane [9]. R and N are not good quantum numbers, if one were to be able to describe all the transitions of this highly spherically symmetric molecule. An update has been performed for the only band of SF_6 present in *HITRAN*, the ν_3 band. New positions and intensities for 22901 lines [163,164] replace the spectroscopic parameters listed in the previous edition [1] of *HITRAN*. A dedicated effort to find theoretical solutions for the simulations and analysis of XY_6 spherical top systems has been in progress at the University of Burgundy in Dijon. Recent success with respect to SF_6 [165] is expected to lead to a more complete line list including hot bands.

A transcriptional error committed in the earlier editions of *HITRAN* in the list of the self-broadened half-widths has been fixed. A single self-broadened half-width of $0.042\,cm^{-1}\,atm^{-1}$ based on Ref. [166] has been assigned to all of the lines.

It should be recognized that the line-by-line parameters for SF_6 are not listed in the main folder for *HITRAN* line-by-line parameters, but are relegated to a supplemental folder (see Fig. 1). The rationale for this is due to the fact that, for such a heavy molecule, there are many very low-lying vibrational levels, often on the order of kT/hc, which is about $200\,cm^{-1}$ in terrestrial atmospheric applications. Most attempts to make high-resolution simulations of spectra would require in the database not only the information on the fundamental bands, but also on a plethora of hot bands and combination bands. Therefore, we recommend the use of cross-sections for these types of molecules; the line-by-line parameters are given for theoretical considerations or very specific cases.

3.31. H_2S (molecule 31)

Significant improvements have been implemented in the database to the air- and self-broadened half-widths for hydrogen sulfide. Average values of $0.074\,cm^{-1}\,atm^{-1}$ for the air-broadened half-widths and $0.158\,cm^{-1}\,atm^{-1}$ for the self-broadened half-widths, generated as the averages of the data reported in Refs. [167–170] and Refs. [167,170,171], respectively, have been used for all H_2S lines. However, when available, we have adopted the measured values from Refs. [167–170] for air-broadened half-widths and the measured values from Refs. [167,170,171] for self-broadened half-widths. The experimental values on γ_{air} amounted to 88 lines (out of a total of 20,788 lines for the H_2S linelist). Experimental values were available for 50 lines for γ_{self}. A constant value of 0.75 has been used for n_{air}.

An average value of the air pressure-induced line shift of $-0.002\,cm^{-1}\,atm^{-1}$ from Ref. [169] has been used for all of the lines in the ν_2 band, and an average value of $-0.003\,cm^{-1}\,atm^{-1}$ from Ref. [168] has been used for all of the lines in the ν_1, ν_3, and $2\nu_2$ bands. Average values of δ_{air} for the remaining combination and overtone bands were estimated by appropriately scaling the mean values from Refs. [168,169] according to the band centers. The resulting values are $\delta_{air} = -0.003\,cm^{-1}\,atm^{-1}$ for 110-010 and 030-010, $\delta_{air} = -0.0042\,cm^{-1}\,atm^{-1}$ for 011-000, 110-000, 021-010, and 120-010, and $\delta_{air} = -0.0045\,cm^{-1}\,atm^{-1}$ for 030-000 and 040-010.

3.32. HCOOH (molecule 32)

The spectral parameters of the pure-rotation lines of formic acid observed between 10 and 100 cm^{-1} were added to the current edition. The data on line positions and intensities come from the calculation of Vander Auwera [172]. These line positions have been substantiated by a recent study of Winnewisser et al. [173].

The new spectral line parameters (positions and intensities) generated by Perrin et al. [174] were used to update the data on the v_6 band. Such an improvement is particularly important for atmospheric applications, since the Q branch of the v_6 band located at 1105 cm^{-1} is used to quantify HCOOH in the troposphere and lower stratosphere. The work of Shepard et al. [175] illustrates well the improvements obtained when using the new data. Vander Auwera et al. [176] have reported the measurement of absolute line intensities in the v_6 band, taking the non-negligible contribution from the dimer $(HCOOH)_2$ into account when determining the partial pressure of the monomer HCOOH.

The constant values of 0.1 and 0.4 $cm^{-1}\,atm^{-1}$ used for the air-broadened and self-broadened half-widths, respectively, for the lines in the v_6 band were based on Refs. [177,174] have been applied to the far-infrared region. Finally, we recognize the recent observations of the v_7 and v_9 bands near 15.8 μm by Perrin et al. [178], which could be considered for a future *HITRAN* update.

3.33. HO_2 (molecule 33)

In the previous edition [1] of *HITRAN*, the notation of the rotational quantum numbers used for the hydroperoxyl radical was inconsistent. In the data provided by Chance et al. [179] for the lines in the pure-rotation region (from 0 to 909 cm^{-1}), N was used instead of J, and in the symmetry field the + or − meant, respectively, $J = F + \frac{1}{2}$ and $F - \frac{1}{2}$. For the v_1, v_2, and v_3 bands in *HITRAN* [1] (arising from Refs. [180–182]), N was used instead of J, and in the hyperfine field the indices 1 or 2 were used, respectively, for $J = N + \frac{1}{2}$ and $N - \frac{1}{2}$. In order to make the notation consistent throughout, we have placed the hyperfine quantum number in the F field, and we have used the character + and − (in the sym field), respectively, for $J = N + \frac{1}{2}$ and $N - \frac{1}{2}$. This is the same notation as we have adopted for NO_2 (see Table 4).

3.34. O (molecule 34)

Slight changes have been made in the data for the line positions, intensities, and lower-state energies of the two transitions of oxygen since the previous edition [1]. *HITRAN* has been updated with newer values in the JPL catalog [15].

3.35. $ClONO_2$ (molecule 35)

The line parameters of chlorine nitrate are the same as in the previous edition of *HITRAN* [1]. The parameters for this molecule are to be found in the supplemental folder.

3.36. NO^+ (molecule 36)

The line parameters of NO^+ are the same as in the previous edition of *HITRAN* [1].

3.37. *HOBr* (molecule 37)

The line parameters of hydrobromous acid are the same as in the previous edition of *HITRAN* [1].

3.38. C_2H_4 (molecule 38)

The line parameters of ethylene are the same as in the previous edition of *HITRAN* [1].

3.39. CH_3OH (molecule 39)

The data on methanol make their debut in this edition. In the microwave spectral region, line positions and intensities of the rotational transitions between 0 and 34 cm^{-1} within the ground vibrational level and the v_1 level (the hot band) from Ref. [183] have been used. Furthermore, a recent work by Xu et al. [184] led to the creation of an empirical line list around 10 μm that has been used in the current edition. This line list contains 15,234 lines belonging to the following bands: $v_8, v_8 + v_{12} - v_{12}, v_8 + 2v_{12} - 2v_{12}, v_7, v_7 + v_{12} - v_{12}, v_6 - v_{12}, v_6 - 2v_{12}, v_6 + v_{12} - v_{12}, v_5 - 2v_{12}$, $3v_{12}$ and $4v_{12}$. The air- and self-broadened half-widths have been fixed, respectively, to assumed values of 0.1 and 0.4 cm^{-1} atm^{-1}. The value of the exponent n_{air} has been assumed to be 0.75. A complete review of the quantum number notation used in *HITRAN* for this molecule is given in Ref. [184].

4. Infrared cross-sections

Many of the infrared cross-sections that were listed in the previous editions have been retained in this edition of the *HITRAN*. The format of the catalogue has also been retained (see Table 1). Therefore, only the new and the updated data are described below.

The data on each molecule (or chemical compound) are stored in a separate file, which is now labeled with the chemical symbol followed by an underscore and Irxx.xsc, where xx stands for the edition that the data were originally introduced or later updated and the file extension xsc signifies that it is a list of cross-sections. It is to be recalled that the files may have many temperature–pressure sets for different spectral regions, as indicated by headers throughout the file. Table 13 is a summary of the molecular species and spectral regions covered in the current edition. It is to be realized that, while the temperature–pressure (T, p) sets are reasonably complete for many species for an adequate simulation of atmospheric transmission in the spectral regions where those species are active, for other species, an insufficiency of the (T, p) sets may become apparent. It is hoped that future measurements at extended sets of (T, p) combinations may help broaden the coverage in the database.

Table 13
Summary of molecules represented by IR cross-section data in *HITRAN*

Molecule	Common name	Temperature range (K)	Pressure range (torr)	Number of T, P sets	Spectral coverage (cm^{-1})
SF_6	Sulfur hexafluoride	180–295	20–760	32	925–955
$ClONO_2$	Chlorine nitrate	189–297	0–117	25	750–830
		189–297	0–117	25	1260–1320
		213–296	0	2	1680–1790
CCl_4	Carbon tetrachloride	208–297	8–760	32	750–812
N_2O_5	Dinitrogen pentoxide	205–293	0	5	540–1380
HNO_4	Peroxynitric acid	220	0	1	780–830
C_2F_6	Hexafluoroethane, CFC-116	181–296	25–760	43	1061–1165
		181–296	25–760	43	1220–1285
CCl_3F	CFC-11	190–296	8–760	55	810–880
		190–296	8–760	55	1050–1120
CCl_2F_2	CFC-12	190–296	8–760	52	850–950
		190–296	8–760	52	1050–1200
$CClF_3$	CFC-13	203–293	0	6	765–805
		203–293	0	6	1065–1140
		203–293	0	6	1170–1235
CF_4	CFC-14	180–296	8–761	55	1250–1290
$C_2Cl_2F_3$	CFC-113	203–293	0	6	780–995
		203–293	0	6	1005–1232
$C_2Cl_2F_4$	CFC-114	203–293	0	6	815–860
		203–293	0	6	870–960
		203–293	0	6	1030–1067
		203–293	0	6	1095–1285
C_2ClF_5	CFC-115	203–293	0	6	955–1015
		203–293	0	6	1110–1145
		203–293	0	6	1167–1260
$CHCl_2F$	HCFC-21	296	1	1	785–840
$CHClF_2$	HCFC-22	181–297	0–765	29	760–860
		181–296	22–761	31	1070–1195
		253–287	0	3	1060–1210
		253–287	0	3	1275–1380
$CHCl_2CF_3$	HCFC-123	253–287	0	3	740–900
		253–287	0	3	1080–1450
$CHClFCF_3$	HCFC-124	287	0	1	675–715
		287	0	1	790–920
		287	0	1	1035–1430
CH_3CCl_2F	HCFC-141b	253–287	0	3	710–790
		253–287	0	3	895–1210
		253–287	0	3	1325–1470
CH_3CClF_2	HCFC-142b	253–287	0	3	650–705
		253–287	0	3	875–1265
		253–287	0	3	1360–1475
$CHCl_2CF_2CF_3$	HCFC-225ca	253–287	0	3	695–865
		253–287	0	3	1010–1420
$CClF_2CF_2CHClF$	HCFC-225cb	253–287	0	3	715–1375

Table 13 (*continued*)

Molecule	Common name	Temperature range (K)	Pressure range (torr)	Number of T, P sets	Spectral coverage (cm^{-1})
CH_2F_2	HFC-32	203–297	0–750	17	995–1236
		203–297	0–750	17	1385–1475
CHF_2CF_3	HFC-125	287	0	1	700–745
		287	0	1	840–890
		287	0	1	1060–1465
CHF_2CHF_2	HFC-134	203–297	0–750	9	600–1700
CFH_2CF_3	HFC-134a	253–287	0	3	815–865
		190–296	20–760	32	1035–1130
		190–296	20–760	33	1135–1340
		253–287	0	3	935–1485
CF_3CH_3	HFC-143a	203–297	0–750	9	580–630
		203–297	0–750	9	750–1050
		203–297	0–750	9	1100–1500
CH_3CHF_2	HFC-152a	253–287	0	3	840–995
		253–287	0	3	1050–1205
		253–287	0	3	1320–1490
SF_5CF_3	Trifluoromethyl sulfur pentafluoride	213–323	760	5	599–624
		213–323	760	5	676–704
		213–323	760	5	740–766
		213–323	760	5	860–920
		213–323	760	5	1150–1280
		213–323	760	5	1280–2600

Note: These data are in the main directory. Additional redundant data for CFC-11 and CFC-12 are stored in a supplemental sub-directory (see Fig. 1).

The cross-sections of chlorine nitrate ($ClONO_2$) have been entirely updated in the 750–1320 cm^{-1} region. These data are the measurements by Wagner and Birk [185], who performed them using spectral resolution between 0.002 and 0.008 cm^{-1} and at pressures between 0.2 and 117 torr. Data at total pressures less than 1 torr are for pure $ClONO_2$, while higher total pressures are for mixtures of $ClONO_2$, which was kept at partial pressures not exceeding 0.8 torr, and dry air (see Ref. [185] for details). These data have been arranged as two separate sets covering the 750–830 and 1260–1320 cm^{-1} regions. The cross-sectional data from Ref. [186] in the 1680–1790 cm^{-1} region, and listed in the previous edition of *HITRAN* [1], have been retained.

Ref. [185] also includes cross-sections of nitrogen pentoxide, N_2O_5. These data have been used to replace the data compiled in the previous edition of *HITRAN*. The new database is deemed superior by more than two orders of magnitude, in so far as the spectral resolution and the spectral coverage, which includes two strong bands and some weaker features in the 540–1380 cm^{-1} region, are concerned. The original data from Ref. [185] contained some negative numbers for values of the cross-sections, which was due to the noise in the recorded spectra. By conforming to the format previously adopted by us, we have set all of the negative cross-sections to zero; users desiring to have the original data should contact the authors of the data.

HNO_4 (peroxynitric acid, PNA) is an important transient reservoir for NO_2 and HO_2 in the stratosphere and high-latitude upper troposphere. The cross-sections measured by May and Friedl [187] at 220 K using a spectral resolution of 0.003 cm^{-1} in the 780–830 cm^{-1} region are included in the current edition. These data replace the earlier cross-sections that were measured at room temperature using a spectral resolution of 0.03 cm^{-1}. Since HNO_4 was formed by the reaction between NO_2 and HNO_3, the total pressure is the sum of the partial pressures of these three gases. Since broadening of HNO_4 is due to NO_2 and/or HNO_3, in the present case, we resorted to listing NO*y* as the broadener in the file header.

Absorption cross-sections of SF_5CF_3 (trifluoromethyl sulfur pentafluoride) are included for the first time in the current version of *HITRAN*. This compound is conceived as a breakdown product of SF_6 in high-voltage equipment. It may have a potentially higher global warming potential than SF_6. While the strongest of the thermal infrared absorption bands, the fundamental and all of the hot bands of SF_6 are located in a single spectral region around 9.6 μm, SF_5CF_3 bands are located throughout the 8–12 μm atmospheric window. The cross-sections were measured at 213, 243, 278, 298, and 323 K at a spectral resolution of 0.112 cm^{-1} in 760 torr of N_2, in the 520–6500 cm^{-1} region at the Pacific Northwest National Laboratory [188]. The cross-sections are tabulated for six wavenumber regions between 599 and 2600 cm^{-1} at the five temperatures mentioned above. Fig. 4 is a display of the cross-sections in one of the bands, and it is an illustration of the dependence of the spectral absorption cross-sections of SF_5CF_3 upon temperature.

The distributions of the (T,p) sets for the three molecules $ClONO_2$, N_2O_5, and SF_5CF_3 are shown in Fig. 5.

Supplemental cross-sections of several other species of interest in the lower and upper troposphere will soon be added to *HITRAN*. Measurements of PAN ($CH_3C(O)O_2NO_2$) by Allen

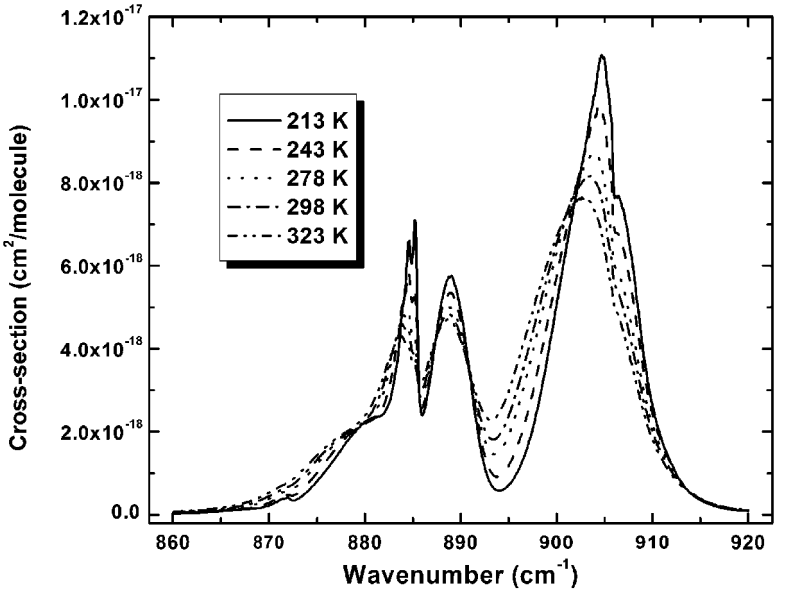

Fig. 4. Cross-sections of SF_5CF_3 [188] in the 11-μm region at five temperatures.

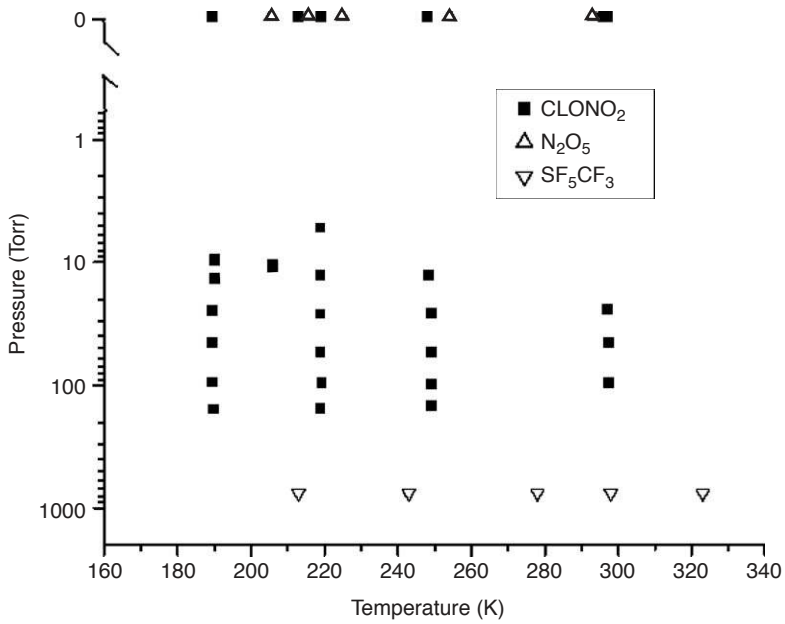

Fig. 5. Pressure and temperature pairs for the new $ClONO_2$, N_2O_5, and SF_5CF_3 cross-section data of the 2004 *HITRAN* edition. Each pair corresponds to a complete cross-section data set included in the compilation.

et al. [189] and measurements of acetone (C_3H_6O) by Orlando and Tyndall [190] are ongoing. Cold-temperature cross-sections of PAN and acetone will lead to retrievals of these species at the cold temperatures commonly encountered in the upper troposphere. Of special interest will be the application of these cross-sections in analysis of TES (Tropospheric Emission Spectrometer) [191] and other remote-sensing observations of air columns associated with biomass fires. Fires in the tropics and boreal regions inject these species (and other organics) into the upper troposphere.

5. Ultraviolet data sets

New cross-sections of a number of molecules in the ultraviolet and visible spectral regions have been introduced into the database. In each case, we have opted to select those data that have proven to be the most useful in the analyses of atmospheric measurements, especially satellite observations. This portion of the *HITRAN* database is projected to grow, and evolve significantly, over the near future as spectroscopic monitoring of atmospheric pollution tends to become more advanced.

5.1. O_3

Absorption cross-sections in the Hartley–Huggins bands, including their dependence upon temperature, are included in the 29,164–40, 798 cm^{-1} region. The data are adopted from Bass and

Paur [192]. They are corrected from the wavelengths in air to the wavelengths in vacuum according to Edlén [193]. Further wavelength corrections have been made from comparison with the FTS measurements on ozone by Voigt et al. [194], and they resulted in an additional shift of the wavelength by $+0.015 \pm 0.040$ nm.

Bass and Paur [192] presented coefficients for the calculation of temperature-dependent cross-sections versus wavelength using a quadratic formula. Their coefficients are included in this new *HITRAN* edition in the *alternate file* on O_3. For the *HITRAN* primary files, cross-sections have been calculated for a range of temperatures from 200 to 300 K, and then the data were interpolated using a fixed increment in the wavenumber. Values were obtained by an interpolation using a cubic spline of the original data with 2 cm^{-1} spacing, which corresponds to more than twice the sampling in the original data.

5.2. NO_3

Cross-sections of nitrogen trioxide at 298 K are taken from Orphal et al. [195]. Note that for the strongest (0-0) band around 662 nm, the temperature dependence of the cross-section, σ, can be modeled readily as:

$$\sigma(T)/\sigma(298\,\mathrm{K}) = [1 - e^{-1096.4/T} - 2e^{-529.5/T}]/0.6364, \tag{26}$$

where T is the absolute temperature in K. This model does not apply for bands outside the 645–675 nm range.

5.3. BrO

Cross-sections for bromine monoxide at 228 and 298 K, at 10 cm^{-1} spectral resolution, are taken from Wilmouth et al. [196].

5.4. $OClO$

Chlorine dioxide cross-sections at two spectral resolutions (1 and 20 cm^{-1}) and five temperatures (213–293 K) are taken from Kromminga et al. [197]. The original data are available at http://www-iup.physik.uni-bremen.de/gruppen/molspec/.

5.5. H_2CO

Cross-sections of formaldehyde are adopted from Cantrell et al. [198], who give a linear dependence for calculating cross-sections vs. temperature. The wavenumber steps in the original data are not perfectly regular, and there are 48 gaps or missing points. For the *HITRAN* primary files, cross-sections have been calculated from the Cantrell et al. data [198] at three temperatures (280, 290, and 300 K) and then cubic-spline interpolated to an even wavenumber increment of 0.244 cm^{-1}, corresponding to more than twice the sampling of the original data. The original data are also available in the *alternate* file folder (see Fig. 1).

5.6. O_2–O_2

Cross-sections for the oxygen collision complex at 296 K are adopted from Greenblatt et al. [199]. (The "cross-sections" are in units of cm^5 $molecule^{-2}$, since the absorption depends on the square of the O_2 density.) They are corrected from air to vacuum wavelengths using Edlén [193]. For the *HITRAN* primary files, cross-sections are interpolated to even wavenumber increments in two ranges, 8794.215–9945.540 cm^{-1} and 15385.100–29823.980 cm^{-1}, by cubic spline interpolation. Spacings correspond to more than twice the sampling of the primary data. The primary data are also available in the alternate file folder.

6. Aerosol refractive indices

Refractive indices of water, ice, aqueous sulfuric and nitric acid, solid hydrates (i.e. nitric acid, mono-, di-, and tri-hydrate), organic nonvolatile aerosol, and crustal material (e.g. quartz, hematite, and sand) in the previous version of *HITRAN* are discussed by Massie and Goldman [200]. It is pointed out in Ref. [200] that the specification of refractive indices for ternary ($H_2O/H_2SO_4/HNO_3$) solution droplets, an important type of composition of the so-called "polar stratospheric clouds" (PSCs), is fairly uncertain, due to the uncertainties in the refractive indices of aqueous sulfuric and nitric acid at stratospheric temperatures.

Recently, Norman et al. [201] published the real and imaginary refractive indices at 220 K for six different ternary compositions, and these data have been added to the current *HITRAN* compilation. We show in Fig. 6 the imaginary refractive indices for the six compositions. The imaginary refractive indices are presented in the figure, since the wavelength dependence of the extinction spectrum of a small droplet is similar to the wavelength dependence of the imaginary

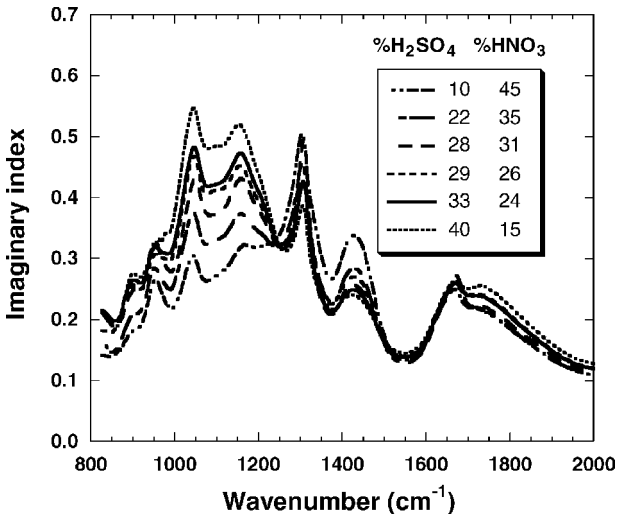

Fig. 6. Imaginary refractive indices at 220 K for six different ternary solution ($H_2O/H_2SO_4/HNO_3$) compositions [201].

refractive index. As temperature decreases below 193 K, the percentage weight of HNO_3 in a ternary droplet increases, and it is expected that the wavelength dependence of its extinction spectrum will also change.

Prior to Ref. [201], the room temperature measurements of Adams and Downing [202] for 75% wt H_2SO_4, 10% wt HNO_3, and 15% wt H_2O, and tabulations of binary (H_2O/H_2SO_4 and H_2O/HNO_3) indices (see Ref. [200]) were available. Biermann et al. [203] and Luo et al. [204] tabulated laboratory measurements of the binary refractive indices, stated a mixing model (i.e. an algebraic expression for obtaining ternary refractive indices from a mixture of the binary components), and tested the mixing model using laboratory measurements of several ternary mixtures. In their measurements, included in *HITRAN*, Norman et al. [201] specified ternary indices directly, and they can be used to perform additional tests on the mixing model.

7. Global data

There are some data, which are necessary for the *HITRAN* compilation and apply in a comprehensive or global manner to the line-by-line parameters or cross-sections. These data are placed in the folder, "Global Data Files, Tables, and References," (see Fig. 1). There are five files in this folder: molparam.txt, bandcent.dat, ref-table2004.pdf, TIPS_2003.zip (containing TIPS_2003.for, BD_TIPS_2003.for, and associated INCLUDE files), and parsum.dat.

The text file, molparam.txt, is a table containing the adopted abundance, the partition sum at 296K, the state-independent degeneracy factor, and the molar mass for all the isotopologues/isotopomers present in *HITRAN*. A list of band centers for all the ro-vibration bands in the database are contained in the file bandcent.dat; this file is used as input for generating statistics on the contents of *HITRAN*. Ref-table2004.pdf is a large list containing all the references for the six line-by-line parameters ($v, S, \gamma_{air}, \gamma_{self}, n_{air}$, and δ_{air}) and the cross-sections. The pointers in the *HITRAN* line transitions and in the cross-section headers refer to the entries in this list.

7.1. Total internal partition sums

For this edition of the database we provide a comprehensive set of total internal partition sums (TIPS) for species of atmospheric interest, calculated to a great degree of accuracy and packaged in a form that allows for easy and rapid recall of the data [205]. Partition sums, $Q(T)$, were calculated for molecular species and isotopologues/isotopomers present in the *HITRAN* database. The calculations of the partition sums address the corrections suggested by Goldman et al. [206]. The correct statistical weights for all isotopologues/isotopomers in the database were implemented, consistent with those used to determine the Einstein A-coefficients [3]. The temperature range of the calculations (70–3000 K) was selected to match a variety of remote-sensing needs (for example, planetary atmospheres, combustion gases, and plume detection). Although there are a number of molecular species for which the partition sum at high temperatures is of no practical importance at present, e.g. ozone or hydrogen peroxide, the aim was to have a consistent set of partition sums for all molecular species in *HITRAN* (partition sums

are also provided for a number of rare isotopic ozone species which are not currently in the *HITRAN* database).

A new method of recall for the partition sums, Lagrange 4-point interpolation, was developed. In previous versions of the *HITRAN* compilation, polynomial fits of $Q(T)$ were used. However, there were a number of species for which the error introduced by the fits was greater than the 1% criterion at certain temperatures and no coefficients were reported. This Lagrange 4-point interpolation method allows all molecular species in *HITRAN* to be considered.

The four-point Lagrange interpolation scheme was coded into a FORTRAN program that uses data tables for $Q(T)$ at 25 K intervals with extra points provided below 70 K and above 3000 K so that a four point interpolation can be used throughout the entire temperature range. In addition to the programs TIPS_2003.for and subroutine BD_TIPS_2003.for, tables at 1 K step size (parsum.dat) are available in the folder Global Data Files.

8. Conclusions

This new edition of the *HITRAN* compilation is a vastly improved one with respect to the line-by-line parameters and IR and UV cross-sections. Mechanisms have been set in place to validate new data being considered for incorporation into the database. We have endeavored to make comparisons with field observations or independent laboratory measurements to verify that the residuals and consistencies have significantly improved.

The new generation of atmospheric remote-sensing satellite instruments is requiring unprecedented high accuracies of the molecular spectroscopic parameters. *HITRAN*'s progress in the future will also require the determination of line parameters for systems of bands in the near-infrared, extending the applicability of the parameters at all wavelengths to high temperatures (often tantamount to archiving atmospheric weak lines), addition of collision-induced absorption bands, characterization of "line coupling" for more molecules, and addition of new molecules that are important for terrestrial, planetary, and astrophysical applications.

Acknowledgements

The *HITRAN* molecular database has been a project with strong international cooperation during its development. Laboratories throughout the world have contributed both experimental data and theoretical calculations. We greatly appreciate the major efforts of P.F. Bernath, C. Boone, J.P. Bouanich, J.W. Brault, C. Camy-Peyret, E.A. Cohen, P.-F. Coheur, M.-R. De Backer-Barilly, B. Drouin, J. Fischer, M. Fukabori, L. Giver, I. Kleiner, M.-F. Mérienne, S. Mikhailenko, C.E. Miller, L. Régalia-Jarlot, J. Schrœder, M. Šimečková, B. Sumpf, M. Tanaka, K. Tang, S. Tashkun, J.-L. Teffo, Vl.G. Tyuterev, and L.H. Xu in support of this new edition. The current endeavor has been funded by the NASA Earth Observing System (EOS), under the grant NAG5-13534, and by the Office of the Secretary of Defense (OSD) High Energy Laser Joint Technology Office.

References

[1] Rothman LS, Barbe A, Benner DC, Brown LR, Camy-Peyret C, Carleer MR, Chance KV, Clerbaux C, Dana V, Devi VM, Fayt A, Flaud JM, Gamache RR, Goldman A, Jacquemart D, Jucks KW, Lafferty WJ, Mandin JY, Massie ST, Nemtchinov V, Newnham D, Perrin A, Rinsland CP, Schrœder J, Smith K, Smith MAH, Tang K, Toth RA, Vander Auwera J, Varanasi P, Yoshino K. The HITRAN molecular spectroscopic database: edition of 2000 including updates through 2001. JQSRT 2003;82:5–44.

[2] Rothman LS, Gamache RR, Goldman A, Brown LR, Toth RA, Pickett HM, Poynter RL, Flaud JM, Camy-Peyret C, Barbe A, Husson H, Rinsland CP, Smith MAH. The HITRAN database: 1986 edition. Appl Opt 1987;26:4058–97.

[3] Šimečková M, Jacquemart D, Rothman LS, Gamache RR, Goldman A. Einstein *A*-coefficients and statistical weights for molecular transitions in the HITRAN database. JQSRT, to appear.

[4] Herzberg G. Molecular spectra and molecular structure, II. Infrared and Raman spectra of polyatomic molecules. Princeton: D Van Nostrand; 1945.

[5] Rothman LS, Young LDG. Infrared energy levels and intensities of carbon dioxide—II. JQSRT 1981;25:505–24.

[6] Jacquemart D, Mandin JY, Dana V, Claveau C, Vander Auwera J, Herman M, Rothman LS, Régalia-Jarlot L, Barbe A. The IR acetylene spectrum in HITRAN: update and new results. JQSRT 2003;82:363–82.

[7] Perrin A, Flaud JM, Camy-Peyret C, Schermaul R, Winnewisser M, Mandin JY, Dana V, Badaoui M, Koput J. Line intensities in the far-infrared spectrum of H_2O_2. J Mol Spectrosc 1996;176:287–96.

[8] Klee S, Winnewisser M, Perrin A, Flaud JM. Absolute line intensities for the v_6 band of H_2O_2. J Mol Spectrosc 1999;195:154–61.

[9] Brown LR, Benner DC, Champion JP, Devi VM, Fejard L, Gamache RR, Gabard T, Hilico JC, Lavorel B, Loëte M, Mellau GC, Nikitin A, Pine AS, Predoi-Cross A, Rinsland CP, Robert O, Sams RL, Smith MAH, Tashkun SA, Tyuterev VG. Methane line parameters in HITRAN. JQSRT 2003;82:219–38.

[10] Tarrago G, Dang Nhu M. Ground state rotational energies of C_{3v} quasi-spherical top molecules: applications to $^{16}OPF_3$ and PH_3. J Mol Spectrosc 1985;111:425–39.

[11] Tarrago G, Delaveau M. Triad $v_n(A_1), v_t(E), v_{t'}(E)$ in C_{3v} molecules: energy and intensity formulation (computers programs). J Mol Spectrosc 1986;119:418–25.

[12] Ramsay DA, Rostas J, Zare RN. The labeling of parity doublet levels in linear molecules. J Mol Spectrosc 1975;55:500–3.

[13] Champion JP, Loëte M, Pierre G. Spherical top spectra. In: Rao KN, Weber A, editors. Spectroscopy of the Earth's atmosphere and interstellar medium. USA: Academic Press; 1992.

[14] Perrin A, Flaud JM, Goldman A, Camy-Peyret C, Lafferty WJ, Arcas Ph, Rinsland CP. NO_2 and SO_2 line parameters: 1996 HITRAN update and new results. JQSRT 1998;60:839–50.

[15] Pickett HM, Poynter RL, Cohen EA, Delitsky ML, Pearson JC, Müller HSP. Submillimeter, millimeter, and microwave spectral line catalog. JQSRT 1998;60:883–90.

[16] Toth RA. Transition frequencies and absolute strengths of $H_2^{17}O$ and $H_2^{18}O$ in the 6.2-μm region. J Opt Soc Am B 1992;9:462–82.

[17] Pearson JC. Private communication. Jet Propulsion Laboratory, Pasadena CA, USA. 1999.

[18] Coudert LH. Line frequency and line intensity analyses of water vapour. Mol Phys 1999;96:941–54.

[19] Lanquetin R, Coudert LH, Camy-Peyret C. High-lying rotational levels of water: an analysis of the energy levels of the five first vibrational states. J Mol Spec 2001;206:83–103.

[20] Flaud JM, Piccolo C, Carli B, Perrin A, Coudert LH, Teffo JL, Brown LR. Molecular line parameters for the MIPAS (Michelson interferometer for passive atmospheric sounding) experiment. Atmos Ocean Opt 2003;16:172–81.

[21] Rothman LS. AFGL atmospheric absorption line parameters compilation: 1980 version. Appl Opt 1981;20:791–5.

[22] Toth RA. Linelists of water vapor parameters from 500 to 8000 cm^{-1}, see http://mark4sun.jpl.nasa.gov.data/spec/H2O/

[23] Camy-Peyret C, Flaud JM, Mandin JY, Bykov A, Naumenko O, Sinitsa L, Voronin B. Fourier-transform absorption spectrum of the $H_2^{17}O$ molecule in the 9711–11335 cm^{-1} spectral region: the first decade of resonating states. JQSRT 1999;61:795–812.
[24] Tanaka M, Naumenko O, Brault JW, Tennyson J. Absorption spectrum of $H_2^{17}O$ and $H_2^{18}O$ in the near-infrared and visible. J Mol Spectrosc 2005, in press.
[25] Tanaka M, Brault JW, Tennyson J. Absorption spectrum of $H_2^{18}O$ in the 12,400–14, 520 cm^{-1} range. J Mol Spectrosc 2002;216:77–80.
[26] Schermaul R, Brault JW, Canas AAD, Learner RCM, Polyansky OL, Zobov NF, Belmiloud D, Tennyson J. Weak line water vapour spectrum in the regions 13,200–15, 000 cm^{-1}. J Mol Spectrosc 2002;211:169–78.
[27] Mérienne MF, Jenouvrier A, Hermans C, Vandaele AC, Carleer M, Clerbaux C, Coheur PF, Colin R, Fally S, Bach M. Water vapor line parameters in the 13000–9250 cm^{-1} region. JQSRT 2003;82:99–117.
[28] Coheur PF, Fally S, Carleer M, Clerbaux C, Colin R, Jenouvrier A, Mérienne MF, Hermans C, Vandaele AC. New water vapor line parameters in the 26000–13000 cm^{-1} region. JQSRT 2002;74:493–510.
[29] Tolchenov RN, Zobov NF, Polyansky OL, Tennyson J, Naumenko O, Carleer M, Coheur PF, Fally S, Clerbaux C, Jenouvrier A, Vandaele AC. Water vapor line assignments in the 9250–26000 cm^{-1} frequency range. J Mol Spectrosc 2005, in press.
[30] Gamache RR, Hartmann JM. An intercomparison of measured pressure-broadening and pressure-shifting parameters of water vapor. Can J Chem 2004;82:1013–27.
[31] Robert D, Bonamy J. Short range force effects in semiclassical molecular line broadening calculations. J Phys 1979;40:923–43.
[32] Gamache RR, Fischer J. Calculated halfwidths and lineshifts of water-vapor transitions in the 0.7 μm region and a comparison with published data. J Mol Spectrosc 2001;207:254–62.
[33] Gamache RR, Fischer J. Half-widths of $H_2^{16}O$, $H_2^{18}O$, $H_2^{17}O$, $HD^{16}O$, and $D_2^{16}O$: I Comparison between isotopomers. JQSRT 2003;78:289–304.
[34] Gamache RR, Fischer J. Half-widths of $H_2^{16}O$, $H_2^{18}O$, $H_2^{17}O$, $HD^{16}O$ and $D_2^{16}O$: II Comparison with measurement. JQSRT 2003;78:305–18.
[35] Gamache RR. Line shape parameters for water vapor in the 3.2–17.76 μm region for atmospheric applications. J Mol Spectrosc 2005;229:9–18.
[36] Gamache RR, Hartmann JM. Collisional parameters of H_2O lines: effects of vibration. JQSRT 2004;83: 119–47.
[37] Jacquemart D, Gamache RR, Rothman LS. Semi-empirical calculation of air-broadened half-widths and air pressure-induced frequency shifts of water-vapor absorption lines. JQRST, this issue, doi:10.1016/j.jqsrt.2004.11.018
[38] Zou Q, Varanasi P. Laboratory measurement of the spectroscopic line parameters of water vapor in the 610–2100 and 3000–4050 cm^{-1} regions at lower-tropospheric temperatures. JQSRT 2003;82:45–98.
[39] Brown LR, Toth RA, Dulick M. Empirical line parameters of $H_2^{16}O$ near 0.94 μm: positions, intensities and air-broadening coefficients. J Mol Spectrosc 2002;212:57–82.
[40] Toth RA, Brown LR, Smith MAH, Malathy Devi V, Benner DC, Dulick M. Temperature dependence of air-broadened line widths and shifts of water at 6 μm. 58th International Symposium on Molecular Spectroscopy, Ohio State University, June 16–20, 2003 (Paper TA01, p. 110).
[41] Tashkun SA, Perevalov VI, Teffo JL, Bykov AD, Lavrentieva NN. CDSD-296, the carbon dioxide spectroscopic databank: version for atmospheric applications. XIV Symposium on High Resolution Molecular Spectroscopy, Krasnoyarsk, Russia, July 6–11, 2003. See also ftp://ftp.iao.ru/pub/CDSD-296/.
[42] Wattson RB, Rothman LS. Direct numerical diagonalization: wave of the future. JQSRT 1992;48:763–80.
[43] Rothman LS, Hawkins RL, Wattson RB, Gamache RR. Energy levels, intensities and linewidths of atmospheric carbon dioxide bands. JQSRT 1992;48:537–66.
[44] Miller CE, Brown LR. Near infrared spectroscopy of carbon dioxide I. $^{16}O^{12}C^{16}O$ line positions. J Mol Spectrosc 2004;228:329–54.
[45] Rothman LS, Gamache RR, Tipping RH, Rinsland CP, Smith MAH, Benner DC, Devi VM, Flaud JM, Camy-Peyret C, Perrin A, Goldman A, Massie ST, Brown LR, Toth RA. The HITRAN molecular database: editions of 1991 and 1992. JQSRT 1992;48:469–507.

[46] Mandin JY. Interpretation of the CO_2 absorption bands observed in the venus infrared spectrum between 1 and 2.5 μm. J Mol Spectrosc 1977;67:304–21.
[47] Rothman LS, Benedict WS. Infrared energy levels and intensities of carbon dioxide. Appl Opt 1978;17: 2605–11.
[48] Goldman A, Stephen TM, Rothman LS, Giver LP, Mandin JY, Gamache RR, Rinsland CP, Murcray FJ. The 1-μm CO_2 bands and the O_2 (0-1) $X^3\Sigma_g - a^1\Delta_g$ and (1-0) $X^3\Sigma_g - b^1\Sigma_g$ bands in the earth atmosphere. JQSRT 2003;82:197–206.
[49] Ding Y, Bertseva E, Campargue A. The $2v_1 + 3v_3$ triad of $^{12}CO_2$. J Mol Spectrosc 2002;212:219–22.
[50] Benner DC. Private communication. College of William and Mary, Williamsburg VA, USA, 2003.
[51] Claveau C, Teffo JL, Hurtmans D, Valentin A, Gamache RR. Line positions and absolute intensities in the laser bands of carbon-12 oxygen-17 isotopic species of carbon dioxide. J Mol Spectrosc 1999;193:15–32.
[52] Mandin JY, Dana V, Allout JY, Régalia L, Barbe A, Plateaux JJ. Line intensities and self-broadening coefficients in the 10012-10001 band of $^{12}C^{16}O_2$ centered at 2224.657 cm^{-1}. J Mol Spectrosc 1995;170:604–7.
[53] Claveau C, Teffo JL, Hurtmans D, Valentin A. Infrared fundamental and first hot bands of $O^{12}C^{17}O$ isotopic variants of carbon dioxide. J Mol Spectrosc 1998;189:153–95.
[54] Teffo JL, Claveau C, Kou Q, Guelachvili G, Ubelmann A, Perevalov VI, Tashkun SA. Line intensities of $^{12}C^{16}O_2$ in the 1.2–1.4 μm spectral region. J Mol Spectrosc 2000;201:249–55.
[55] Teffo JL, Claveau C, Valentin A. Infrared fundamental bands of $O^{13}C^{17}O$ isotopic variants of carbon dioxide. JQSRT 1998;59:151–64.
[56] Henningsen J, Simonsen H. The (22^01-00^00) band of CO_2 at 6348 cm^{-1}: linestrengths, broadening parameters, and pressure shifts. J Mol Spectrosc 2000;203:16–27.
[57] Kshirsagar RJ, Giver LP, Chackerian C, Brown LR. The rovibrational intensities of the $2v_3$ band of $^{16}O^{12}C^{18}O$ at 4639 cm^{-1}. JQSRT 1999;61:695–701.
[58] Kshirsagar RJ, Giver LP, Chackerian C. Rovibrational intensities of the (00^03) ← (10^00) dyad absorption bands of $^{12}C^{16}O_2$. J Mol Spectrosc 2000;199:230–5.
[59] Giver LP, Brown LR, Chackerian C, Freedman RS. The rovibrational intensities of five bands of $^{12}C^{16}O_2$ between 5218 and 5349 cm^{-1}. JQSRT 2003;78:417–36.
[60] Devi VM, Benner DC, Rinsland CP, Smith MAH. Absolute rovibrational intensities of $^{12}C^{16}O_2$ absorption bands in the 3090–3850 cm^{-1} spectral region. JQSRT 1998;60:741–70.
[61] Campargue A, Charvat A, Permogorov D. Absolute intensity measurement of CO_2 overtone transitions in the near-infrared. Chem Phys Lett 1994;223:567–72.
[62] Lucchesini A. Private communication, IPCF, Pisa, Italy, 2004.
[63] Campargue A, Bailly D, Teffo JL, Tashkun SA, Perevalov VI. The $v_1 + 5v_3$ dyad of $^{12}CO_2$ and $^{13}CO_2$. J Mol Spec 1999;193:204–12.
[64] Devi VM, Benner DC, Smith MAH, Rinsland CP. Air- and N_2-broadening coefficients and pressure-shift coefficients in the $^{12}C^{16}O_2$ laser bands. JQSRT 1998;59:137–49.
[65] Miller CE, Montgomery MA, Onorato RM, Johnstone C, McNicholas TP, Kovaric B, Brown LR. Near infrared spectroscopy of carbon dioxide II. $^{16}O^{13}C^{16}O$ and $^{16}O^{13}C^{18}O$ line positions. J Mol Spectrosc 2004;228:355–74.
[66] Rodrigues R, Jucks KW, Lacome N, Blanquet G, Walrand J, Traub WA, Khalil B, Le Doucen R, Valentin A, Camy-Peyret C, Bonamy L, Hartmann JM. Model, software, and database for computation of line-mixing effects in infrared Q-branches of atmospheric CO_2: I. Symmetric isotopomers. JQSRT 1999;61:153–84.
[67] Jucks KW, Rodrigues R, Le Doucen R, Claveau C, Traub WA, Hartmann JM. Model, software, and database for computation of line-mixing effects in infrared Q-branches of atmospheric CO_2: II. Minor and asymmetric isotopomers. JQSRT 1999;63:31–48.
[68] Wagner G, Birk M, Schreier F, Flaud JM. Spectroscopic database for ozone in the fundamental spectral regions. J Geophys Res 2002;107:D22.
[69] Mikhailenko S. Institute of Atmospheric Optics, Tomsk, Russia, private communication (2002), using calculation based on Mikhailenko S, Barbe A, Plateaux JJ, Tyuterev VG. New analysis of $2v_1 + v_2$, $v_1 + v_2 + v_3$, and $v_2 + 2v_3$ bands of ozone in the 2600–2900 cm^{-1} region. J Mol Spectrosc 1999;196:93–101;
Flaud JM, Camy-Peyret C, Devi VM, Rinsland CP, Smith MAH. The v_1 and v_3 bands of $^{16}O_3$ line positions and intensities. J Mol Spectrosc 1987;124:209–17;

Flaud JM, Camy-Peyret C, Rinsland CP, Smith MAH, Devi VM. Line parameters of $^{16}O_3$ in the 7-μm region. J Mol Spectrosc 1989;134:106–12.
[70] Flaud JM, Wagner G, Birk M, Camy-Peyret C, Debacker-Barilly MR, Barbe A, Piccollo C. Ozone absorption around 10 μm. J Geophys Res 2003;108(D9) doi:10.1029/2002JD002755.
[71] Devi VM, Benner DC, Smith MAH, Rinsland CP. Air-broadening and shift coefficients of O_3 lines in the v_2 band and their temperature dependence. J Mol Spectrosc 1997;182:221–38.
[72] Smith MAH, Devi VM, Benner DC, Rinsland CP. Temperature dependence of air-broadening and shift coefficients of O_3 lines in the v_1 band. J Mol Spectrosc 1997;182:239–59.
[73] Smith MAH. Characterization of line broadening and shift parameters of ozone for spectroscopic databases. 56th International symposium on molecular spectroscopy, Ohio State University, June 11–15, 2001 (Paper ME03); Smith MAH. Infrared spectroscopic parameters of ozone and other atmospheric gases. NASA workshop on laboratory spectroscopic needs for atmospheric sensing, San Diego, California, October 22–26, 2001.
[74] Smith MAH, Rinsland CP, Devi VM. Measurements of self-broadening of infrared absorption lines of ozone. J Mol Spectrosc 1991;147:142–54.
[75] Drouin BJ, Fischer J, Gamache RR. Temperature dependent pressure induced lineshape of O_3 rotational transitions in air. JQSRT 2004;83:63–81.
[76] Smith MAH, Rinsland CP, Devi VM, Prochaska ES. Measurements of pressure broadening and shifts of O_3 lines in the 3-μm region. J Mol Spectrosc 1994;164:239–59.
[77] Smith MAH, Rinsland CP, Devi VM, Prochaska ES. Erratum: measurements of pressure broadening and shifts of O_3 lines in the 3-μm region. J Mol Spectrosc 1994;165:596.
[78] Toth RA. Linelist of N_2O parameters from 500 to 7500 cm^{-1}, see http://mark4sun.jpl.nasa.gov.data/spec/N2O/.
[79] Johns JWC, Lu Z, Weber M, Sirota JM, Reuter DC. Absolute intensities in the v_2 fundamental of N_2O at 17 μm. J Mol Spectrosc 1996;177:203–10.
[80] Daumont L, Claveau C, Debacker-Barilly MR, Hamdouni A, Régalia-Jarlot L, Teffo JL, Tashkun S, Perevalov VI. Line intensities of $^{14}N_2{}^{16}O$: the 10 micrometer region revisited. JQSRT 2002;72:37–55.
[81] Lyulin OM, Perevalov V, Teffo JL. Effective dipole moment and band intensities of nitrous oxide. J Mol Spectrosc 1995;174:566–80.
[82] Toth RA. Line strengths (900–3600 cm^{-1}) self-broadened linewidths and frequency shifts (1800–2660 cm^{-1}) of N_2O. Appl Opt 1993;32:7326–65.
[83] Daumont L, Vander Auwera J, Teffo JL, Perevalov V, Tashkun SA. Line intensity measurements in $^{14}N_2{}^{16}O$ and their treatment using the effective dipole moment approach: I. the 4300- to 5200-cm^{-1} region. J Mol Spectrosc 2001;208:281–91.
[84] Toth RA. Line positions and strengths of N_2O between 3515 and 7800 cm^{-1}. J Mol Spectrosc 1999;197:158–87.
[85] Toth RA. N_{2-} and air-broadened linewidths and frequency-shifts of N_2O. JQSRT 2000;66:285–304.
[86] Lacome N, Levy A, Guelachvili G. Fourier transform measurement of self-, N_{2-}, and O_{2-} broadening of N_2O lines: temperature dependence of linewidths. Appl Opt 1984;23:425–34.
[87] Nemtchinov V, Sun C, Varanasi P. Measurements of line intensities and line widths in the v_3-fundamental band of nitrous oxide at atmospheric temperatures. JQSRT 2003;83:267–84.
[88] Brault JW, Brown LR, Chackerian C, Freedman R, Predoi-Cross A, Pine AS. Self-broadened $^{12}C^{16}O$ line shapes in the $v = 2 \leftarrow 0$ band. J Mol Spectrosc 2003;222:220–39.
[89] Zou Q, Varanasi P. New laboratory data on the spectral line parameters in the 1-0 and 2-0 bands of $^{12}C^{16}O$ relevant to atmospheric remote sensing. JQSRT 2002;75:63–92.
[90] Devi VM, Benner DC, Smith MAH, Rinsland CP, Mantz AW. Determination of self- and H_2-broadening and shift coefficients in the 2-0 band of $^{12}C^{16}O$ using a multispectrum fitting procedure. JQSRT 2002;75:455–71.
[91] Fukabori M, Aoki TA, Aoki TE, Ishida H, Watanabe T. Measurements of the line strengths and halfwidths of the (2-0) and (3-0) band of CO. Proceedings of the fifth HITRAN database conference, 23–25 September 1998.
[92] Picqué N, Guelachvili G, Dana V, Mandin JY. Absolute line intensities, vibrational transition moment, and self-broadening coefficients for the 3-0 band of $^{12}C^{16}O$. J Mol Struct 2000;517-8:427–34.
[93] Chackerian C, Freedman RS, Giver LP, Brown LR. Absolute rovibrational intensities and self-broadening and self-shift coefficients for the $X^1\Sigma^+$ $V = 3 \leftarrow V = 0$ band of $^{12}C^{16}O$. J Mol Spectrosc 2001;210:119–26.

[94] Sung K, Varanasi P. Intensities, collision-broadened half-width, and collision-induced line shifts in the second overtone band of $^{12}C^{16}O$. JQSRT 2004;82:445–58.
[95] Régalia-Jarlot L, Thomas X, Von der Heyden P, Barbe A. Pressure-broadened line widths and pressure-induced line shifts coefficients of the (1-0) and (2-0) bands of $^{12}C^{16}O$. JQSRT 2005;91:121–31.
[96] Smith MAH, Brown LR, Devi VM, Pittman TJ. CO broadening and shift parameters for TES. Proceedings of the eighth HITRAN database conference, Cambridge, MA, June 15–18. 2004.
[97] Connor BJ, Radford HE. Pressure broadening of the CO $J = 1 - 0$ rotational transition by N_2, O_2 and air. J Mol Spectrosc 1986;119:229–31.
[98] Predoi-Cross A, Bouanich JP, Benner DC, May AD, Drummond JR. Broadening, shifting, and line asymmetries in the $2 \leftarrow 0$ band of CO and CO–N_2: experimental results and theoretical calculations. J Chem Phys 2000;113:1–11.
[99] Henningsen J, Simonsen H, Møgelberg T, Trudsø E. The $0 \rightarrow 3$ overtone band of CO: precise linestrengths and broadening parameters. J Mol Spectrosc 1999;193:354–62.
[100] Swann WC, Gilbert SL. Pressure-induced shift and broadening of 1560–1630-nm carbon monoxide wavelength-calibration lines. J Opt Soc Am B 2002;19:2461–7.
[101] Jacquemart D, Mandin JY, Dana V, Picqué N, Guelachvili G. A multispectrum fitting procedure to deduce molecular line parameters: application to the 3-0 band of $^{12}C^{16}O$. Eur Phys J D 2001;14:55–69.
[102] Devi VM, Benner DC, Smith MAH, Rinsland CP. Self-broadening and self-shift coefficients in the fundamental band of $^{12}C^{16}O$. JQSRT 1998;60:815–24.
[103] Sun JNP, Griffiths PR. Temperature dependence of the self-broadening coefficients for the fundamental band of carbon monoxide. Appl Opt 1981;20:1691–5.
[104] Nakazawa T, Tanaka M. Measurements of intensities and self- and foreign-gas-broadened half-widths of spectral lines in the CO fundamental band. JQSRT 1982;28:409–16.
[105] Lowder JE. Self-broadened half-width measurements in the CO fundamental. JQSRT 1971;11:1647–57.
[106] Hunt RH, Toth RA, Plyler EK. High-resolution determination of the line widths of the self-broadened lines of carbon monoxide. J Chem Phys 1968;49:3909–12.
[107] BelBruno JJ, Gelfand J, Radigan W, Verges K. Helium and self-broadening in the first and second overtone bands of $^{12}C^{16}O$. J Mol Spectrosc 1982;94:336–42.
[108] Brown LR. Empirical line parameters of methane from 1.1 to 2.1 μm. JQSRT this issue, doi:10.1016/j.jqsrt.2004.12.037.
[109] Camy-Peyret C, LPMA, Paris, France, private communication based on Camy-Peyret C, Payan S, Jeseck P, Té Y, Hawat T. High resolution balloon-borne spectroscopy within the O_2 A-band: observations and radiative transfer modeling. Paper E4, Proceedings of the international radiation symposium, Saint Petersburg, Russia, 2000.
[110] Goldman A, Brown LR, Schoenfeld WG, Spencer MN, Chackerian Jr C, Giver LP, Dothe H, Rinsland CP, Coudert LH, Dana V, Mandin JY. Nitric oxide line parameters: review of 1996 HITRAN update and new results. JQSRT 1998;60:825–38.
[111] Gillis JR, Goldman A. Nitric oxide IR line parameters for the upper atmosphere. Appl Opt 1982;21:1616–27.
[112] Chackerian C, Freedman RS, Giver LP, Brown LR. The NO vibrational fundamental band: O_2-broadening coefficients. J Mol Spectrosc 1998;192:215–9.
[113] Spencer MN, Chackerian C, Giver LP, Brown LR. The nitric oxide fundamental band: frequency and shape parameters for ro-vibrational lines. J Mol Spectrosc 1994;165:506–24.
[114] Allout MY, Dana V, Mandin JY, Von der Heyden P, Décatoire D, Plateaux JJ. Oxygen-broadening coefficients of first overtone nitric oxide lines. JQSRT 1999;61:759–65.
[115] Mandin JY, Dana V, Régalia L, Thomas X, Barbe A. Nitrogen-broadening in the nitric oxide first overtone band. JQSRT 2000;66:93–100.
[116] Pine AS, Maki AG, Chou NY. Pressure broadening lineshapes and intensity measurements in the $2 \leftarrow 0$ band of NO. J Mol Spectrosc 1985;114:132–47.
[117] Spencer MN, Chackerian C, Giver LP, Brown LR. Temperature dependence of nitrogen broadening of the NO fundamental vibrational band. J Mol Spectrosc 1997;181:307–15.

[118] Pine AS, Johns JWC, Robiette AG. Λ-Doubling in the $v = 2 \leftarrow 0$ overtone band in the infrared spectrum of NO. J Mol Spectrosc 1979;74:52–69.
[119] Chu PM, Wetzel SJ, Lafferty WJ, Perrin A, Flaud JM, Arcas Ph, Guelachvili G. Line intensities for the 8-μm bands of SO_2. J Mol Spectrosc 1998;189:55–63.
[120] Sumpf B. Line intensity and self-broadening investigations in the ν_1 and the ν_3 bands of SO_2. J Mol Struct 2001;599:39–49.
[121] Henningsen J. Private communication. Danish Institute for Fundamental Metrology, Lyngby, Denmark, 2004.
[122] Benner DC, Blake TA, Brown LR, Devi VM, Smith MAH, Toth RA. Air-broadening parameters in the ν_3 band of $^{14}N^{16}O_2$ using a multispectrum fitting technique. J Mol Spectrosc 2004;228:593–619.
[123] Kleiner I, Tarrago G, Cottaz C, Sagui L, Brown LR, Poynter RL, Pickett HM, Chen P, Pearson JC, Sams RL, Blake GA, Matsuura S, Nemtchinov V, Varanasi P, Fusina L, Di Lonardo G. NH_3 and PH_3 line parameters: the 2000 HITRAN update and new results. JQSRT 2003;82:293–312.
[124] Zu L, Hamilton PA, Davies PB. Pressure broadening and frequency measurements of nitric acid lines in the 683 GHz region. JQSRT 2002;73:545–56.
[125] Petkie DT, Helminger P, Winnewisser BP, Winnewisser M, Butler RAH, Jucks KW, De Lucia FC. The simulation of infrared bands from the analyses of rotational spectra: the $2\nu_9 - \nu_9$ and $\nu_5 - \nu_9$ hot bands of HNO_3. JQSRT 2005;92:129–41.
[126] Toth RA, Brown LR, Cohen EA. Line intensities of HNO_3. J Mol Spectrosc 2003;218:151–68.
[127] Rothman LS, Rinsland CP, Goldman A, Massie ST, Edwards DP, Flaud JM, Perrin A, Camy-Peyret C, Dana V, Mandin JY, Schrœder J, McCann A, Gamache RR, Wattson RB, Yoshino K, Chance KV, Jucks KW, Brown LR, Nemtchinov V, Varanasi P. The HITRAN molecular spectroscopic database and HAWKS (HITRAN atmospheric workstation): 1996 edition. JQSRT 1998;60:665–710.
[128] Goldman A, Rinsland CP, Perrin A, Flaud JM. HNO_3 Line parameters: 1996 HITRAN update and new results. JQSRT 1998;60:851–61.
[129] Perrin A, Flaud JM, Camy-Peyret C, Winnewisser BP, Klee S, Goldman A, Murcray FJ, Blatherwick RD, Bonomo FS, Murcray DG. First analysis of the $3\nu_9 - \nu_9$, $3\nu_9 - \nu_5$ and $3\nu_9 - 2\nu_9$ bands of HNO_3: torsional splitting in the ν_9 vibrational mode. J Mol Spectrosc 1994;166:224–43.
[130] Flaud JM, Perrin A, Orphal J, Kou Q, Flaud PM, Dutkiewicz Z, Piccolo C. New analysis of the $\nu_5 + \nu_9 - \nu_9$ hot band of HNO_3. JQSRT 2003;77:355–64.
[131] Chackerian C, Sharpe SW, Blake TA. Anhydrous nitric acid integrated absorption cross sections: 820–5300 cm^{-1}. JQSRT 2003;82:429–41.
[132] Giver LP, Valero FPJ, Goorvitch D, Bonomo FS. Nitric-acid band intensity and band-model parameters from 610 to 1760 cm^{-1}. J Opt Soc Am B 1984;1:715–22.
[133] Boone C, Bernath PF, Private communication. University of Waterloo, Canada, 2004. See also http://www.ace.uwaterloo.com
[134] Brockman P, Bair CH, Allario F. High resolution spectral measurement of the HNO_3 11.3-μm band using tunable diode lasers. Appl Opt 1978;17:91–9.
[135] Goldman A, Schoenfeld WG, Goorvitch D, Chackerian C, Dothe H, Mélen F, Abrams MC, Selby JEA. Updated line parameters for OH $X^2\Pi$—$X^2\Pi(v'', v')$ transitions. JQSRT 1998;59:453–69.
[136] Colin R, Coheur PF, Kisaleva M, Vandaele AC, Bernath PF. Spectroscopic constants and term values for the $X^2\Pi_i$ state of OH ($v = 0$–10). J Mol Spectrosc 2002;214:225–6.
[137] Bulanin MO, Domanskaya AV, Kerl K. High-resolution FTIR measurement of the line parameters in the fundamental band of HI. J Mol Spectrosc 2003;218:75–9.
[138] Goldman A, Coffey MT, Hannigan JW, Mankin WG, Chance K, Rinsland CP. HBr and HI line parameters update for atmospheric spectroscopy databases. JQSRT 2003;82:313–8.
[139] Régalia-Jarlot L, Hamdouni A, Thomas X, Von der Heyden P, Barbe A. Line intensities of the $\nu_3, 4\nu_2, \nu_1 + \nu_3, 3\nu_1$, and $2\nu_1 + \nu_2$ bands of the $^{16}O^{12}C^{32}S$ molecule. JQSRT 2002;74:455–70.
[140] Vander Auwera J, Fayt A. Absolute line intensities for carbonyl sulfide from 827 to 2939 cm^{-1}. J Mol Struct 2005, in press.
[141] Rbaihi E, Belafhal A, Vander Auwera J, Naïm S, Fayt A. Fourier transform spectroscopy of carbonyl sulfide from 4800 to 8000 cm^{-1} and new global analysis of $^{16}O\ ^{12}C^{32}S$. J Mol Spectrosc 1998;191:32–44.

[142] Strugariu T, Naim S, Fayt A, Bredohl AH, Blavier JF, Dubois I. Fourier transform spectroscopy of ^{18}O-enriched carbonyl sulfide from 1825 to 2700 cm^{-1}. J Mol Spectrosc 1998;189:206–19.
[143] Bermejo D, Domenech JL, Santos J, Bouanich JP, Blanquet G. Absolute line intensities in the $2\nu_3$ band of $^{16}O^{12}C^{32}S$. J Mol Spectrosc 1997;185:26–30.
[144] Perrin A, Keller K, Flaud JM. New analysis of the ν_2, ν_3, ν_4 and ν_6 bands of formaldehyde $H_2^{12}C^{16}O$ line positions and intensities in the 5–10 μm spectral region. J Mol Spectrosc 2003;221:192–8.
[145] Flaud JM, Birk M, Wagner G, Orphal J, Klee S, Lafferty WJ. The far-infrared spectrum of HOCl: line positions and intensities. J Mol Spectrosc 1998;191:362–7.
[146] Vander Auwera J, Kleffmann J, Flaud JM, Pawelke G, Burger H, Hurtmans D, Petrisse R. Absolute ν_2 line intensities of HOCl by simultaneous measurements in the infrared with a tunable diode laser and far-infrared region using a Fourier transform spectrometer. J Mol Spectrosc 2000;204:36–47.
[147] Shorter JH, Nelson DD, Zahniser MS. Air-broadened linewidth measurements in the ν_2 vibrational band of HOCl. J Chem Soc Faraday Trans 1997;93:2933–5.
[148] Bernath PF. Private communication. University of Waterloo, Canada, 2004.
[149] Maki AG, Mellau GC, Klee S, Winnewisser M, Quapp W. High-temperature infrared measurements in the region of the bending fundamental of $H^{12}C^{14}N$, $H^{12}C^{15}N$, and $H^{13}C^{14}N$. J Mol Spectrosc 2000;202:67–82;
Maki AG, Quapp W, Klee S, Mellau GC, Albert S. Infrared transitions of $H^{12}C^{14}N$ and $H^{12}C^{15}N$ between 500 and 10000 cm^{-1}. J Mol Spectrosc 1996;180:323–36.
[150] Devi VM, Benner DC, Smith MAH, Rinsland CP, Sharpe SW, Sams RL. A multispectrum analysis of the ν_1 band of $H^{12}C^{14}N$: I. Intensities, self-broadening and self-shift coefficients. JQSRT 2003;82:319–42.
[151] Devi VM, Benner DC, Smith MAH, Rinsland CP, Sharpe SW, Sams RL. A multispectrum analysis of the $2\nu_2$ spectral region of $H^{12}C^{14}N$: intensities, broadening and pressure-shift coefficients. JQSRT 2004;87: 339–66.
[152] Rinsland CP, Devi VM, Smith MAH, Benner DC, Sharpe SW, Sams RL. A multispectrum analysis of the ν_1 band of $H^{12}C^{14}N$: II. Air- and N_2-broadening, shifts and their temperature dependences. JQSRT 2003; 82:343–62.
[153] Malathy Devi V, Benner DC, Smith MAH, Rinsland CP, Predoi-Cross A, Sharpe SW, Sams RL, Boulet C, Bouanich JP. A multispectrum analysis of the ν_2 band of $H^{12}C^{14}N$: Part I. Intensities, broadening and shift coefficients. J Mol Spectrosc 2005;231:66–84 Bouanich JP, Boulet C, Predoi-Cross A, Sharpe SW, Sams RL, Smith MAH, Rinsland CP, Benner DC, Malathy Devi V. A multispectrum analysis of the ν_2 band of $H^{12}C^{14}N$: Part II. Theoretical calculations of self-broadening, self-induced shifts and their temperature dependences. J Mol Spectrosc 2005;231:85–95.
[154] Chackerian C, Brown LR, Lacome N, Tarrago G. Methyl chloride ν_5 region line shape parameters and rotational constants for the ν_2, ν_5 and $2\nu_3$ vibrational bands. J Mol Spectrosc 1998;191:148–57.
[155] Bouanich JP, Blanquet G, Populaire JC, Walrand J. N_2-Broadening for methyl chloride at low temperature by diode-laser spectroscopy. J Mol Spectrosc 2001;208:72–8.
[156] El Hachtouki R, Vander Auwera J. Absolute line intensities in acetylene: the 1.5-μm region. J Mol Spectrosc 2002;216:355–62.
[157] Kou Q, Guelachvili G, Abbouti Temsamani M, Herman M. The absorption spectrum of C_2H_2 around $\nu_1 + \nu_3$: energy standards in the 1.5 μm region and vibrational clustering. Can J Phys 1994;72:1241–50.
[158] Nakagawa K, De Labachelerie M, Awaji Y, Kourogi M. Accurate optical frequency atlas of the 1.5 microns band of acetylene. J Opt Soc Am B 1996;13:2708–14.
[159] Pine AS, Rinsland CP. The role of torsional hot bands in modeling atmospheric ethane. JQSRT 1999;62:445–58.
[160] Brown LR, Sams RL, Kleiner I, Cottaz C, Sagui L. Line intensities of the phosphine dyad at 10 μm. J Mol Spectrosc 2002;215:178–203.
[161] Tarrago G, Lacome N, Levy A, Guelachvili G, Benzard B, Drossart P. Phosphine spectrum at 4–5 μm: analysis and line-by-line simulation of $2\nu_2, \nu_2 + \nu_4, 2\nu_4, \nu_1$, and ν_3 bands. J Mol Spectrosc 1992;154:30–42.
[162] Cohen EA. Private communication. Jet Propulsion Laboratory. 2001.
[163] Acef O, Bordé CJ, Clairon A, Pierre G, Sartakov B. New accurate fit of an extended set of saturation data for the ν_3 band of SF_6: comparison of Hamiltonians in the spherical and cubic tensor formalisms. J Mol Spectrosc 2000;199:188–204.

[164] Boudon V, Pierre G. In: Pandalai SG, editor. Rovibrational spectroscopy of sulphur hexafluoride: a review in recent research developments in molecular spectroscopy. Vol. 1. Trivandrum, India: Transworld Research Network; 2002; p. 25–55.
[165] Boudon V, Lacome N. High-resolution FTIR spectrum and analysis of the $\nu_2 + \nu_4$ combination band of $^{32}SF_6$. J Mol Spectrosc 2003;222:291–5.
[166] Tejwani GDT, Fox K. Calculated self- and foreign-gas-broadened linewidths for SF_6. JQSRT 1987;37:541–6.
[167] Sumpf B, Meusel I, Kronfeldt HD. Self- and air-broadening in the ν_1 and ν_3 bands of H_2S. J Mol Spectrosc 1996;177:143–5.
[168] Kissel A, Kurtz O, Kronfeldt HD, Sumpf B. Quantum number and perturber dependence of pressure-induced line shift and line broadening in the $2\nu_2, \nu_1$, and ν_3 bands of H_2S. 15th International Conference on High Resolution Molecular Spectroscopy, Prague, Czech Republic, August 30–September 3, 1998.
[169] Kissel A, Sumpf B, Kronfeldt HD, Tikhomirov BA, Ponomarev YN. Molecular-gas-pressure-induced line-shift and line-broadening in the ν_2-band of H_2S. J Mol Spectrosc 2002;216:345–54.
[170] Waschull J, Kuhnemann F, Sumpf B. Self-, air- and helium broadening of the ν_2 band of H_2S. J Mol Spectrosc 1994;165:150–8.
[171] Sumpf B. Experimental investigation of the self-broadening coefficients in the $\nu_1 + \nu_3$ band of SO_2 and the $2\nu_2$ band of H_2S. J Mol Spectrosc 1997;181:160–7.
[172] Vander Auwera J. ULB, Brussels, Belgium, private communication (2004), based on Vander Auwera J. High-resolution investigation of the far-infrared spectrum of formic acid. J Mol Spectrosc 1992;155:136–42.
[173] Winnewisser M, Winnewisser BP, Stein M, Birk M, Wagner G, Winnewisser G, Yamada KMT, Belov SP, Baskakov OI. Rotational spectra of cis-HCOOH, trans-HCOOH, and trans-$H^{13}COOH$. J Mol Spectrosc 2002;216:259–65.
[174] Perrin A, Rinsland CP, Goldman A. Spectral parameters for the ν_6 region of HCOOH and its measurement in the infrared tropospheric spectrum. J Geophys Res 1999;104:18661–6.
[175] Shepard MW, Goldman A, Clough SA, Mlawer EJ. Spectroscopic improvements providing evidence of formic acid in AERI-LBLRTM validation spectra. JQSRT 2003;82:383–90.
[176] Vander Auwera J, Didriche K, Perrin A, Keller F, Flaud JM. Absolute line intensities in the ν_6 band of trans-formic acid. Proceedings of the eighth HITRAN database conference, Cambridge, MA, 16–18 June, 2004. p. 21.
[177] Goldman A, Gillis JR. Line parameters and line-by-line calculations for molecules of stratospheric interest. Progress report, Department of Physics, University of Denver, 1984.
[178] Perrin A, Flaud JM, Bakri B, Demaison J, Basakov O, Sirota SV, Herman M, Vander Auwera J. New high-resolution analysis of the ν_7 and ν_9 fundamental bands of trans-formic acid by Fourier transform infrared and millimeter-wave spectroscopy. J Mol Spectrosc 2002;216:203–13.
[179] Chance K, Jucks KW, Johnson DG, Traub WA. The Smithsonian Astrophysical Observatory Database SAO92. JQSRT 1994;52:447–57.
[180] Yamada C, Endo Y, Hirota E. Difference frequency laser spectroscopy of the ν_1 band of the HO_2 radical. J Chem Phys 1983;78:4379–84.
[181] Nagai K, Endo Y, Hirota E. Diode laser spectroscopy of the HO_2 ν_2 band. J Mol Spectrosc 1981;89:520–7.
[182] Nelson DD, Zahniser MS. Diode laser spectroscopy of the ν_3 vibration of the HO_2 radical. J Mol Spectrosc 1991;150:527–34.
[183] Müller HSP, Thorwirth S, Roth DA, Winnewisser G. The Cologne Database for Molecular Spectroscopy. CDMS. Astronomy & Astrophysics 2001;370:L49–52.
[184] Xu LH, Lees RM, Wang P, Brown LR, Kleiner I, Johns JWC. New assignments, line intensities, and HITRAN database for CH_3OH at 10 μm. J Mol Spectrosc 2004;228:453–70.
[185] Wagner G, Birk M. New infrared spectroscopic database for chlorine nitrate. JQSRT 2003;82:443–60.
[186] Ballard J, Johnston WB, Gunson MR, Wassell PT. Absolute absorption coefficients of $ClONO_2$ infrared bands at stratospheric temperatures. J Geophys Res 1988;93:1659–65.
[187] May RD, Friedl RR. Integrated band intensities of HO_2NO_2 at 220 K. JQSRT 1993;50:257–66.
[188] Rinsland CP, Sharpe SW, Sams RL. Temperature-dependent cross-sections in the thermal infrared bands of SF_5CF_3. JQSRT 2003;82:483–90.

[189] Allen G, Remedios JJ, Newnham DA, Smith KM, Monks PS. High resolution mid-infrared cross-sections for peroxyacetyl nitrate (PAN) vapour. Atmos Chem Phys Discuss 2004;4:5656–81.
[190] Orlando JJ, Tyndall GS. Private communication. National Center for Atmospheric Research, Boulder CO, USA. 2004.
[191] Beer R, Glavich TA, Rider DM. Tropospheric emission spectrometer for the Earth Observing System's *AURA* satellite. Appl Opt 2001;40:2356–67.
[192] Bass AM, Paur RJ. UV absorption cross-sections for ozone: the temperature dependence. J Photochem 1981;17:41;
Bass AM, Paur RJ. The ultraviolet cross-sections of ozone: I the measurements. In: Zerefos CS, Ghazi A, editors. Atmospheric ozone. Dordrecht: Reidel D; 1985. p. 606–10;
Bass AM, Paur RJ. The ultraviolet cross-sections of ozone: II results and temperature dependence. In: Zerefos CS, Ghazi A, editors. Atmospheric ozone. Dordrecht: Reidel D; 1985. p. 611–6.
[193] Edlén B. The refractive index of air. Metrologia 1966;2:71–80.
[194] Voigt S, Orphal J, Bogumil K, Burrows JP. The temperature dependence (203–293 K) of the absorption cross sections of O_3 in the 230–850 nm region measured by Fourier-transform spectroscopy. J Photochem Photobiol A: Chem 2001;143:1–9.
[195] Orphal J, Fellows CE, Flaud PM. The visible absorption spectrum of NO_3 measured by high-resolution Fourier-transform spectroscopy. J Geophys Res 2003;108(D3):4077.
[196] Wilmouth DM, Hanisco TF, Donahue NM, Anderson JG. Fourier transform ultraviolet spectroscopy of the $A\ ^2\Pi_{3/2} \leftarrow X\ ^2\Pi_{3/2}$ transition of BrO. J Phys Chem 199; 103:8935–8945.
[197] Kromminga H, Orphal J, Spietz P, Voigt S, Burrows JP. The temperature dependence (213–293 K) of the absorption cross-sections of OClO in the 340–450 nm region measured by Fourier-transform spectroscopy. J Photochem Photobiol A: Chem 2003;157:149–60.
[198] Cantrell CA, Davidson JA, McDaniel AH, Shetter RE, Calvert JG. Temperature-dependent formaldehyde cross sections in the near-ultraviolet spectral region. J Phys Chem 1990;94:3902–8.
[199] Greenblatt GD, Orlando JJ, Burkholder JB, Ravishankara AR. Absorption measurements of oxygen between 330 and 1140 nm. J Geophys Res 1990;95:18577–82.
[200] Massie ST, Goldman A. The infrared absorption cross-section and refractive-index data in HITRAN. JQSRT 2003;82:413–28.
[201] Norman ML, Miller RE, Worsnop DR. Ternary $H_2O/HNO_3/H_2O$ optical constants: new measurements from aerosol spectroscopy under stratospheric conditions. J Phys Chem 2002;106:6075–83.
[202] Adams RW, Downing HD. Infrared optical constants of ternary system of 75% H_2SO_4 10% HNO_3 and 15% H_2O. J Opt Soc Am 1986;3:22–8.
[203] Biermann UM, Luo BP, Peter T. Absorption spectra and optical constants of binary and ternary solutions of H_2SO_4, HNO_3, and H_2O in the mid infrared at atmospheric temperatures. J Phys Chem 2000;104:783–93.
[204] Luo B, Krieger UK, Peter T. Densities and refractive indices of $H_2SO_4/HNO_3/H_2O$ solutions to stratospheric temperatures. Geophys Res Lett 1996;23:3707–10.
[205] Fischer J, Gamache RR, Goldman RR, Rothman LS, Perrin A. Total internal partition sums for molecular species on the 2000 edition of the HITRAN database. JQSRT 2003;82:401–12.
[206] Goldman A, Gamache RR, Perrin A, Flaud JM, Rinsland CP, Rothman LS. HITRAN partition functions and weighted transition probabilities. JQSRT 2000;66:455–86.